EFFECT OF BOLUS VISCOSITY ON CARBOHYDRATE DIGESTION AND GLUCOSE ABSORPTION PROCESSES: AN *IN VITRO* GASTROINTESTINAL STUDY AND DEVELOPMENT OF A MATHEMATICAL MODEL

By

KARTHIKEYAN JAGADEESAN SANKARAN

A dissertation submitted to the

School of Graduate Studies

Rutgers, The State University of New Jersey

In partial fulfillment of the requirements

For the degree of

Doctor of Philosophy

Graduate Program in Food Science

Written under the direction of

Dr. Mukund V. Karwe

And approved by

_____

_____

_____

_____

New Brunswick, New Jersey

October 2019

ABSTRACT OF THE DISSERTATION

Effect of Bolus Viscosity on Carbohydrate Digestion and Glucose Absorption Processes: An *In vitro* Gastrointestinal Study and Development of a Mathematical Model

by KARTHIKEYAN JAGADEESAN SANKARAN

Dissertation Director:

Dr. Mukund V. Karwe

Digestion is the process of breaking down food into smaller nutrient components which can be easily absorbed in the intestinal tract. Research in human digestion is limited due to the complex multistage process of digestion and technical difficulties in completely understanding the process. This dissertation research was aimed at analyzing carbohydrate digestion and glucose absorption processes in the human small intestine using *in vitro* experimental procedure in a gastrointestinal model system and by subsequently developing a mathematical model to simulate and predict these processes.

Based on prior research it could be inferred that the viscosity of gastrointestinal content plays a significant role in reducing the amount of nutrients available for absorption. In this study, the aim of *in vitro* experiments was to investigate the influence of bolus (gastric content) viscosity on digestion and nutrient absorption processes, using an *in vitro* gastrointestinal model, the TIM-1 system. Two types of simple carbohydrates, namely glucose and maltodextrin, were used as simple food bases. The initial bolus viscosity was varied (~1 mPa·s, ~15 mPa·s, and ~100 mPa·s) using different glycerol-water proportions. A fluorescence emitting dye (Fast Green) was used to monitor the changing patterns of the viscosity of gastrointestinal content during digestion in the stomach and in the small intestine. By analyzing the nutrient absorption data, it was found that the bolus viscosity did not significantly affect the nutrient absorption process in the small intestine. An increase in the initial bolus viscosity from ~1 mPa·s to ~15 mPa·s, significantly reduced the maltodextrin to glucose conversion by 35%. However, increasing the initial bolus viscosity further from ~15 mPa·s to ~100 mPa·s did not significantly reduce the maltodextrin to glucose conversion.

The aim of the numerical simulation was to develop a fluid flow-based numerical model mimicking human small intestine to predict the glucose absorption process during carbohydrate digestion. COMSOL Multiphysics® software was used to numerically simulate two-dimensional axisymmetric fluid flow induced by peristaltic movement. From the literature, the intestinal geometry parameters, motility parameters, and amylase enzyme kinetics were obtained. To predict the glucose absorption process, it was assumed that the intestine is enclosed in a cylindrical casing with an intermediate diffusive wall. The

numerical predictions were experimentally validated by analyzing *in vitro* digestion of 5 g glucose and 5 g maltodextrin. The numerical model with the intermediate diffusive wall of thickness 2 mm and glucose diffusivity value of 5.25×10^{-9} m^2/s for the jejunal section and 2.5×10^{-8} m^2/s for the ileal section, predicted the experimental cumulative glucose absorption value with an average error of 0.1 g.

This research elucidates the influence of viscosity on the digestion of food. This work also demonstrates the possibility of numerically simulating the human digestive process. Research in this direction could guide the food researchers to engineer novel food products with an optimal viscosity behavior for controlled caloric intake/release which might eventually reduce obesity-related risks.

ACKNOWLEDGEMENTS

This dissertation would not have been possible without the support and help of many people. I am happy to acknowledge their contribution towards the completion of this research work.

First and foremost, I would like to express my sincere thanks to my advisor and mentor, Dr. Mukund V. Karwe for his guidance, support, and encouragement throughout my graduate career (Masters and Ph.D.). I am grateful to him for providing me the opportunity to be a part of his lab and work on this project. I have learned a great deal of skills by being a part of this lab and as his student, such as, how to be a good teacher, a good researcher, a group leader, a team member, etc. I will always be happy and proud to address myself as 'Dr. Karwe's student'.

I would also like to extend my gratitude to Dr. Deepti Salvi and Dr. Maria G. Corradini, for sharing their valuable experience, suggestions, and for their constant support throughout this project. I would sincerely like to thank Dr. Kit Yam and Dr. Paul Takhistov, for agreeing to serve on my thesis committee. Their inputs, suggestions, and comments are appreciated.

I would like to thank the New Jersey Institute of Food Nutrition and Health (IFNH) for partially funding this project. I would like to thank, Dr. David Ribnicky and Dr. Richard Ludescher at Rutgers University, Dr. Michael Rogers (University of Guelph), and Dr.

Serafim Bakalis (University of Birmingham) for their suggestions regarding my experiments and research work, and for allowing me to use their lab resources for this research. I would like to thank Fatemah, Yaqi, Sawali, Pango, Haoxin, and Yuejia, for their help while performing experiments. Special mention to Dr. Donald Schaffner (Graduate Program Director), Dr. Chitra Ponnusamy (Undergraduate Program Director), and Irene Weston (Departmental Administrator), for all their help, during my stay at Rutgers Department of Food Science.

I want to thank all my lab mates for making the lab my second home, actually my *first* home - Noopur, Ender, Tina, Shruthi, Isha, Sawali, Soundharya, Swetha, Siddharth, Meenakshi, Jose, Kiran, Rajay, Tanya, Neha, Pango, Siddhi, Lin, Vahini, and Manasi, for their support and help. I would like to thank my friends, near (Varsha, Sarath, and Krithiga) and far, for their support and for sticking by my side during my ups and downs. I am also grateful to my family members, therapists, and well-wishers for their support and encouragement.

No words of mine can adequately express my regards and love to my parents, Madiniyar and Sankaran, for their constant support and encouragement. Their moral support has always been my side and has provided me with the confidence to accomplish my goals.

TABLE OF CONTENTS

LIST OF TABLES

LIST OF FIGURES

1. BACKGROUND

1.1. Obesity

Obesity is defined as an abnormal or excessive fat accumulation that may impair health **(WHO, 2015)**. Obesity can be caused by different reasons. The primary reason is the lack of energy balance, which is the imbalance between calories consumed and calories spent. The energy imbalance can be attributed due to unhealthy diet/eating habits, overeating (excessive caloric intake), and lack of physical activity **(Linton et al., 1972; Kopelman, 2000; NIH, 2012)**. Other reasons for obesity are genetic/hereditary, specific health conditions (such as hormonal imbalance), side effects of some medicines, smoking, lack of sleep, etc. **(NIH, 2012)**. The common health consequences of obesity are non-communicable diseases such as cardiovascular diseases (heart disease and stroke), diabetes, and musculoskeletal disorders **(WHO, 2015)**. In the past, obesity was considered as a problem only in affluent countries, however in recent years the prevalence of obesity has been increasing in low- and middle-income countries, concentrating more in urban settings **(WHO, 2015)**. In 2014, approximately 13% of the world's adult population (11% of men and 15% of women) were obese. Also, the worldwide prevalence of obesity increased by two times between 1980 and 2014 **(WHO, 2015)**. According to an obesity-related survey study across the U.S., in 2013-2014, the overall prevalence of obesity was 37.7% (35.0% of men and 40.4% of women) **(Flegal et al., 2016)**. In the U.S., obesity has reached epidemic proportions and needs new strategies for prevention and medical treatment

There are a number of ways to prevent and treat obesity. The most important and healthier way is to make lifestyle changes such as eating fewer calories and being physically active. A healthy eating plan can give body sufficient nutrients it needs with enough calories for good health. Reducing the portion size is a good way to eat fewer calories and reduce gaining weight **(NIH, 2012)**. The portion sizes of all the common foods have increased over the years, and with less physical activity, the incidence of obesity has increased drastically due to energy imbalance. In severe cases of obesity, people are medically advised to seek medication to lose weight as part of programs that includes diet, physical activity, and behavioral changes. According to an obesity-related survey study across the U.S., in the year 2006, per capita medical costs for people who are obese were $ 1,429 (USD) higher than those of normal weight **(Finkelstein et al., 2009)**. Some of the weight loss medicines approved by the USFDA are Xenical®, Alli®, Locaserine Hydrochloride (Belviq®), and Qsymia™. The functionalities of these medicines include reducing the absorption of fats, fat calories, and some vitamins. Some other over-the-counter (OTC) products like Hoodia (a cactus that is native to Africa) are also used by people, as appetite suppressants to reduce caloric intake **(NIH, 2012)**. To analyze the nutrient absorption process and caloric consumption, a detailed understanding of the human digestive system and the digestive process is required.

1.2. The human digestive system

Digestion is the process of breaking down food into smaller components, by mechanical and enzymatic action in the digestive tract, so that these small nutrient components can be more easily absorbed by the body **(Gropper et al., 2009)**. The human digestive system is a complex series of organs and glands which assist the digestion of food. **Figure 1.1** illustrates the human digestive tract and accessory organs.

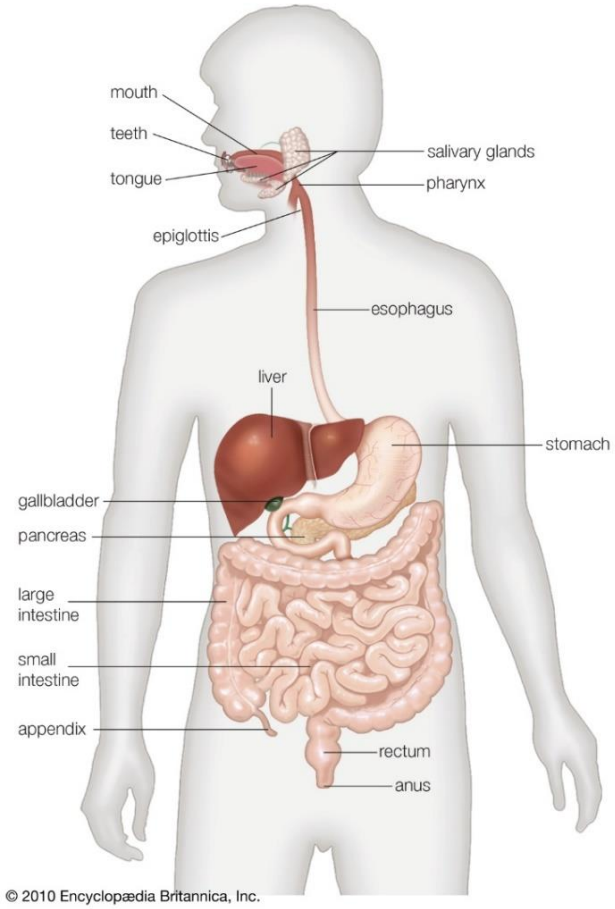

Figure 1.1: The human digestive system

(http://kids.britannica.com/comptons/art-193071/The-organs-of-the-human-digestive-system-work-together-to)

The human digestive tract is approximately 5 m long. The main parts of the digestive tract include the oral cavity, esophagus, stomach, small intestine, and large intestine. The accessory organs include the pancreas, liver, and gall bladder. The accessory organs produce secretions that are delivered to the digestive tract to aid the digestive and absorptive processes **(Gropper et al., 2009)**. The food intake is controlled by neuronal circuits in the central nervous system. The nervous system of the gastrointestinal tract is referred as the enteric nervous system. This system includes millions of neurons embedded in the walls of the gastrointestinal tract beginning from the esophagus and extending to the anus **(Gropper et al., 2009)**. Subsequent sections describe the structures and the digestive processes that occur in each part of the digestive tract.

1.2.1. The oral cavity and the esophagus

The digestive process begins in the oral cavity and proceeds sequentially through the esophagus, stomach, small intestine, and finally into the large intestine. The oral cavity includes the mouth and pharynx/throat. In the mouth, food is chewed by the actions of the teeth and jaw muscles and is mixed with saliva secreted from the salivary glands, for swallowing. Saliva is majorly comprised of water (99.5%). The primary enzyme in saliva is α-amylase which hydrolyzes the internal α-(1→4) bonds within starch. Another enzyme present in saliva is lingual lipase which hydrolyzes dietary triacylglycerols in the stomach **(Gropper et al., 2009)**. The food mixed with saliva is called as the bolus and passes through the pharynx into the esophagus. The esophagus is a flexible tube about 25 cm long. The bolus of food moves into and down the esophagus with the help of voluntary and involuntary muscles. These muscles result in a progressive wavelike motion, peristalsis,

which moves the bolus through the esophagus. Bolus usually takes 10 seconds to travel through the esophagus and reach the stomach **(Gropper et al., 2009)**.

1.2.2. The stomach

The stomach is a J-shaped organ located on the left side of the abdomen under the diaphragm. The stomach acts as the major reservoir of food and it can hold up to 1 L to 1.5 L of food. The stomach comprises of four main regions (as shown in **Figure 1.2).**

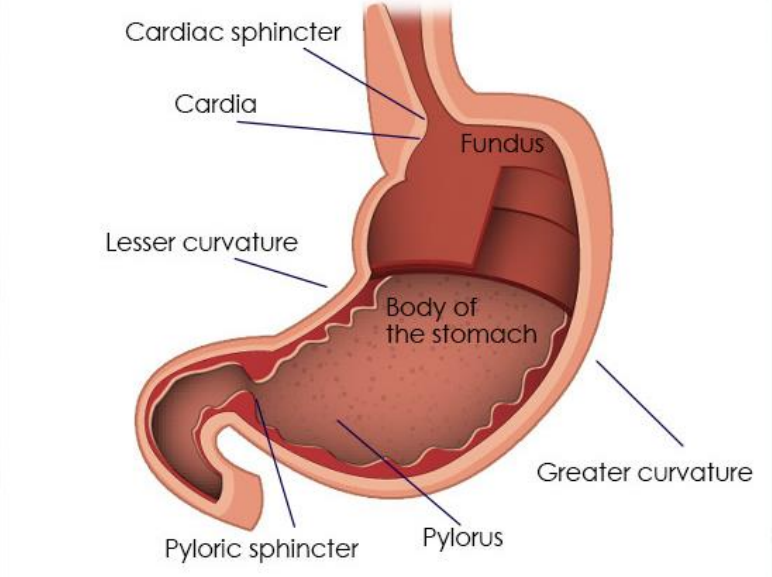

Figure 1.2: Parts of the human stomach

(http://www.buzzle.com/articles/understanding-the-human-stomach-anatomy-with-labeled-diagrams.html)

(i) The cardia region follows immediately after the gastro-esophageal sphincter receiving bolus, (ii) the fundus region lies next to the cardia, (iii) the body of the stomach is the large central region of the stomach; it primarily serves as the reservoir of bolus and is the main production site for gastric juice, and (iv) the pyloric portion which is the distal portion of the stomach **(Gropper et al., 2009)**. The pyloric portion provides strong peristaltic waves for grinding of food and gastric emptying. At this region, the food gets mixed with gastric juice and forms a partially digested thick semiliquid mass called chyme. The chyme passes through the pyloric sphincter, which is found at the juncture of the stomach and the small intestine **(Gropper et al., 2009).**

Gastric juice

Gastric juice secreted in the body of the stomach is comprised of water, electrolytes, enzymes, hydrochloric acid, mucus, and a glycoprotein called intrinsic factor. The main enzyme found in gastric juice is pepsin which hydrolyzes protein. Another enzyme present in gastric juice is gastric lipase which hydrolyzes short- and medium-chain triacylglycerols **(Gropper et al., 2009)**. The high concentration of hydrochloric acid present in the gastric juice is responsible for the low pH (~2) of the contents in the stomach. Mucus, secreted in the stomach, lubricates the chyme and also it coats and protects the inner walls of the stomach. The glycoprotein - intrinsic factor facilitates the absorption of vitamin B_{12} in the small intestine **(Gropper et al., 2009)**.

Regulation of gastric emptying

The movement in the walls of the stomach is generated by circular, longitudinal, and oblique smooth muscles of the stomach. Once the food reaches the stomach, its proximal portion relaxes to accommodate the ingested food. Peristaltic waves originate along the greater curvature of the stomach and migrate distally towards the pyloric sphincter, facilitating gastric emptying. Due to high rate of contractions in the pyloric region of the stomach the food gets liquefied to chyme. Food particles that have been disintegrated to a diameter of ~3 mm or less can pass through the pyloric sphincter into the small intestine. Following a meal, gastric emptying usually takes between 2 h to 6 h **(Gropper et al., 2009)**. Gastric emptying is influenced by physical factors such as volume, concentration, and composition of chyme. With respect to the composition of chyme, carbohydrate-rich and protein-rich foods were observed to have similar gastric emptying rate. High-fat foods tend to slower the gastric emptying rate **(Gropper et al., 2009)**. Gut motility and gastric emptying are regulated by different hormones, receptors, and peptides such as secretin, gastric inhibitory peptide (GIP), somatostatin, peptide YY (PYY), and enterogastrone. A large volume of chyme in the stomach increases the pressure on the stomach walls which promotes gastric emptying. If very concentrated (hypertonic) or much diluted (hypotonic) chyme enters the small intestine, a receptor called osmoreceptor gets activated. This receptor reduces the gastric emptying rate and facilitate the formation of isotonic chyme. Also, the exposure of nutrients or the low pH chyme to the small intestine triggers enterogastric reflex and peptides (GIP and PYY), which decrease or inhibit gastric motility **(Gropper et al., 2009; Patton and Thibodeau, 2016)**.

1.2.3. The small intestine

The small intestine is the main site for nutrient digestion and absorption. It is composed of three sections: the duodenum, jejunum, and ileum **(Figure 1.3).** The duodenum is the first 25 cm of the small intestine and it is shaped roughly like the letter C. The duodenum is followed by the jejunum and the jejunal portion continues for approximately the next 1.2 m. The final section – the ileum is approximately 1.8 m long **(Betts et al. 2013; Jamieson and Wong, 2006).**

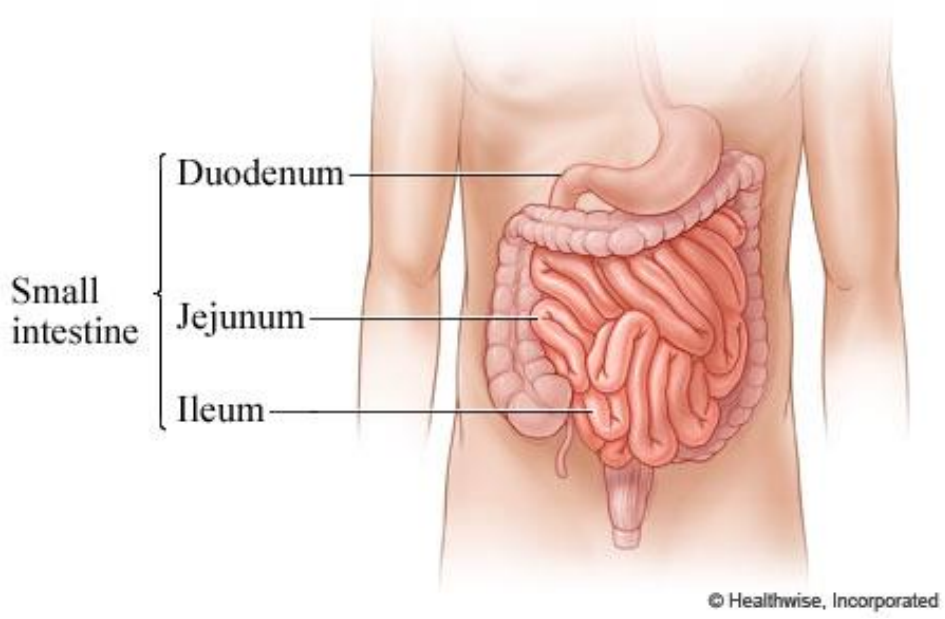

Figure 1.3: The small intestine

(http://www.webmd.com/digestive-disorders/small-intestine)

No clear demarcation between the jejunum and ileum can be seen. However there are clear differences between the proximal part of the jejunum and the distal part of the ileum, such as, wider lumen diameter (3 cm - 4 cm) to narrower lumen diameter (2.5 cm – 3.5 cm), prominent circular mucosal folds less intense, color (pink to white), less dense fat deposit in mesentery to denser, numerous villi to less villi, simple arcades to complicated arcade branches etc. **(Gropper et al., 2009; Patton and Thibodeau, 2016; Jamieson and Wong, 2006).**

The structure of the small intestine

Chyme moving from the stomach has an initial pH of about 2 because of the gastric acid. Mucus secreted from the mucosal lining of the small intestine protects the interior surface of the proximal end from the acidic chyme. The intestinal lining or mucosa has circular plicae (folds) that have many projections called villi **(Figure 1.4)**. Villi are fingerlike projections that project out in the lumen of the small intestine and consist of hundreds of epithelial cells, also called as enterocytes. Villi are present along with blood capillaries and a central lacteal (lymphatic vessel) for transport of nutrients out of epithelial cells **(Gropper et al., 2009)**. Each villus is about 1 mm in diameter. Microscopic view of epithelial cells on the surface of villi resembles a fine brush and hence called brush border. Each epithelial cell has about 1700 ultrafine microvilli. Each microvillus is about 1 μm in length and 0.1 μm in diameter. The presence of villi and microvilli increases the internal surface area of the small intestine (~200 m^2) by approximately 600 times. Thus making the small intestine the primary site of nutrient absorption **(Caspary, 1992)**. Most of the digestive enzymes produced by the intestinal mucosal cells are found along the brush

border and are called brush border enzymes. These enzymes hydrolyze already-partially digested carbohydrates and proteins. Between the villi, small pits or pockets are present and they are called crypts of Lieberkün. Cells and glands in the crypts of Lieberkün secrete intestinal juices and electrolytes to facilitate nutrient digestion **(Gropper et al., 2009)**.

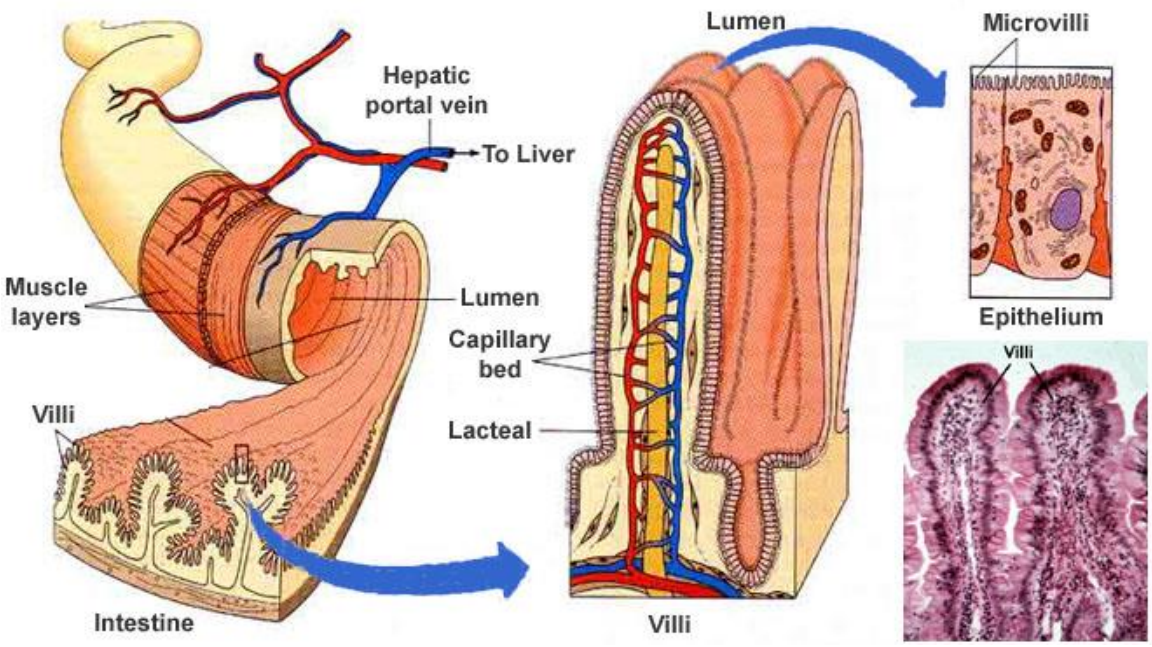

Figure 1.4: Villi in the small intestine

(http://www.daviddarling.info/encyclopedia/S/small_intestine.html)

Accessory organs

The three organs that facilitate the digestive and absorptive processes in the small intestine are the pancreas, liver, and gall bladder. The pancreas is a slender, elongated organ which lies between the stomach and the duodenum **(Figure 1.1)**. The pancreatic juice secreted by the pancreas contains bicarbonate (for neutralizing the acidic chyme), electrolytes, and pancreatic digestive enzymes. The enzymes released by the pancreas are responsible for digestion of approximately 50% of ingested carbohydrates, 50% of proteins, and almost 80% to 90% of ingested fat. One of the enzymes secreted by the pancreas, pancreatic α-amylase digests carbohydrates **(Gropper et al., 2009)**. Pancreas also secretes insulin, a peptide hormone which regulates the synthesis and storage of glucose, lipid, and protein. Insulin plays an important role in regulating blood glucose level. In the case of high blood glucose levels, insulin catalyzes the conversion of glucose to glycogen process, and stores glycogen in liver. If the blood glucose levels are low, insulin converts glycogen stored in liver back to glucose and stabilizes the glucose levels. The liver is the largest gland in the body which is found behind the greater curvature of the stomach **(Figure 1.1)**. The absorbed nutrients from the digestive tract get transported to the liver through the portal vein. Liver cells carry out many important steps in the metabolism of proteins, fats, and carbohydrates. Liver cells store components such as iron and vitamins A, B_{12}, and D **(Gropper et al., 2009; Patton and Thibodeau, 2016)**. The liver also produces bile, a yellowish brown fluid that aids the digestion and absorption of lipids in the small intestine. The gall bladder, a small organ located on the surface of the liver **(Figure 1.1)** concentrates and stores bile. Both pancreatic secretions and bile are emptied into the duodenum through different ducts **(Patton and Thibodeau, 2016)**.

Movements in the small intestine

The muscle coat of the small intestine is made of two smooth muscle layers: a thick inner layer of circumferentially oriented smooth muscle cells and a thin outer layer of longitudinally oriented muscle cells. The nervous system influences/regulates various contractions in these muscle layers for the mixing and movement of the chyme through the small intestine. The motility produced by smooth muscles is of two main types: peristalsis and segmentation. Peristalsis is progressive wavelike contractions that are primarily accomplished through the action of the circular muscles (**Figure 1.5A**).

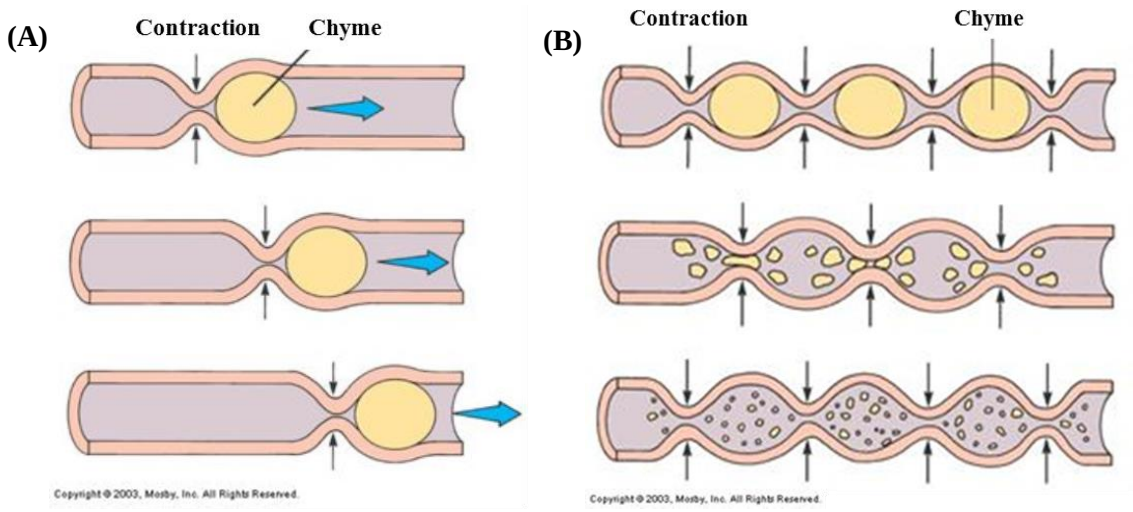

Figure 1.5: Movement of chyme in the gastrointestinal tract:

(A) Peristalsis and (B) Segmentation.

(http://slideplayer.com/slide/7068265/)

Segmentation movement can be described as a mixing movement. It causes a forward and backward movement within a single region or segment of the small intestine (**Figure 1.5B**). Segmentation movement is caused by the contractions of longitudinal smooth muscles. Segmentation movement is responsible for the mechanical breakdown of food particles, mixing of food and digestive juices, and it brings the digested food in contact with the intestinal wall to facilitate nutrient absorption **(Gropper et al., 2009)**. The unabsorbed chyme is distally pushed along the small intestine by peristaltic waves towards the large intestine. Chyme normally takes 3 h to 4 h to pass all the way through the small intestine **(Davis et al., 1986; Yuen, 2010; Billa et al., 2000; Coupe et al., 1991; Yuen et al., 1993).**

Regulation of intestinal motility and secretions

Similar to the regulation of gastric motility and gastric emptying, several hormones and peptides influence the gut motility and release of intestinal secretions. The presence of chyme and absorbed nutrients in the small intestine stimulate the hormones and peptides like cholecystokinin (CCK), neuropeptide P, and motilin, which positively influences the intestinal motility. On the other hand, peptide YY, secretin, and glucagon-like peptide (GLP) inhibit gut motility. A peptide named vasoactive intestinal peptide (VIP) has been shown to regulate intestinal secretions. Also, the distension of the stomach wall triggers gastro-ileal reflux, which causes peristalsis in the ileum and the opening of the ileocecal valve, the valve that separates the small intestine and the large intestine **(Gropper et al., 2009)**.

1.2.4. The large intestine

From the terminal section of the small intestine, unabsorbed materials pass into the cecum, the right side of the large intestine **(Figure 1.6)**. The components of the large intestine are ascending, transverse, descending, and sigmoid sections. The large intestine is almost 1.5 m long and is larger in diameter than the small intestine. The intestinal material entering the large intestine will be still in the fluid state. The intestinal contents are gently mixed and are allowed to stay in the ascending colon for a longer time to allow nutrients to be absorbed. The intestinal content can take 12 h to 70 h to pass through the large intestine and the unabsorbed materials are progressively dehydrated.

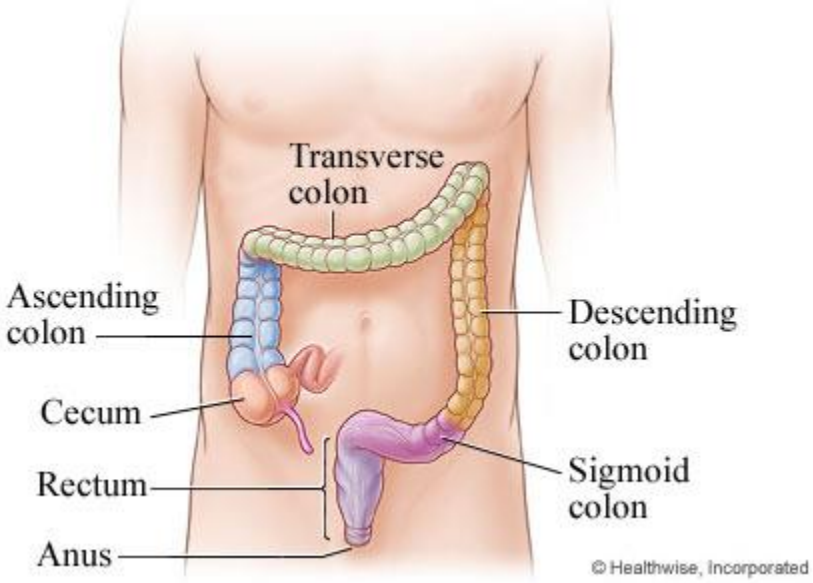

Figure 1.6: The large intestine

(http://www.webmd.com/digestive-disorders/large-intestine)

Each day, about 90% to 95% of water and sodium entering large intestine are absorbed. Typically, 1 L of intestinal content entering the large intestine each day is reduced to less than about 200 g of defecated material containing sloughed gastrointestinal cells, inorganic matter, water, small amounts of unabsorbed nutrients, unabsorbed food residues, constituents of digestive juices, and bacteria that are present in the gastrointestinal tract **(Gropper et al., 2009)**. The last 17 cm to 20 cm of the gastrointestinal tract is called the rectum. The terminal inch of the rectum is called the anal canal. The defecated material is eliminated from the body through this canal **(Patton and Thibodeau, 2016).**

1.3. Previous research

As discussed in previous sections, the human digestive tract evokes numerous signals regulating gastrointestinal motility and secretions which can directly influence food intake and available nutrients for absorption. Many studies have been conducted in the past to understand the influence of different food items on appetite regulation which in turn can reduce caloric intake. As discussed earlier, the passive over-consumption of calories (energy) is recognized as a major cause for the development of obesity **(Kopelman, 2000)**. According to **Pan and Hu (2011)**, many factors of food influence appetite regulation and subsequent functions of gastrointestinal tract. Some of these factors are palatability, macronutrient composition, cooking methods, food quality, portion size, energy content, energy density, form of the food either solid or liquid, physical properties (viscosity, texture), etc. To study and analyze the role of these factors on the human digestive process three different methodologies have been used, namely (1) *in vivo* feeding methods using

human volunteers, (2) *in vitro* gastrointestinal models, and (3) advanced computational software.

1.3.1. *In vivo* experimental procedure

Studies conducted with human volunteers by **Paddon-Jones et al. (2008), Potier et al. (2009),** and **Halton and Hu (2004)** showed that the macronutrient protein has the most satiating effect followed by carbohydrates; fat has the least satiating effect. Satiation refers to physiological processes that act to reduce or terminate consumption of a meal and the feeling of satisfaction associated with this **(Blundell, 1999; Maljaars et al., 2007)**. Consumption of food that can increase satiety and consequently reduce food intake may be beneficial in controlling body weight **(Clark and Slavin, 2013)**. A two-year long clinical trial with 811 overweight adults was conducted to compare the satiating effect of diets with different compositions of fat, protein, and carbohydrate. This study did not find any significant differences in satiation generated with respect to the macronutrient composition **(Sacks et al., 2009)**. Fiber is a major component of a carbohydrate-based diet and is considered beneficial for health. Epidemiological studies show that intake of dietary fiber and whole grains reduces the risk of overweight and obesity. A possible reason for this could be the satiation generated by the fiber-rich diet **(Howarth et al., 2001; Liu et al., 2003; Slavin and Green, 2007; Williams et al., 2008; Kristensen et al., 2010)**. In a study conducted by **Tighe et al**. **(2010)**, 233 healthy volunteers were monitored for a period of 12 weeks with their diets including three different portions of whole grains. This study did not find any significant difference in the participant's energy intake and body weight with respect to the different whole grains diet plans. From these studies, it can be concluded that

factors other than the macronutrient composition and fiber-rich diet may also influence the caloric intake process. In general, *in vivo* feeding studies with humans provide the most accurate results. However, these procedures are time-consuming and expensive. To overcome these challenges, research has been carried out to develop reliable *in vitro* experimental procedures **(Boisen and Eggum, 1991)**.

1.3.2. *In vitro* experimental procedure

Ideally, *in vitro* experimental procedures can be a useful alternative to human models by rapidly screening food materials and could provide accurate results **(Coles et al., 2005)**. *In vitro* methods are not limited by ethical constraints and do not need Institutional Review Boards (IRB) approvals. They avoid biological variations among subjects and allow manipulation of experimental conditions **(Minekus et al., 1995)**. In spite of this, none of these methods has yet been widely accepted **(Hur et al., 2011)**. According to **Coles et al. (2005)**, due to the inherent complexity of the digestive process, the accuracy of *in vitro* method is incomparable to that of an *in vivo* study and some compromise is needed between the accuracy of the results and the effort in developing and operating an *in vitro* model.

In the past few years, food scientists and animal scientists have developed and used many *in vitro* digestion models to study the structural and chemical changes that a food undergoes under simulated gastrointestinal conditions **(Hur et al., 2011)**. According to a survey conducted by **Hur et al. (2011)**, from the year 2000 to 2010, the predominant food samples tested by *in vitro* digestive models were plant-based food products, such as starch,

tea, rice, or bread (45%), meats (18%), dairy foods (9%), marine foods (9%), and emulsions (9%). Based on this survey, the important differences in these *in vitro* digestive studies were the food component being analyzed, the nature of the food matrix, and the sophistication of the *in vitro* digestion model used. Also, *in vitro* digestive models used in these studies primarily differed from one another in their procedure, such as the number of steps included in the digestion process from mouth to large intestine, the composition of digestive fluids used in each step such as enzymes and buffers, and the geometries used, applied mechanical stresses, and fluid flows generated **(Hur et al., 2011)**.

Research conducted by **Kong et al. (2011)**, used a dynamic stomach model to study the effect of structural differences in white and brown rice on gastric digestion. According to that research, properties of brown rice, namely larger particle size, high viscosity, low water absorption capacity, reduced the rates of gastric emptying and starch digestion (**Kong et al., 2011)**. A small intestinal *in vitro* model that consists of an inner porous flexible membrane and an outer flexible tube was developed by **Tharakan et al. (2010)**, to study the effect of intestinal content viscosity on transport phenomena and mass transfer of the nutrient molecule, riboflavin (vitamin B2). The results of this research showed that the addition of guar gum to the system significantly decreased the mass transfer coefficient. Also, when starch was used as the food system, an increase in intestinal content viscosity significantly decreased glucose absorption **(Tharakan et al., 2010)**. However, their study was conducted at room temperature (22 °C) and not at the physiological body temperature (37 °C) and also the *in vitro* model developed by them was not validated with the human digestive process **(Tharakan et al., 2010)**.

1.3.2.1. The TIM-1 system

One of the commercially available *in vitro* gastrointestinal models was developed by The Netherlands Organization (TNO) and is called as TNO's intestinal model or TIM. According to **Guerra et al. (2012)**, the TIM system is considered as the most advanced *in vitro* digestive model. The main advantages of the TIM system are its accuracy, reproducibility, and that it allows to collect samples at any level of the gastrointestinal tract and at any time period during digestion **(Etienne-Mesmin et al., 2011)**.

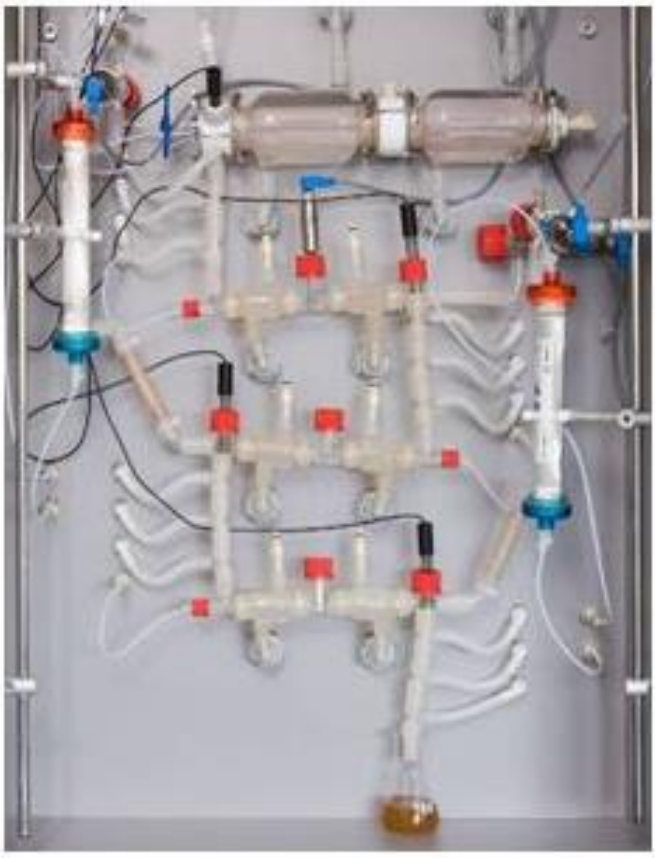

Figure 1.7: Front panel of the TIM-1 system

(http://botanical.pbrc.edu/cores_botanical.html)

The TIM comprises of two different systems TIM-1 and TIM-2. The TIM-1 system **(Figure 1.7)** represents the human upper digestive system - stomach and small intestine (duodenum, jejunum, and ileum). The TIM-1 system is a very sophisticated model because it simulates many parameters of the human digestive system namely, body temperature, gastrointestinal transit times, peristalsis, churning, the flow of saliva, gastric and pancreatic juices including digestive enzymes and bile, and regulation of gastric and intestinal pH, etc. **(Minekus et al., 1995; Etcheverry et al., 2012)**. The functionalities of the TIM-1 system are discussed in detail in section 3.3. Low molecular compounds in the small intestinal section are removed continuously through dialysis or filtrate membrane systems and they represent the bioaccessible fraction. The material that exits the system represents the non-bioaccessible fraction and is used to study colonic fermentation products in the TIM-2 system which represents the human large intestine **(Anson et al., 2009)**. Previous studies conducted with the TIM-1 system concluded that the slower gastric emptying rate and prolonged intestinal transit time improves nutrient (iron and calcium) absorption **(Salovaara et al., 2003; Smeets-Peeters et al., 1999)**.

1.3.3. Mathematical modeling

To completely understand and predict the process of food digestion it is important to understand the fluid dynamics and transport of the food at all sites of the gastrointestinal tract **(Lentle and Janssen, 2010; Schulze, 2006)**. Though the advanced mapping techniques and real-time imaging tools have been used for characterizing *in vivo* fluid dynamic behavior, their capabilities are limited (**Schulze, 2006)**. Since peristalsis is the common mechanism of transport of the gastrointestinal contents, analytical solutions of

peristaltic flows can be solved to characterize the fluid dynamics of the gastrointestinal content **(Ferrua and Singh, 2013)**. However, these analytical models could not accurately incorporate the complex geometry and functionality of the GI tract **(Pozrikidis, 1987; Taghipoor 2014; Moxon et al., 2016)**. In recent years, the use of computational fluid dynamics (CFD) techniques has been a unique and promising approach to characterize and model the fluid dynamics in the human digestive process **(Schulze, 2006)**. The possibility of numerically analyzing the dynamics of food in the human gastrointestinal tract can enhance the understanding of the human digestive process.

Pal et al. (2004) modeled gastric flow and mixing using the Lattice-Boltzmann method and MRI data. In this study, a 2D model of the stomach geometry was developed to analyze the gastric flow behavior by simplifying the gut motility and the gastric emptying rate. Based on the **Pal et al. (2004)** research, **Singh (2007)** developed a 3D mathematical model of the human stomach to study the effect of gastric motility on the dynamics of a water-like fluid during digestion. The results of this study indicated that the viscosity of the fluid had a significant effect on the gastric flow behavior. **Ferrua and Singh (2010)** used computational fluid dynamics (CFD) to develop a 3D model of the stomach geometry during digestion as shown in **Figure 1.8**. They observed that the flow field behavior within the pyloric region of the stomach was significantly affected by the rheological properties of the fluid. The authors extended their work to investigate the effect of viscosity of gastric fluids on the intragastric distribution of a series of discrete particles of food **(Ferrua and Singh, 2011)**. As expected, the rate of gastric emptying decreased with an increase in the viscosity. The velocity field predicted by this model was in a good

agreement with experimental data obtained from an *in vivo* stomach model in which the velocity field was quantified using a non-intrusive particle image velocimetry **(Ferrua and Singh, 2011)**.

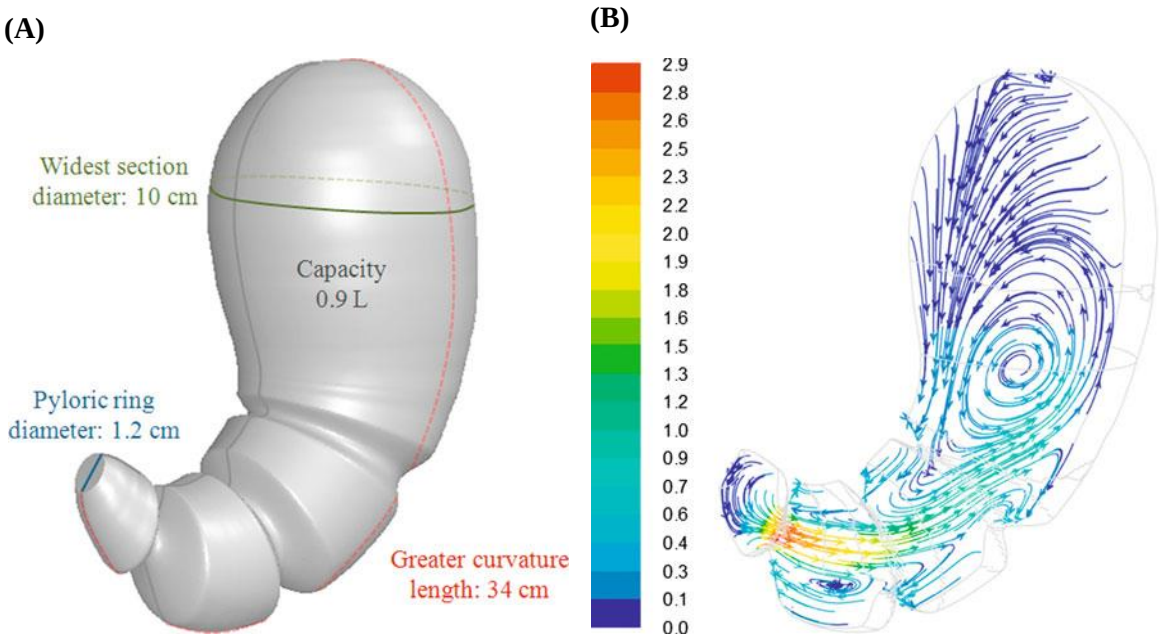

Figure 1.8: (A) 3D model of a human stomach and (B) Instantaneous streamlines of a water-like fluid flow within the 3D model developed by Ferrua and Singh (2010), colored by velocity magnitude (cm/s)

Tharakan et al. (2010) reported that more mathematical models have been developed to study drug release and drug absorption in the small intestine than to analyze food digestion and nutrient uptake. The small intestinal slow wave activity was first simulated by **Lin et al. (2006)**. They developed an anatomically based cylindrical model to analyze the velocity field throughout the small intestine and the results were validated with the experimental data obtained from the canine small intestine. **Tharakan (2008)**

developed a 2D axisymmetric model of length 0.25 m and radius 0.015 m, approximating a section of the small intestine and discussed the effect of fluid viscosity on average velocity and shear rate developed within the system. **Brasseur et al. (2009)** developed a 2D model approximating the human small intestine using the Lattice-Boltzmann framework to study the contribution of peristaltic and segmental contractions on transport, mixing, absorption of chyme in the small intestine. They found that the rate of peristaltic motion negatively influenced the nutrient absorption, whereas the segmentation movement enhanced nutrient absorption. **Hari et al. (2012)** developed a 2D axisymmetric model of the human duodenum with the flow of chyme induced by peristaltic motions on the wall. They incorporated starch hydrolysis reaction to the model to observe the flux of resulted glucose through the duodenum wall. The results obtained from this model are yet to be validated with experimental data. Although more work needs to be done for accurately predicting the intestinal flow dynamics and nutrient absorption, these previous work highlight the possibility of using CFD to understand the physics behind them.

1.4. Viscosity of gastrointestinal content

As discussed in the last section, research related to the human digestive process shows that the viscosity of the gastrointestinal content significantly affects the fluid flow, mixing, particle distribution, and nutrient absorption in the gastrointestinal tract. To completely understand the effect of the viscosity of food on the results of these processes, it is imperative to track the viscosity changes of gastrointestinal content during digestion. **Villemejane et al. (2015)** monitored the changes in gastrointestinal content viscosity during *in vitro* digestion of short-dough biscuits in the TIM-1 system. During the digestion

process, these researchers periodically collected samples from different compartments of the TIM-1 system (stomach, duodenum, jejunum, and ileum). Using a dynamic rheometer, they measured the viscosity of the collected samples. However, collecting samples from the gastric and intestinal sections of the TIM-1 system, in the middle of the experiment, would disrupt the equilibrium of the experimental run. To overcome this challenge, a 'non-invasive' and 'non-disruptive' method should be used to monitor the viscosity changes during *in vitro* digestion. One such technique is the usage of an optical 'generally recognizes-as-safe (GRAS)' chromophore, which based on molecular rotor principle, emits fluorescence with respect to the local viscosity of the surrounding medium **(Du et al., 2014)**. Molecules that consist of two or more parts that can rotate easily relative to each other are called molecular rotors **(Kottas et al., 2005)**. The structure of one of the molecular rotors, Azorubine, is shown in **Figure 1.9**. The red color arrow in the figure indicates the possible intramolecular rotation spot and the chemical structure at that spot is represented by N=N **(Kashi et al., 2015)**.

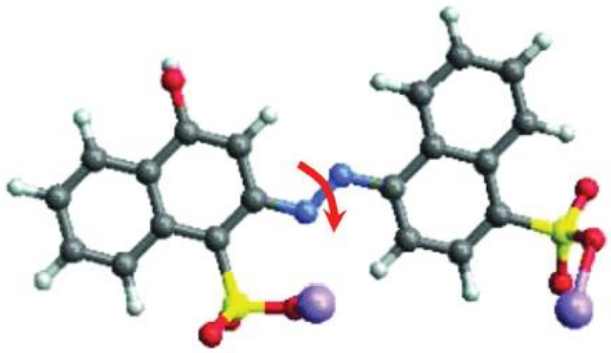

Figure 1.9: Structure and possible intramolecular rotation in Azorubine (Kashi et al., 2015)

When molecular rotors are photoexcited, they get excited to either local singlet state or twisted intramolecular charge transfer state (TICT), depending on the extent of rotation of one of the parts of the molecule with respect to the other **(Du et al., 2014; Uzhinov et al., 2011).** Deactivation from the local singlet state occurs radiatively and deactivation from the TICT state occurs predominantly through a non-radiative pathway. In a high viscous environment **(Figure 1.10A)**, the rate of molecular rotation (the rate of TICT state formation) is lower which results in a radiative decay. In a low viscous environment **(Figure 1.10B)**, the molecule undergoes faster internal rotation and thus decays without any radiation. These two competing decay pathways help in determining the local viscosity of the surrounding environment. The radiative decay results in a photon emission which could be observed using appropriate instrumentation **(Uzhinov et al., 2011; Du et al., 2014)**. In the past, researchers have correlated the changes in emission properties of molecular rotor molecules, such as fluorescence quantum yield, intensity, and lifetime, to the local and bulk viscosity of the medium **(Turro, et al., 2010; Corradini and Ludescher, 2015; AlHasawai et al., 2018)**. Some of the commonly used molecular rotor compounds to analyze the local and bulk viscosity of a medium are Allura red and Fast Green **(Corradini and Ludescher, 2015)**. Based on the results of **Kashi et al. (2015)**, the molecular rotor property of these compounds is highly sensitive to the changes in the viscosity of glycerol-water mixture than its alternatives like sucrose-water mixture, methylcellulose (MC), carboxymethyl cellulose (CMC). **Corradini and Ludescher (2015)** reported that the compound Fast Green is more sensitive than Allura red for monitoring viscosity changes during digestive studies using an *in vitro* gastrointestinal model.

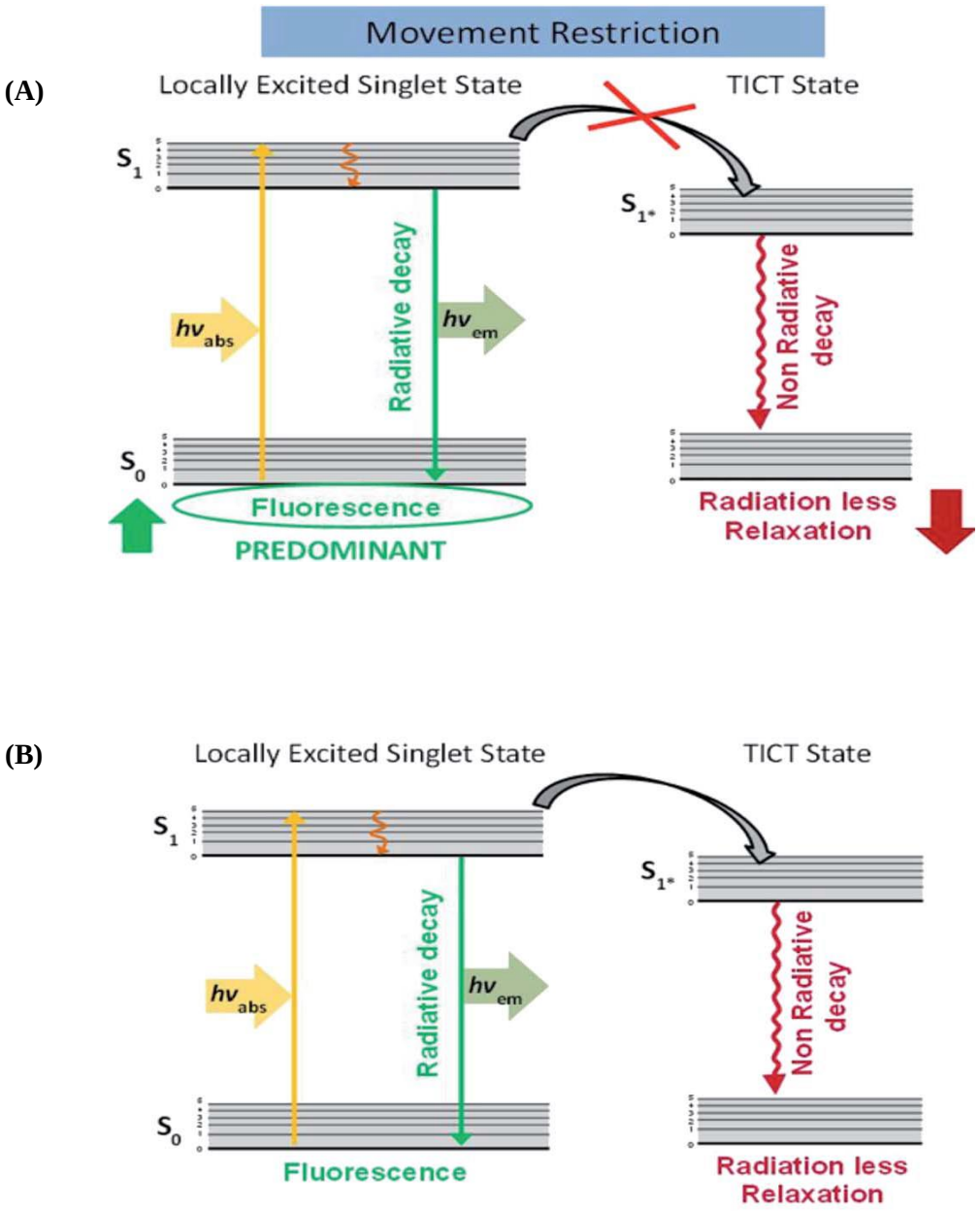

Figure 1.10: Jablonski diagram of a single emission band molecular rotor - (A) Restriction of the twisted state increases radiative fluorescence emission and (B) Relaxation from the TICT state occurs without fluorescence emission.

(**Du et al., 2014** adapted it from **Haidekker and Theodorakis, 2010**)

1.5. Carbohydrates

In the average human diet, carbohydrate is the major source of energy fuel. Carbohydrates are polyhydroxy aldehydes or ketones and are constructed from the atoms of carbon, oxygen, and hydrogen. Carbohydrates can be classified into two major classes, namely, simple carbohydrates and complex carbohydrates. Simple carbohydrates include monosaccharides (1 saccharide unit) and disaccharides (2 saccharide units). Complex carbohydrates include oligosaccharides which contain 3 to 10 saccharide units, and polysaccharides which contain more than 10 saccharide units. Carbohydrates supply half or more of the total caloric intake. Approximately half of the dietary carbohydrate is in the form of polysaccharides such as starches and dextrins, derived majorly from cereal grains and vegetables. Starch is an easily accessible form of energy when compared to glycogen which is also a type of polysaccharides but found in certain animal tissues. Dietary carbohydrates sources also include simple sugars such as sucrose, lactose, which are disaccharides. Monosaccharides are not commonly present in the diet in significant quantities; however free glucose and fructose are present in honey, certain fruits, and the high fructose corn syrup fortified processed food products **(Gropper et al., 2009)**. Other forms of carbohydrates include the non-starch polysaccharides (NSP), such as pectin, inulin, hemicelluloses, and food gums (guar, locust bean, gum arabic, agar). This form of carbohydrates resists digestion in the small intestine by influencing the rheology of gastrointestinal content and compromising mixing. These substances may undergo microbial digestion in the large intestine **(Lentle and Janssen, 2011)**.

1.5.1. Polysaccharides

Starch, the most common digestible polysaccharides in plants, can exist in two forms: amylose and amylopectin. They both are polymers of D-glucose units. Glucose is a six-carbon monosaccharide with an aldehyde functional group, hence also called as an aldohexose. The chemical formula of glucose is $C_6H_{12}O_6$. Based on the optical activity, a D-glucose solution can rotate a plane polarized light passing through it, to the right side, hence called as D-glucose (dextrorotatory configuration). On the other hand, levorotatory configuration, L-glucose can rotate the plane polarized light passing through it to the left side. A D-glucose compound exists naturally in dietary carbohydrate and is metabolized in the same D-form. Hence, D-glucose is more nutritionally important than L-glucose.

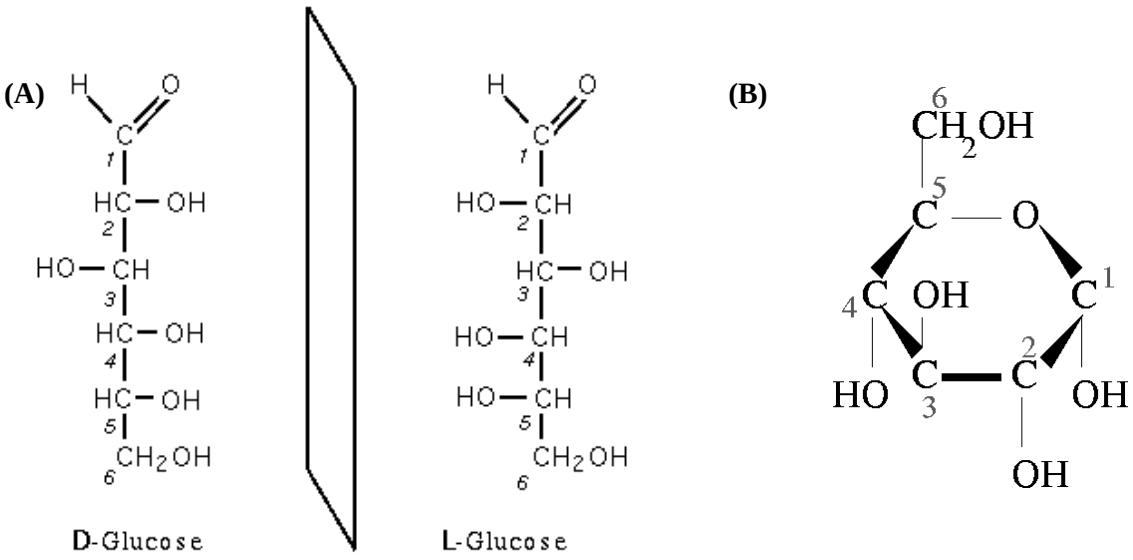

Figure 1.11: (A) Open chain models of the D and L forms of glucose and (B) Cyclic structure of the D-glucose

(https://commons.wikimedia.org/wiki/File:D_et_l_glucose.png)

(https://commons.wikimedia.org/wiki/File:Alpha-d-glucose.png)

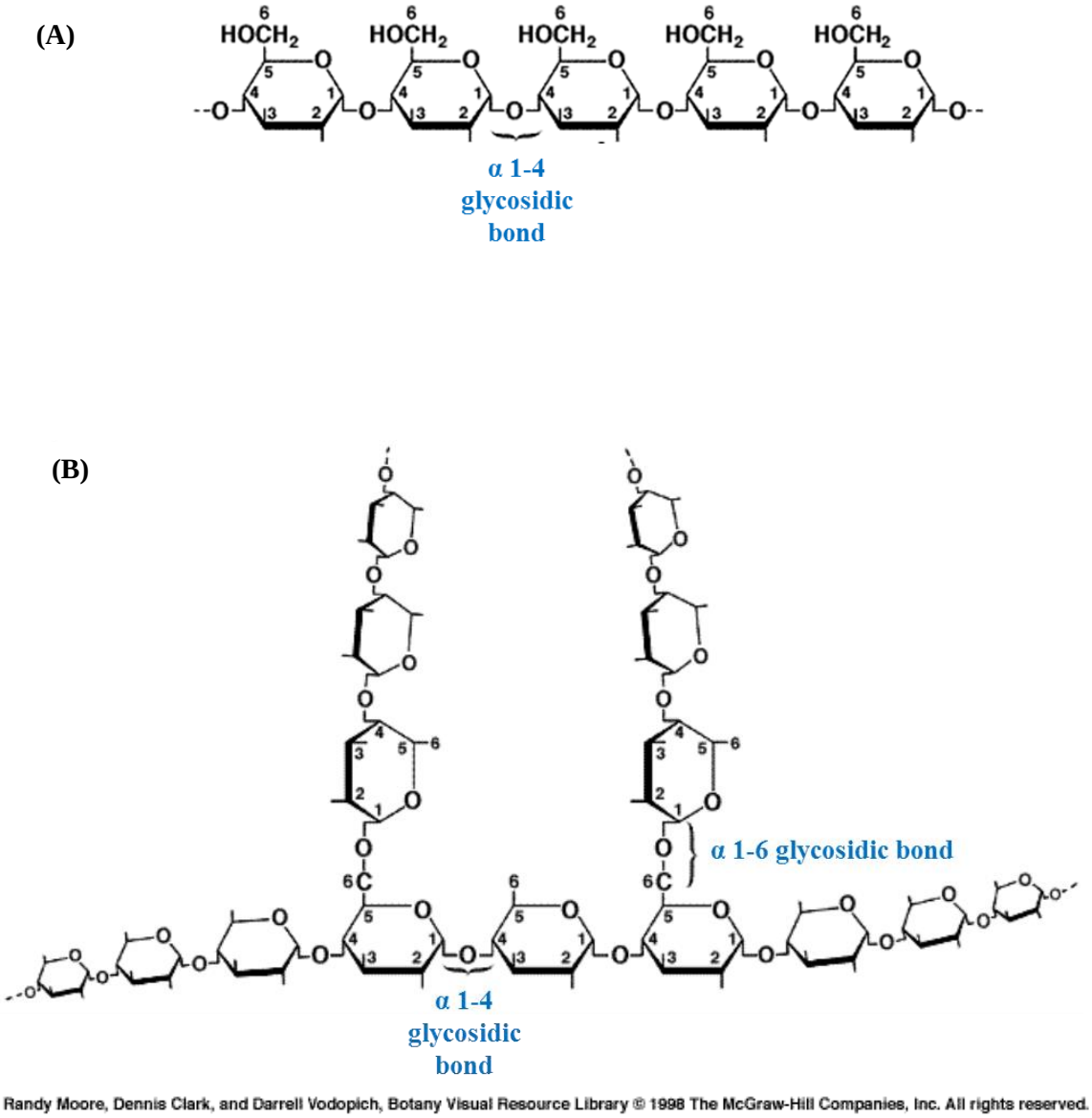

Figure 1.12: Structures of (A) amylose and (B) amylopectin

(https://biochemable.wordpress.com/2013/03/18/deeper-into-starches-we-go/)

Figure 1.11A shows the D- and L- form of glucose as open-chain models. In liquid solutions, the monosaccharides do not exist in an open-chain form. Instead, the molecules cyclize by a reaction between the carbonyl group (aldehyde) and the hydroxyl group to form a cyclic structure. The cyclic structure of D-glucose is given in **Figure 1.11B (Gropper et al., 2009)**. The structures of amylose and amylopectin are shown in **Figure 1.12**. The amylose molecule is a linear, unbranched chain of D-glucose molecules, which are attached only through α-(1→4) glycosidic bonds. On the other hand, amylopectin is a branched chain polymer. It has both α-(1→4) glycosidic bonds and α-(1→6) glycosidic bonds, with branch points occurring through α-(1→6) glycosidic bonds **(Gropper et al., 2009)**.

1.5.2. Digestion of polysaccharides

The summary of the digestion of polysaccharides is shown in **Figure 1.13**. A polysaccharides digestion starts in the mouth. The enzyme salivary α-amylase specifically hydrolyzes α-(1→4) glycosidic bonds. The α-(1→6) bonds of the amylopectin are resistant to this enzyme. After the short period of stay in the mouth, once the food reaches the stomach, the enzymatic activity continues for some time until the gastric acid lowers the pH of the gastric content (~2) sufficient enough to inactivate the salivary enzyme. By this point, amylose and amylopectin have been partially hydrolyzed to dextrins which are short chain polysaccharides and maltose **(Gropper et al., 2009)**. Further digestion of the dextrins is resumed in the small intestine by the enzyme pancreatic α-amylase which is secreted in the duodenum. Secretion of bicarbonate in the duodenum elevates the pH (~6) to a favorable condition for amylase enzyme activity.

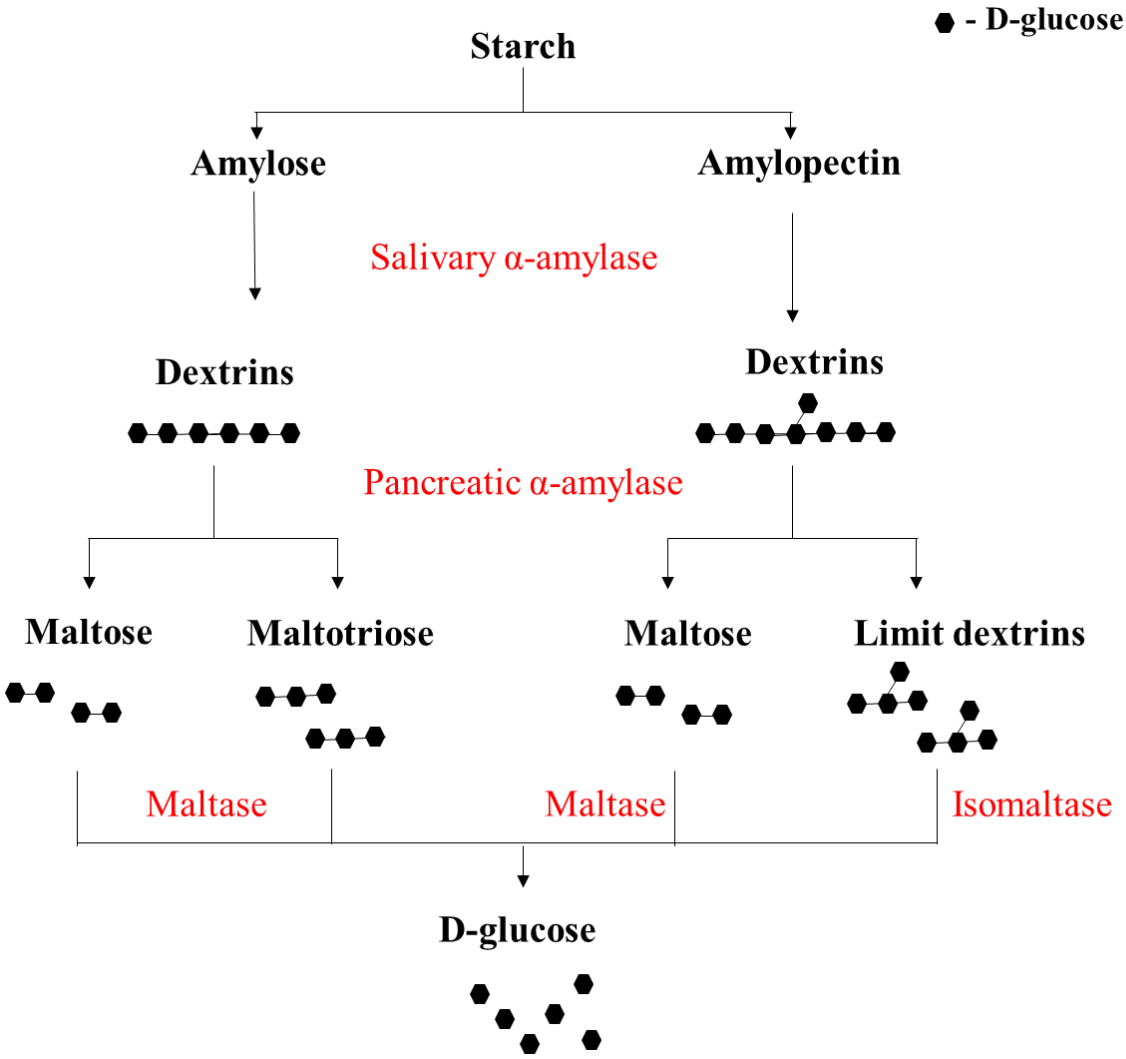

Figure 1.13: Digestion of starch

(Adapted from **Gropper et al., 2009**)

If the dietary polysaccharide is unbranched amylose, the product of pancreatic α-amylase hydrolysis is maltose and maltotriose (trisaccharide). In the case of the branched amylopectin, the pancreatic α-amylase hydrolysis results in maltose, isomaltose (α-(1→6) linked disaccharide) and limit dextrin (branched short chain dextrins). As mentioned earlier, the α-(1→6) glycosidic bonds are resistant to the α-amylase enzyme, even in the small intestine. The disaccharides and limit dextrins are further digested to glucose in the microvilli, by the brush border enzymes namely maltase and isomaltase (α-dextrinase). The enzyme maltase hydrolyzes maltose and maltotriose to 2 and 3 D-glucose units, respectively. The enzyme isomaltase can cleave α-(1→6) glycosidic bonds. In summary, nearly all dietary polysaccharides are hydrolyzed completely by specific enzymes to their constituent monosaccharide units, in the small intestine **(Gropper et al., 2009)**.

1.5.3. Glucose absorption

D-glucose molecules are absorbed from the intestinal content into the walls of the small intestine by active transport, as explained in **Figure 1.14**. Active transport is one of the modes of nutrient transport that requires energy and the involvement of a specific carrier. A protein complex present in the microvilli of the small intestine called sodium-glucose transporter 1 (SGLT1) is the designated carrier of the D-glucose molecule. This carrier transports glucose into the epithelial cells. This transporter is also called as a symporter because for each glucose molecule two sodium ions are transported into the mucosal cell at the same time. A glucose molecule cannot attach to the carrier until the carrier has been preloaded with sodium ions. To maintain a concentration gradient of sodium ions between the intestinal lumen and epithelial cells, sodium ions are transported

outside the epithelial cells into the bloodstream using the Na+/K+-ATPase pump. At the expense of ATP, this pump transports two potassium ions in the opposite direction for every three sodium ions transport. Glucose molecules are transported outside the epithelial cells into the bloodstream using a facilitated carrier called glucose transporter 2 (GLUT2) **(Gropper et al., 2009)**.

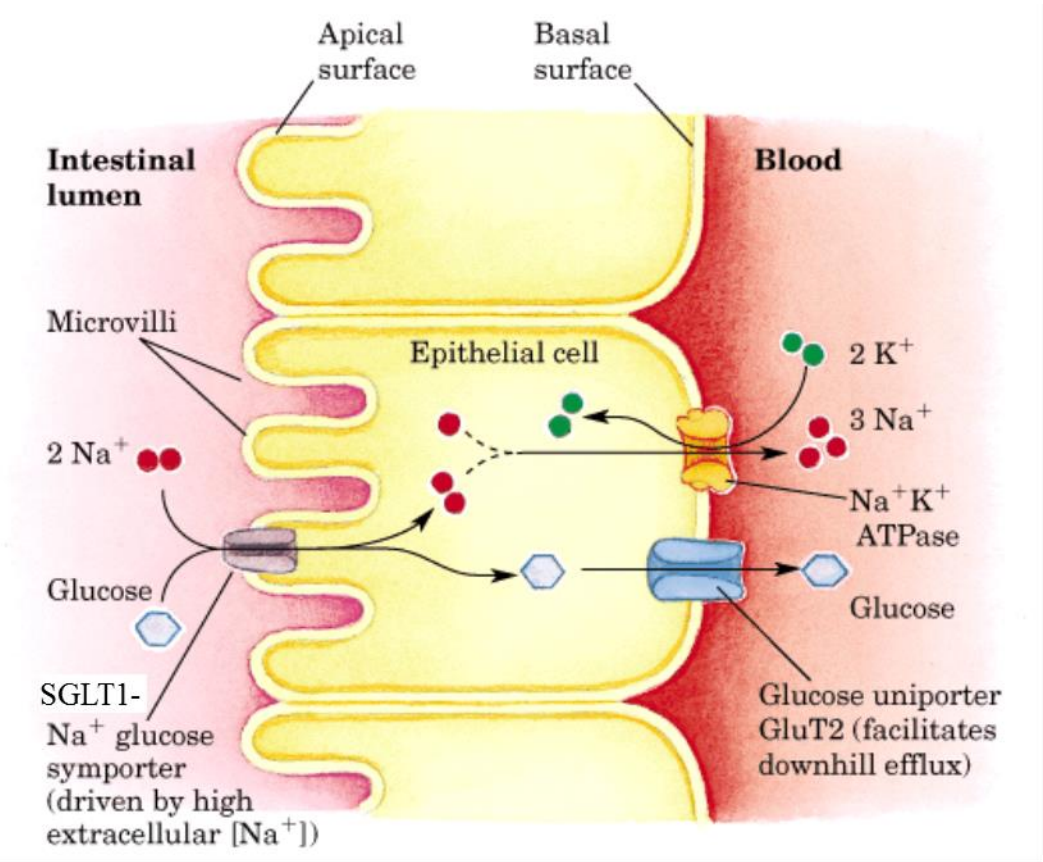

Figure 1.14: Active transport of glucose through the small intestine

(http://web.ics.purdue.edu/~smills/ANSC230/Digestive%20Physiology/Absorption.html)

The rate at which glucose is absorbed from the intestinal tract is an important parameter influencing blood glucose concentration, insulin release, obesity, and possibly weight loss. Elevated blood glucose concentration can lead to the development of chronic diseases and obesity. **Wachters-Hagedoorn et al. (2006)** reported that the rate of glucose absorption in the bloodstream as 181.7 mmol/(L·2 h) ± 40.1 mmol/(L·2 h) when 7 healthy men ingested 55 g of glucose. The glucose absorption rate was quantified by analyzing blood samples collected periodically from the volunteers for the first two hours after the ingestion of food. When the volunteers ingested uncooked corn starch (53.5 g) and corn pasta (50.4 g), the blood glucose absorption rate dropped to 74.7 mmol/(L·2 h) ± 21.1 mmol/(L·2 h) and 65.3 mmol/(L·2 h) ± 17.3 mmol/(L·2 h), respectively **(Wachters-Hagedoorn et al., 2006)**. The rate of glucose absorption was observed to be affected by the available glucose, gastric emptying rate, and the extent of digestion.

1.5.4. Glycemic response

The extent of carbohydrate-based food item's influence on blood glucose concentration is categorized using a term called glycemic index. According to **Gropper et al (2009)**, the glycemic index is defined as "the increase in blood glucose level over the baseline level during a 2 h period following the consumption of a defined amount of carbohydrate (usually 50 g) compared with the same amount of carbohydrate in a reference food." Pure glucose or white bread can be used as the reference food and their glycemic index value is assigned as 100. In practice, the glycemic index value of a given food product is determined by monitoring the blood glucose levels of healthy human volunteers for 2 h following the ingestion of that particular food. The area under the curve of the blood

glucose level of the given food divided by the area under the curve of the blood glucose level of the reference food gives the glycemic index value of the given food **(Figure 1.15) (Gropper et al., 2009)**.

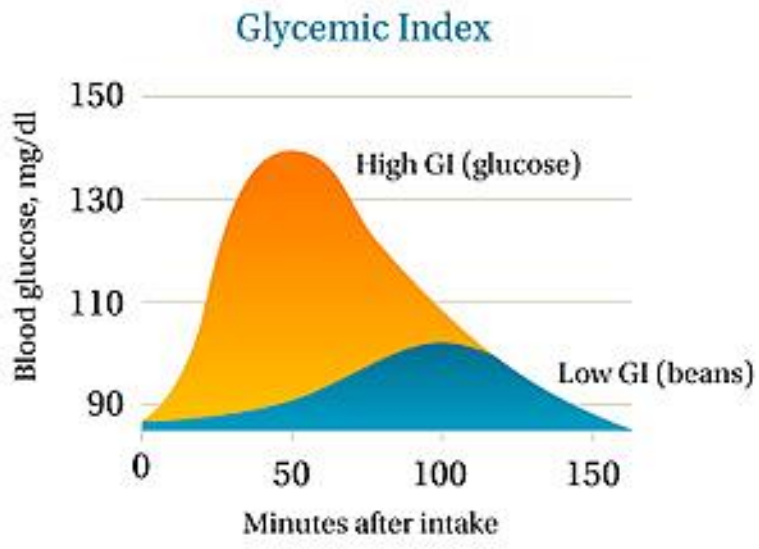

Figure 1.15: Representation of Blood glucose level of glucose and beans after consumption

(http://www.weightlossforall.com/gly-index.htm)

Table 1.1 provides glycemic indices of selected food items **(Foster-Powell et al., 2002)**. Glycemic index refers to the carbohydrate quality of the food. Whereas, Glycemic Load considers both the quality and the quantity of the carbohydrate in a meal. The glycemic load of a given food is calculated by multiplying its glycemic index with the grams of carbohydrate in a serving of that food. For example, boiled white rice has 43 g of carbohydrates per serving (150 g). Based on its glycemic index (~69), the glycemic load of boiled white rice was calculated to be 30/serving. On the other hand, boiled brown rice has 33 g of carbohydrates per serving (150 g). Based on its glycemic index (~50), the

glycemic load of boiled brown rice is 16/serving. In cases like watermelon, even if the glycemic index is as high as 72, the low available carbohydrates (6 g) per serving (120 g) can lead to a low glycemic load of 4/serving **(Foster-Powell et al., 2002)**. Researchers have found that the long-term consumption of a diet with a relatively high glycemic load is associated with an increased risk of type 2 diabetes and coronary heart diseases **(Gropper et al., 2009; Liu et al., 2000)**.

Table 1.1: Glycemic index of selected food items with glucose as the reference food (Foster-Powell et al., 2002)

Food	Glycemic index
White bread (USA)	70
Coca cola (USA)	63
Boiled white rice (India)	69 ± 15
Boiled brown rice (India)	50 ± 19
Watermelon, raw (Australia)	72 ± 13
Green lentils, dried, boiled (Canada)	22
Sucrose	58
Maltose	105 ± 12

2. INTRODUCTION TO THE RESEARCH

2.1. Justification of the research

As discussed in the previous section **(Section 1.3)**, many studies have been conducted in the past to understand the influence of different food products, based on composition and physical form, on inducing caloric intake reduction. From these studies, it could be inferred that viscosity plays a significant role in affecting the residence time of gastrointestinal content in the digestive tract as well as the amount of nutrients available for absorption. High-viscous gastric content (bolus) would lower the gastric emptying rate, which would lead to delayed exposure of nutrients to the small intestine. In contrast, low-viscous intestinal content would assist the interaction between food and enzyme, increase the diffusivity of nutrients in the intestinal content (chyme), and enhance the nutrient absorption by the small intestinal walls. A comprehensive study on the effects of viscosity on the residence time of the food in the digestive tract, the rates of digestion, nutrient release, and absorption, can potentially provide useful information for engineering food products that can reduce caloric absorption and nutrient intake rates. On the other hand, the complex geometry and motility in the human gastrointestinal tract impose challenges in characterizing the local gastrointestinal fluid behavior and the nutrient absorption process. Analyzing the fluid dynamics of gastrointestinal content during digestion of a given food, is an important element to understand and model the digestive and nutrient absorption processes. In the past, researchers have been successful to an extent in analyzing the flow behavior in the human stomach through numerical simulation. With respect to the human small intestine, many researchers have developed CFD based models to simulate fluid flow

induced by gut motility. They have studied the effect of peristaltic motion and rheology of intestinal content on the flow behavior. However, incorporating digestion and nutrient processes to these fluid flow models are still in the preliminary stage. This dissertation research proposed to address some of the experimental and numerical procedure limitations by analyzing carbohydrate digestion and glucose absorption processes in a human small intestine using *in vitro* experimental procedure and by subsequently developing a mathematical model to simulate and predict these processes.

2.2. Objectives of the research

This study includes both an *in vitro* experimental procedure and numerical simulation. The aim of *in vitro* experimental procedure was to investigate the influences of bolus (gastric content) viscosity on the carbohydrate digestion process and the rate of glucose absorption in the small intestine, using an *in vitro* gastrointestinal model, the TIM-1 system. The aim of numerical simulation procedure was to develop a fluid flow-based computational model mimicking the human small intestine to predict the glucose absorption process during carbohydrate digestion. The specific objectives of this study were:

A: *In vitro* experimental procedure

1. To experimentally analyze different glucose-based food systems to evaluate the effect of bolus viscosity on the glucose absorption process in the TIM-1 system.
2. To experimentally analyze different maltodextrin-based food systems and evaluate the effect of bolus viscosity on the digestive process in the TIM-1 system.

3. To develop an experimental procedure based on molecular rotor principle to monitor viscosity changes of the gastrointestinal content during digestion in the TIM-1 system.

B: Numerical simulation

4. To develop a fluid flow numerical model mimicking the human small intestine with flow induced by peristaltic waves.
5. To incorporate carbohydrate digestion kinetics and diffusion physics to the fluid flow model and simulate the nutrient absorption process.
6. To experimentally validate and improve the numerical model for accurate prediction of the human digestive process.

3. MATERIALS AND METHODS

3A. *In vitro* experimental procedure

3.1. Food composition

Two different types of simple carbohydrates, namely glucose (Product code: D9439, Sigma-Aldrich) and maltodextrin (Product code: 419699, Sigma-Aldrich), were used as the food base. Glucose is a monosaccharide and maltodextrin is a readily digestible starch. Maltodextrin is a polysaccharide produced by partial hydrolysis of starch and they can be metabolized in a similar way to starch **(Kennedy et al., 1995)**. It consists of D-glucose units linked primarily by α-(1→4) glycosidic linkages with a general formula of $(C_6H_{10}O_5)_n$. **Figure 3.1** shows the chemical structure of maltodextrin.

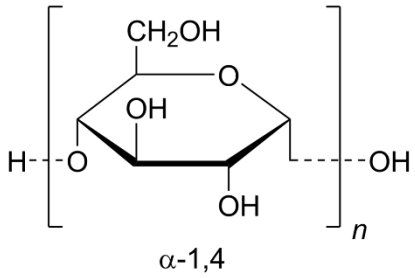

Figure 3.1: Chemical structure of maltodextrin

Maltodextrin can be classified on the basis of dextrose equivalent (DE) and the degree of polymerization (DP). DE is defined as the percentage of reducing sugar (containing a free aldehyde group) in the carbohydrate product, relative to dextrose (glucose), on a dry weight basis. Maltodextrin has a DE that ranges between 3 and 20. DP is the number of monomeric units in a polymer molecule. The DP of maltodextrin ranges

from 2 to 20 glucose units. In this study, maltodextrin with the DE of 16.5-19.5 and DP of approximately 7 glucose units was used. Among the commercially available maltodextrin products, DE in the range of 16.5-19.5 has the highest water solubility. The viscosity of the solution was controlled by varying the proportions of glycerol and water. To increase the viscosity, the available water proportion has to be reduced. Hence, the type of maltodextrin with the highest water solubility was chosen. 5 g glucose and 5 g maltodextrin were used as the feed.

3.2. Viscosity measurement

For the purpose of monitoring viscosity changes of gastrointestinal content during digestion (Objective A3), a molecular rotor compound - Fast Green was used in this study, which is discussed in detail in section 3.7. As mentioned in the introduction, the Fast Green dye is highly sensitive to changes in viscosity of the glycerol-water mixture. So, with the constant 5 g carbohydrate (glucose or maltodextrin) as the dry food base, the viscosity of the solution was altered by varying glycerol to water ratio. Model bolus solutions (without gastric juices) were prepared and their viscosity values were measured using a TA - Discovery HR-2 Rheometer (TA Instruments, New Castle, DE) **(Figure 3.2**). The average capacity of the gastric compartment in the TIM-1 system is 300 g. Model bolus solutions were prepared with 5 g carbohydrate and in the remaining 295 g of the solution, the ratio between glycerol and water was varied as 0:100, 50:50, 70:30, 80:20, and 90:10 (w/w). A 60 mm cone (4.0°) and plate geometry (Peltier plate steel - 988987) was used for the viscosity measurements. To measure the viscosity of each sample, approximately 4 ml of the solution was loaded between the cone and the plate. Shear rate vs. shear stress curves

were obtained for each solution by ramping up the shear rate from 0 s^{-1} to 150 s^{-1} (run time – 10 min). By calculating the slope of the curves, the respective viscosity values were evaluated. The measurements were conducted in triplicates while maintaining the samples at 37 °C (body temperature). Based on the results, three glycerol to water ratios were chosen to study the *in vitro* digestibility.

Figure 3.2. TA - Discovery HR-2 Rheometer

3.3. *In vitro* digestive experiment

The TIM-1 system was used to study the *in vitro* digestibility of the chosen food system. As mentioned in the introduction, the TIM-1 system is a multi-compartmental, dynamic, computer-controlled model of the human upper gastrointestinal tract **(Minekus et al., 1995)**. The TIM-1 system consists of four consecutive sections representing the stomach, duodenum, jejunum, and ileum, as shown in **Figure 3.3**. Each section consists of two connected glass units with a flexible interior membrane, which contains the

gastrointestinal content. The intermediate space between the glass wall and the flexible interior membrane is filled with circulating water to maintain the temperature at 37 °C. The circulating water applies pressure on the flexible interior membrane to generate alternate cycles of compression and relaxation which enables mixing of gastrointestinal content **(Kostewicz et al., 2014)**. The experimental parameters and chemicals being used were based on previous studies with some modifications, to simulate the digestive conditions of a healthy adult after intake of a meal (fed state) (**Dickinson et al., 2012; Speranza et al., 2013; Nimalaratne et al., 2015; Minekus, 2015**).

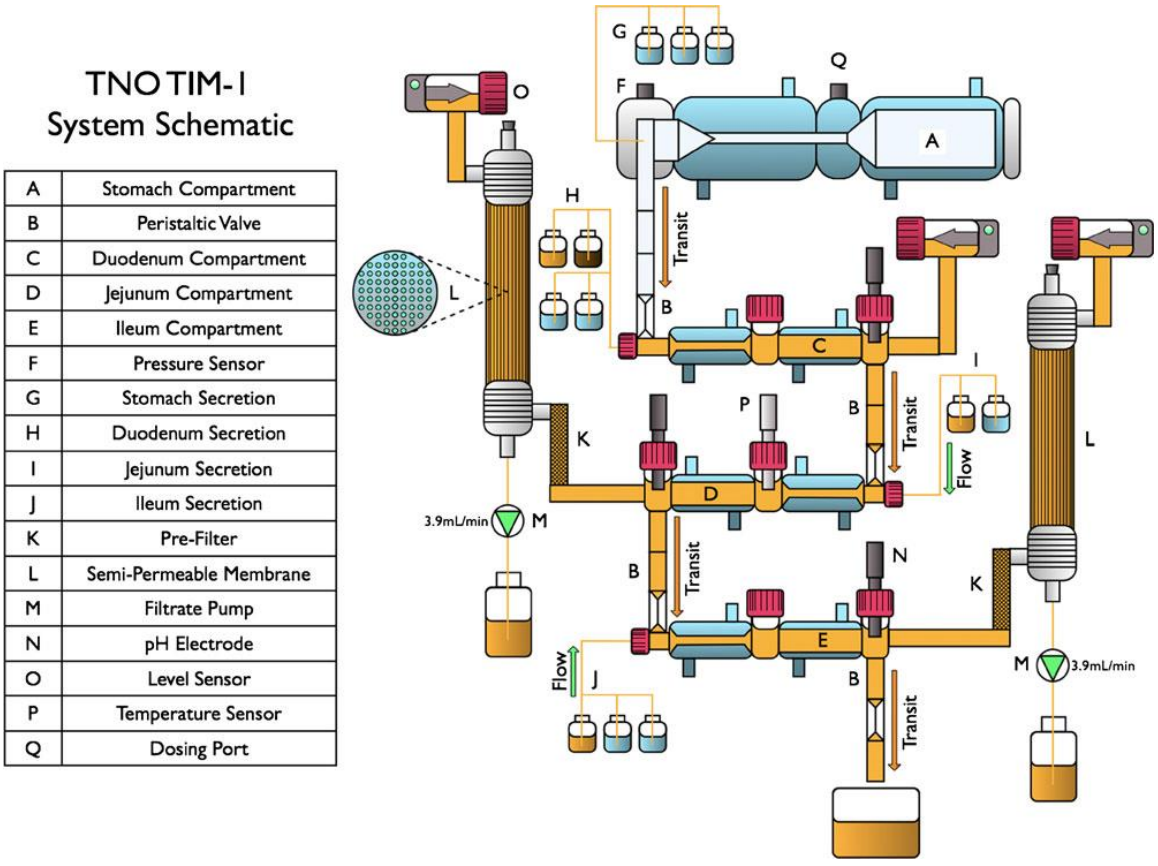

Figure 3.3: Schematic diagram of the TIM-1 system

(Dickinson et al., 2012)

Chemicals and enzymes

The two electrolyte solutions, gastric electrolyte solution (GES) and small intestinal electrolyte solution (SIES), were prepared as concentrated stocks and diluted on the day of use. All the solutions were prepared using de-ionized water. The diluted GES contained sodium chloride - NaCl (4.8 g/L), potassium chloride - KCl (2.2 g/L), calcium chloride - $CaCl_2$ (0.3 g/L), and sodium bicarbonate - $NaHCO_3$ (1.25 g/L). The diluted SIES contained sodium chloride - NaCl (5.0 g/L), potassium chloride - KCl (0.6 g/L), and calcium chloride - $CaCl_2$ (0.25 g/L). All these chemicals were obtained from Sigma-Aldrich. Fresh pig bile was collected from a local slaughterhouse (Farm-to-Pharm, NJ, USA), aliquoted, and stored at -18 °C until use. The required enzymes, α-amylase (~30 U/mg, 10065, from *Aspergillus oryzae*), pepsin (3200 U/mg, P68887, from porcine gastric mucosa), lipase (100-500 U/mg, L3126, from porcine pancreas), trypsin (7500 U/mg, T9201, from bovine pancreas), and pancreatin (4 × USP, P1750, from porcine pancreas), were obtained from Sigma-Aldrich.

Start residue

Before beginning the experiment, each compartment was filled with respective starting contents to mimic *in vivo* conditions. Gastric start residue composed of 5 g of GES with 5200 U of pepsin and 200 U of lipase. Duodenal start residue composed of 15 g of pancreatin solution (7%), 30 g of fresh porcine bile, 1 ml of trypsin solution (2 mg/ml), and 15 g of SIES. Jejunal start residue composed of 40 g of SIES, 80 g of fresh porcine bile, and 40 g of pancreatin solution (7%). Ileal start residue composed of 160 g of SIES. All start residues were prepared on the day of use.

Secretions

Throughout the entire experiment, GES with 1040 U/ml of pepsin and 40 U/ml of lipase was secreted into the gastric compartment at a rate of 0.5 ml/min. 7% pancreatin solution (0.25 ml/min), fresh porcine bile (0.5 ml/min), and SIES (3.2 ml/min) were secreted in to the duodenal section. SIES containing 10 % porcine bile was secreted into the jejunal section at a rate of 3.2 ml/min. SIES was secreted in the Ileal section at a rate of 3 ml/min. All secretion solutions were prepared with deionized water on the day of use. The secretion rates of all the solutions were regulated by a computer controlled pumping system.

Bolus preparation

The average capacity of the stomach section in the TIM-1 system is 300 g. Each bolus solution had 5 g of maltodextrin or glucose, 5 g of gastric start residue, 9.5 g of concentrated GES (10X concentrated), 11 mg of α-amylase, and 280.5 g of glycerol-water mixture. The proportion of the glycerol-water mixture was varied to adjust the initial viscosity of the bolus solution. The prepared bolus solution was injected into the gastric section. The circulation water (between the glass wall and the flexible interior membrane) was allowed to reach the experimental temperature of 37 °C. The digestive experiment was carried out for 5 h.

pH maintenance

Each section of the TIM-1 system has an individual pH probe to monitor pH. Based on predetermined values, the gastric content pH gradually dropped from 5.5 to ~2 in 2 h

and then equilibrated at 1.7 for the rest of the run. The pH of the duodenal, jejunal, and ileal contents was maintained at 6.5, 6.8, and 7.2, respectively. A computer controlled pumping system regulated the pH of the gastric content by secreting either water or 1 M hydrochloric acid into the stomach section at a rate of 0.5 ml/min. The pH of the intestinal content in the duodenum, jejunum, and ileum sections were maintained by secreting either SIES or 1 M sodium bicarbonate at a rate of 0.25 ml/min.

Transit time

Computer-controlled peristaltic pumps regulated the transit of gastrointestinal content between adjacent sections of the TIM-1 system. The transit rate of gastric, duodenal, jejunal, and ileal contents was modeled using a power exponential formula as given by **Eq. 3.1 (Elashoff et al., 1982; Minekus et al., 1995)**.

$$f = 1 - 2^{\left(\frac{t}{t_{1/2}}\right)^{\beta}} \quad \textbf{(3.1)}$$

In **Eq. 3.1**, *f* represents the fraction of gastrointestinal content delivered to the next section, *t* is the time of delivery in min, $t_{1/2}$ is the half-time of delivery, and β is the coefficient describing the shape of the curve. The predetermined halftime delivery and the β coefficient of the gastric section were 80 min and 2, respectively. The halftime delivery and the β coefficient of all the intestinal (duodenal, jejunal, and ileal) sections were fixed as 220 min and 2.5, respectively.

Sample collection

The jejunal and ileal sections were connected to two different hollow-filter membranes (Spectrum Milikros modules M80S-300-01P), to collect digested nutrients. These filter membranes have a pore size of 0.05 μm and they separate available micellar fraction from the intestinal content as dialysate fluids. Through the jejunal and ileal sections, SIES was circulated at a rate of 4.5 ml/min and the filtered fluid was collected in separate containers. The collected digested nutrients represent bioaccessible nutrients rather than bioavailable nutrients. In the human digestive process, bioaccessible nutrients are defined as the fraction of nutrients available for absorption through the intestinal wall. Bioavailable nutrients are nutrients that are absorbed by the gut wall and are available for physiological functions. Filtered fluid from the jejunal and ileal sections was collected every 20 min for the first 2 h and every 30 min for the remaining 3 h. Unabsorbed efflux was collected three times during the run, at 100 min, 210 min, and 300 min. The samples were weighed and were frozen until analysis. All the experiments were performed in triplicates.

3.4. Glucose and maltose assay method

In the TIM-1 system, due to the absence of brush border enzyme (maltase), final products of maltodextrin digestion were glucose (monosaccharide), maltose (disaccharide), and traces of maltotriose (trisaccharides). Previous TIM-1 digestive study indicated that trisaccharides and short chained oligosaccharides would only be in a negligible amount in the collected digested nutrients **(AlHasawi et al., 2017)**. Therefore, in this study, only the amount of glucose and maltose were quantified. For the glucose-based bolus experiments,

glucose concentrations of the collected samples were quantified. For the maltodextrin-based bolus experiments, glucose and maltose concentrations were quantified in the collected samples.

Glucose concentration in each sample was evaluated using a glucose (GO) assay kit purchased from Sigma-Aldrich (Product code: GAGO-20). This kit quantifies the glucose concentration based on an enzymatic method. The two primary chemicals of this kit are glucose oxidase and o-dianisidine reagent. This kit is suitable for glucose concentration ranges from 20 μg/ml to 80 μg/ml. Therefore, the samples collected from the TIM-1 system were diluted with distilled water such that their glucose concentration fell in this range. Using this kit, glucose present in the sample was oxidized to gluconic acid and hydrogen peroxide by the enzyme glucose oxidase. Hydrogen peroxide reacted with the o-dianisidine reagent in the presence of the enzyme peroxidase to form a brown colored product, oxidized o-dianisidine. For the reactions to occur, the test tubes containing samples and the enzymes were kept at 37 °C hot water bath for 30 min. By the end of the heat treatment, sulfuric acid - 12 N (Product code 25,810-5) was added to the test tube so that the brown colored product reacted with sulfuric acid to form a more stable pink colored product. The intensity of pink color was measured as absorbance at 540 nm using a BIO-TEK Synergy HT spectrophotometer (Winooski, Vermont) **(Figure 3.4)**. Correlation between the glucose standards and corresponding spectrophotometric absorbance value was developed and used to predict glucose concentrations in collected samples. The correlation experimented was performed in triplicates.

Figure 3.4: BIO-TEK spectrophotometer - Synergy HT

Maltose concentration was evaluated using a maltose assay kit purchased from Sigma-Aldrich (Product code: MAK019). This kit uses an enzymatic method to convert each maltose unit to two glucose units and the total-glucose concentration was quantified. The total-glucose concentration is the summation of the concentration of glucose already present in the sample (base-glucose), which was measured using the glucose assay kit, and the concentration of glucose converted from maltose. The chemicals present in this maltose kit are maltose assay buffer, maltose probe, α-D-glucosidase, and enzyme mix. This kit is ideally suitable for samples containing maltose in the range of 1 nmol/50 µl to 5 nmole/50 µl. Therefore, the samples collected from the TIM-1 system were diluted with distilled water such that their maltose concentration fell in this range. Using this kit, maltose present in the sample was converted to two glucose units by the enzyme α-D-glucosidase. Glucose

was further oxidized using a mixture of maltose assay buffer, maltose probe, and enzyme mix. For the reactions to occur, the 96 well plate containing samples and the added chemicals were mixed well using a horizontal shatter and incubated at 37 °C for 60 min. By the end of incubation, the oxidation step resulted in a stable pink colored product. The intensity of pink color was measured as absorbance at 570 nm using a BioTek Epoch spectrophotometer (Winooski, Vermont). Correlation between the maltose standards and corresponding spectrophotometric absorbance value was developed and used to predict total-glucose concentrations in collected samples. The correlation experiment was performed in triplicates.

3.5. Statistical analysis

The total mass of absorbed nutrients (base-glucose and total-glucose) based on different initial bolus viscosity values were subjected to one-way analysis of variance (ANOVA) and means were compared using Tukey honest significant difference (HSD) test with a p-value of 0.05. Statistical analysis was performed using Microsoft Excel 2013.

3.6. Fluorescence emission measurement

Fast Green dye (Sigma-Aldrich Product code: 68724) was used to monitor the changes of the gastrointestinal content viscosity in the TIM-1 system during digestion. As mentioned earlier, the molecular rotor property of Fast Green dye is sensitive to the glycerol-water mixture and the fluorescence emission depends on the viscosity of the surrounding medium. Stock solutions of the Fast Green dye (1 mM) were prepared using deionized water and diluted to a concentration of 10 μM in required solutions to obtain

fluorescence signals. The final concentration of the dye was chosen based on preliminary experiments to minimize the disturbances in the fluorescence signals due to inner filters of the spectrofluorometer. Steady-state fluorescence excitation and emission spectra were recorded using a Cary Eclipse spectrofluorometer equipped with a fiber optic attachment (Agilent Technologies, Santa Clara, CA). The fluorescence emission spectra of samples with and without the dye were collected over the range from 600 nm to 750 nm, using an excitation wavelength of 580 nm. Excitation and emission slits were set at 5 nm and 20 nm, respectively. The data obtained from the spectrofluorometer were analyzed using Microsoft Excel 2013. The emission spectra of control samples (without the dye) was subtracted from the emission spectra of the respective samples with the Fast Green dye, to negate the interference of background signals. The final emission spectra were normalized towards the highest intensity value.

Preliminary experiments were carried out to correlate the fluorescence emission intensity with viscosity. Three hundred grams of model bolus solutions with 5 g glucose and 5 g maltodextrin and different glycerol to water ratios (0:100, 50:50, 70:30, 80:20, and 90:10) were prepared. Fast Green dye was added to these solutions at a concentration of 10 μM and control solutions were prepared without the addition of the dye, as shown in **Figure 3.5**. The samples were filled in transparent glass tubes and equilibrated at 37 °C before measuring the fluorescence excitation and emission intensity. After negating the influence of background signals (control solutions), the normalized peak intensity of the samples were evaluated and correlated with the respective viscosity of the solution. All samples were analyzed in triplicates and the measurements were carried out in a dark environment.

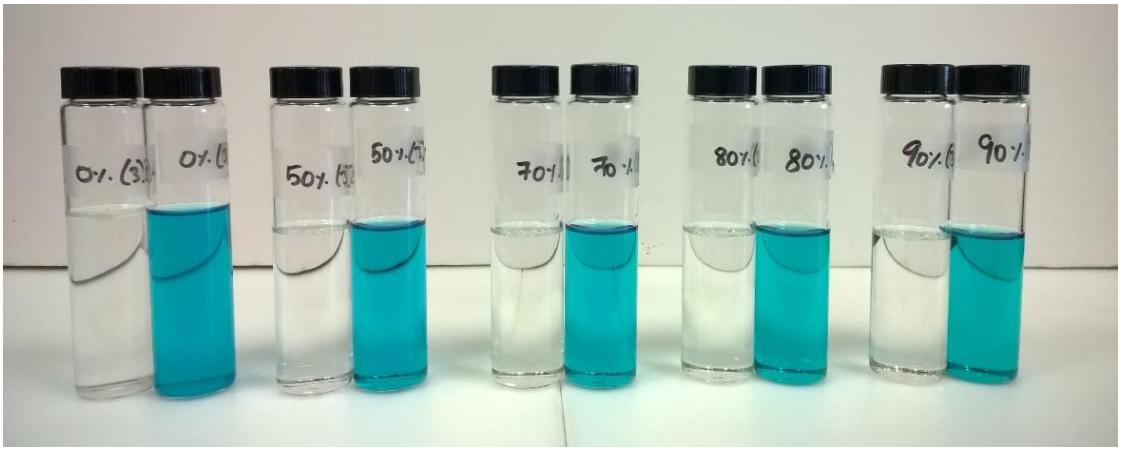

Figure 3.5: Two sets of 5 g maltodextrin solutions with different glycerol to water ratio in w/w (0:100, 50:50, 70:30, 80:10, and 90:10), one (on the left) without any dye - control and the other with the Fast Green dye of concentration 10 µM

3.6.1. In-line fluorescence intensity monitoring

The 10 µM concentration of Fast Green was added to all the secretions of the TIM-1 system, the start residues, and the bolus solution. The experiments with the dye were performed in triplicates and the control experiment (without the addition of the dye) was performed once. During digestion, the fluorescence emission spectra were recorded at four different locations of the TIM-1 system, one in each section (stomach, duodenum, jejunum, and ileum). As mentioned earlier in the description of the TIM-1 system, each section consists of two connected glass units. The fluorescence signals were recorded at the connecting glass chamber between the two units (as shown in **Figure 3.6**) using the fiber optic probe attached to the Cary Eclipse spectrofluorometer. The measurements were carried out for every 15 min in a dark environment. The normalized peak intensity as a

function of time was plotted for each section. From the signals obtained from each section, the normalized peak intensity as a function of time was evaluated. These curves were used to understand the viscosity changing pattern of the gastrointestinal content during digestion.

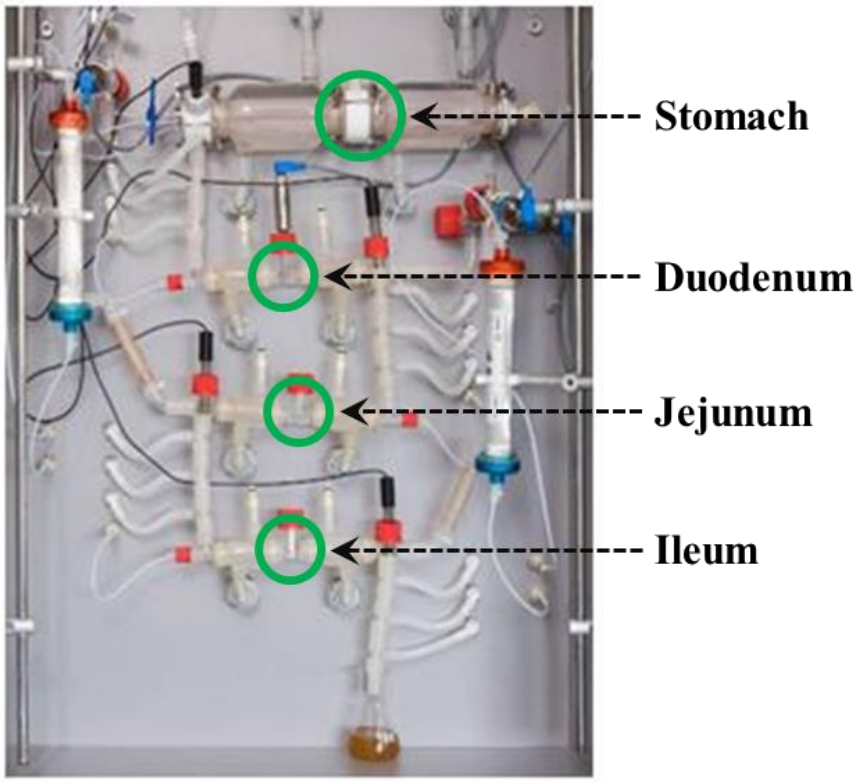

Figure 3.6: Front panel of the TIM-1 system with the locations were fluorescence signals were monitored (Adapted from http://botanical.pbrc.edu/cores_botanical.html)

3B. Numerical simulation

3.7. Fluid flow model

A finite element based commercial computational software, COMSOL Multiphysics® (Version 5.4, COMSOL Inc., Burlington, MA), was used to develop the numerical fluid flow model approximating the small intestinal geometry and motility. As discussed in the introduction section, two types of intestinal motility are peristalsis and segmentation. In this study, only the peristalsis movement was incorporated into the numerical model because peristalsis is the most dominant intestinal movement and it is involved in the propagation of food through the intestine. In case of the segmentation movement, its major purpose is the mixing of chyme. Since a liquid food was used in this study, a better distribution of digested food in the small intestine can be expected even in the absence of segmentation motion. Hence the effect of segmentation movement was not accounted in this study. For numerical purposes, the geometry of small intestine was assumed as a perfect cylinder. The length of jejunum cylinder was assumed to be 1.2 m and the length of ileum geometry was assumed to be 1.8 m **(Betts et al., 2013; Jamieson and Wong, 2006).** Other intestinal geometry and motility parameters were obtained from a study performed by **Ohkubo et al. (2013).** This study assessed the small intestinal motility in healthy human volunteers using an MRI technique. A specific type of MRI technique, Cine-MRI was used to analyze the small intestinal motility for a scan time of 16 s and a total of 30 images were obtained in that scan time. To measure the changes in the inner (luminal) diameter, three sections of the small intestine containing large amounts of intestinal fluids were selected. Images of a healthy volunteer showing changes in inner

diameter of two sections of the small intestine at different time intervals are shown in **Figure 3.7 (Ohkubo et al., 2013)**.

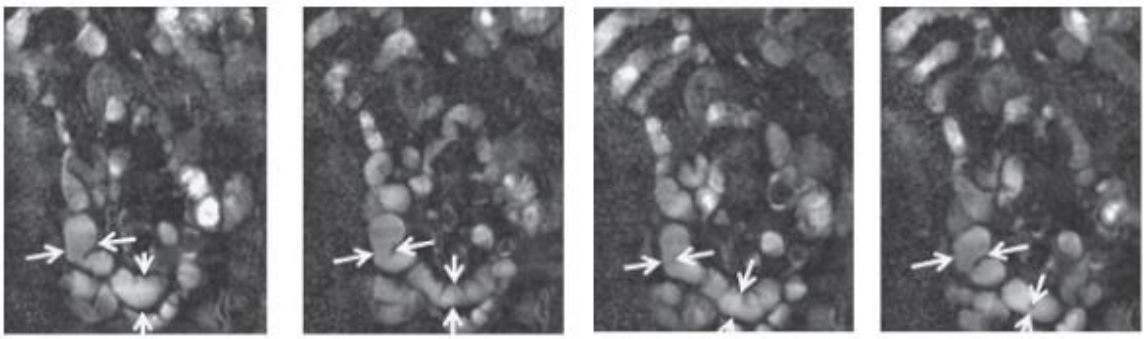

t = 0 s **t = 5 s** **t = 10 s** **t = 15 s**

Figure 3.7: MRI images of a healthy small intestine at four time intervals (Ohkubo et al., 2013)

Figure 3.8 shows a typical intestinal contraction with normal luminal (inner) diameters in a healthy volunteer **(Ohkubo et al., 2013)**. Based on this study, the diameter of the cylinder was assumed to be 17.3 mm **(Ohkubo et al., 2013; Pallotta et al., 1999)**, which is the diameter of the small intestinal lumen under relaxed condition. The contraction cycle, which is the time between subsequent maximum contractions, was assumed to be 7s **(Ohkubo et al., 2013)**. The average contraction ratio (amplitude) of the cycle, which is calculated based on the difference between maximum extension and maximum contraction was assumed to be 78 % **(Ohkubo et al., 2013)**. Using this intestinal geometry and motility information, a numerical model was developed. The peristaltic wave motion was incorporated into the model based on the movement explained in **Figure 1.5** (Introduction chapter), also shown below. The slight expansion of the walls which immediately follows the compression (as seen in **Figure 1.5**) was ignored in the model.

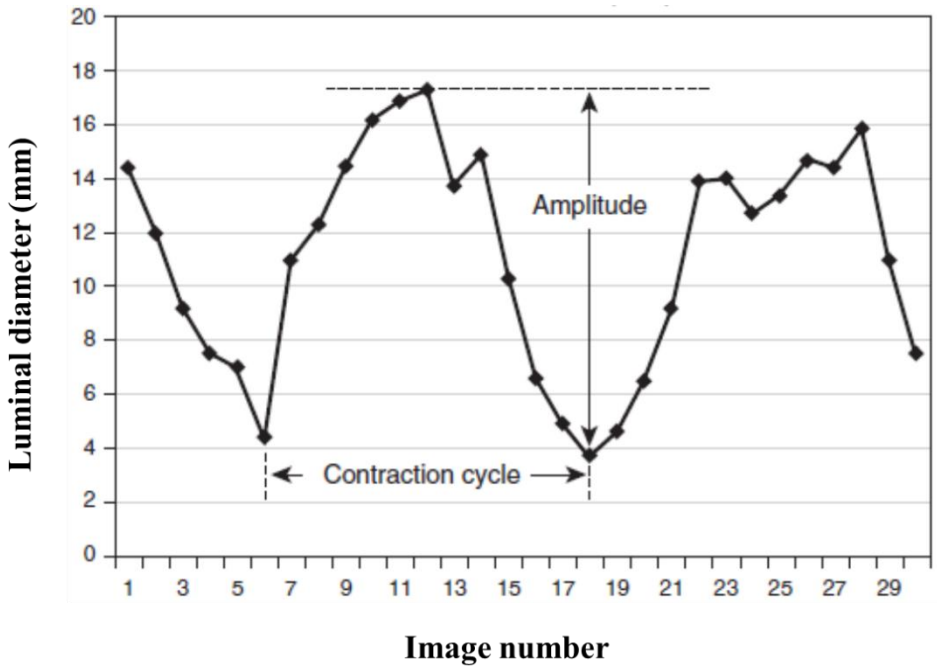

Figure 3.8: A typical intestinal contraction with normal luminal diameter, regular contraction cycle and high contraction ratio in a healthy volunteer, obtained from thirty MRI images within a scan time of 16 s at a selected location (Ohkubo et al., 2013)

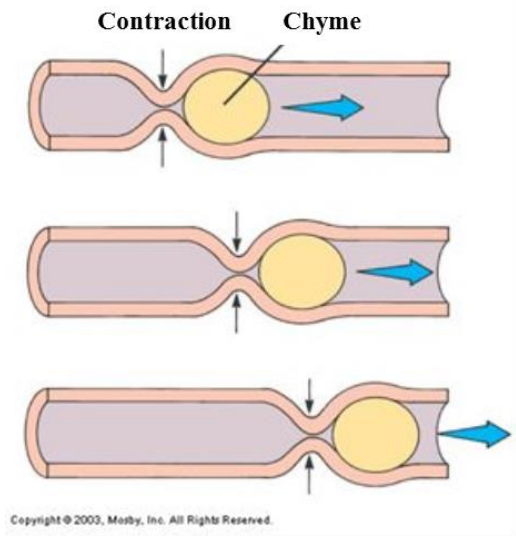

(From the introduction chapter) Figure 1.5: Peristaltic wave motion

(http://slideplayer.com/slide/7068265/)

3.7.1. Geometry

For numerical purposes, the geometry of small intestine was assumed as a perfect cylinder. The flow in the cylindrical tube was assumed to be axisymmetric. Two separate 2-D axisymmetric geometries, one for jejunum (length - 1.2 m) and one for ileum (length - 1.8 m), were built, both with a radius of 8.65 mm. **Figure 3.9A** shows the 2-D axisymmetric geometry built for the jejunum fluid flow model. A similar geometry 2-D axisymmetric with 1.8 m length was develop for the ileum fluid flow model.

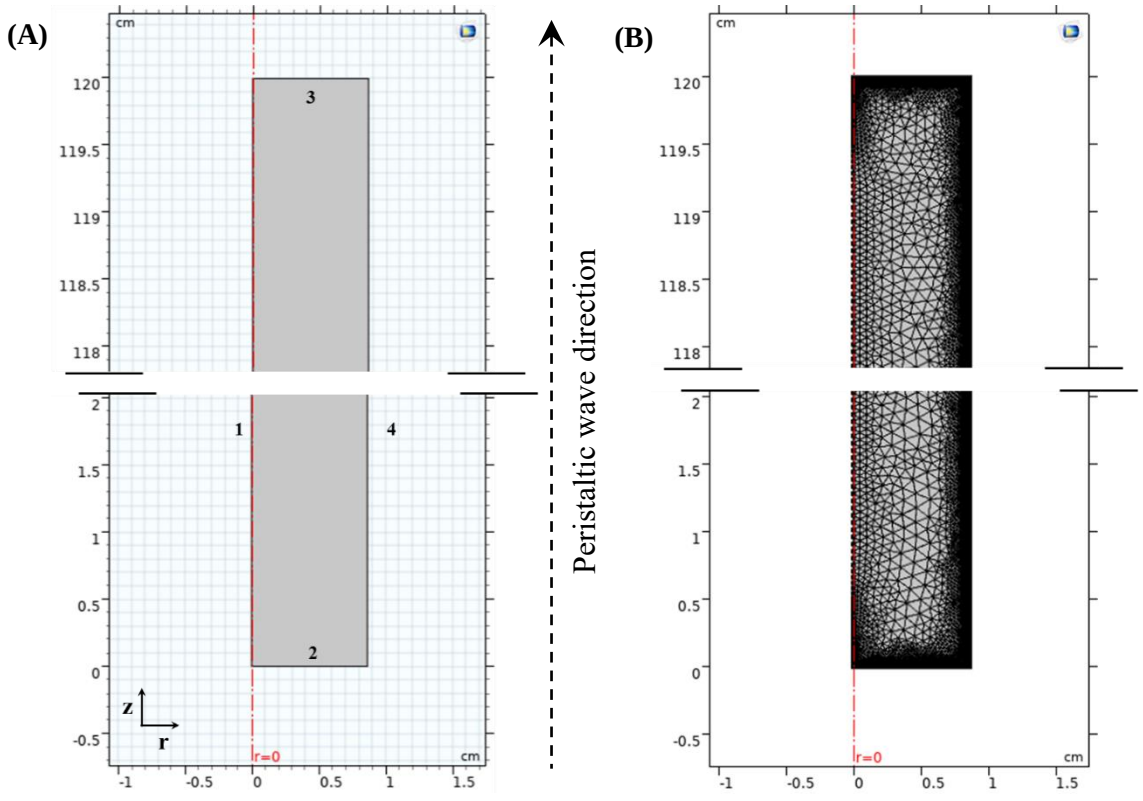

Figure 3.9: (A) 2-D axisymmetry geometry of jejunum used for developing fluid flow model and corresponding (B) schematic diagram of mesh used for solving governing equations

3.7.2. Governing equations

In the geometry shown in **Figure 3.9A**, the peristaltic wave travels from bottom to top along the z-axis direction. The velocity field imposed by peristalsis was assumed to be laminar, because the expected Reynolds number was ~3. Therefore, the numerical model was developed in COMSOL Multiphysics® using the available modules *laminar flow* physics and the gut motility was incorporated using the *moving mesh* physics.

3.7.2.1. Laminar flow physics

Fluid properties

The fluid was assumed to be incompressible and the fluid flow was solved based on the continuity equation **(Eq. 3.2)** and the Navier-Stokes equation **(Eq. 3.3)**. The continuity equation signifies the conservation of mass i.e., the net flux in a given volume with respect to all the directions (radial component r and transverse component z) is zero. In **Eq. 3.2**, ρ is the density in kg/m^3 and u is the velocity vector in m/s.

$$\boldsymbol{\rho \nabla \cdot (u) = 0} \tag{3.2}$$

$$\boldsymbol{\rho \frac{\partial u}{\partial t} + \rho(u \cdot \nabla)u = \nabla \cdot [-p + \mu(\nabla u + (\nabla u)^t)] + \rho g} \tag{3.3}$$

The Navier-stokes equation solves for the gradient of velocity with respect to the pressure force, viscous force, and gravitation force. In **Eq. 3.3**, t is the time in s, p is the pressure in Pa, μ is the dynamic viscosity in Pa·s, ∇u is the velocity gradient tensor in s^{-1}, $(\nabla u)^t$ is the transpose of ∇u in s^{-1}, and g is the gravitational force vector expressed in m/s^2.

In this study, the gravitation force was assumed to be zero. The material properties of intestinal content used were density (ρ) of 1040 kg/m^3 **(Snyder et al., 1992)** and dynamic viscosity (μ) of 0.0014 Pa·s **(McDonald et al., 2001)**.

Open boundary

The two opposite edges of the axisymmetric geometry (boundaries 2 and 3 in **Figure 3.9A**), were defined as open boundaries. The open boundary condition describes boundaries in contact with a large volume of fluid. **Eq. 3.4** was solved for these two edges which shows that the summation of pressure force and viscous force was assumed to be zero. Because of no external stress, fluid can enter and leave the domain freely. In **Eq. 3.4**, *n* represents the boundary normal pointing out of the domain.

$$[-\boldsymbol{p} + \boldsymbol{\mu}(\boldsymbol{\nabla u} + (\boldsymbol{\nabla u})^{\boldsymbol{t}})]\boldsymbol{n} = \mathbf{0} \quad \textbf{(3.4)}$$

Moving wall

The moving wall boundary condition was imposed on the outer wall of the geometry (boundary 4 of **Figure 3.9A**). This condition allows the wall to move at a translational velocity (u_{tr}) as shown in **Eq. 3.5**. The translational velocity of the moving wall in the direction of r- and z-coordinates was defined using the *moving mesh* physics.

$$\boldsymbol{u} = \boldsymbol{u_{tr}} \quad \textbf{(3.5)}$$

3.7.2.2. Moving mesh physics

In COMSOL Multiphysics®, the *moving mesh* interface can be used to create models where the geometry (represented by mesh) changes due to some physical phenomena without the material being removed or added.

Prescribed deformation

The prescribed deformation condition was used on the entire domain to simulate the peristaltic wave motion. Using this condition, the spatial coordinates of the geometry follow a defined equation for deformation. The intestinal motility parameters were modeled as an exponential function as shown in **Eq. 3.6** and the equation's graphical representation is shown in **Figure 3.10**.

$$\boldsymbol{peristalsis_r = -0.78 * R * exp\left(-\left(Z-\left(60+0.0035*mod(t,7)\right)\right)\text{^}2/0.006\right) * contraction(t)} \quad \textbf{(3.6)}$$

$$\boldsymbol{contraction = flc2hs(mod(t,7)-1.75,1.75) * flc2hs(5.25-mod(t,7),1.75)} \quad \textbf{(3.7)}$$

In **Eq. 3.6**, 0.78 represents the amplitude of the curve (78%), 60 represents the starting location of the peristaltic wave in cm (midpoint of the entire geometry), 0.0035 represents the rate of peristaltic wave progression in cm/s, 0.006 defines the shape of the peristaltic wave curve, R and Z represents the r- and z- coordinate values, respectively, and *contraction(t)* represents the contraction cycle of each peristaltic wave which was defined

using the available step function option called Heaviside function (*flc2hs*) as shown in **Eq. 3.7**. Each peristaltic wave cycle starts at 0 s, reaches the peak (amplitude) in 3.5 s and drops back to zero in 7 s. In **Eq. 3.7**, 1.75 represents the half time (s) at which the curve reaches 50% of the amplitude value while moving towards the peak and 5.25 represents the half time (s) at which the curve reaches 50% of the amplitude value while moving towards zero. The cycle continues for every 7 s which was defined using the *mod* function. **Eq. 3.6** repeatedly generates peristaltic waves only at one location (60 cm) in the entire geometry of the jejunum and results in an average velocity of 0.24 mm/s. This equation was designed to achieve the average residence time of intestinal content in the small intestine which ranges from 3 h to 4 h **(Davis et al., 1986; Yuen, 2010; Billa et al., 2000; Coupe et al., 1991; Yuen et al., 1993)**. Similarly, for the ileum geometry of 1.8 m long, peristaltic waves were generated at one location (90 cm) to achieve the average intestinal content residence time of ~3.5 h. For the ileum geometry, the only change in **Eq. 3.6** was, instead of 60, 90 was used as the starting location of the peristaltic wave.

In **Figure 3.10**, the length of the geometry is represented by the x-axis, the time is represented by the y-axis, and the amplitude (78%) is shown in the negative z-axis direction. The exponential equation **(Eq. 3.6)** was given as the input in the prescribed deformation boundary condition and solved for the entire geometry.

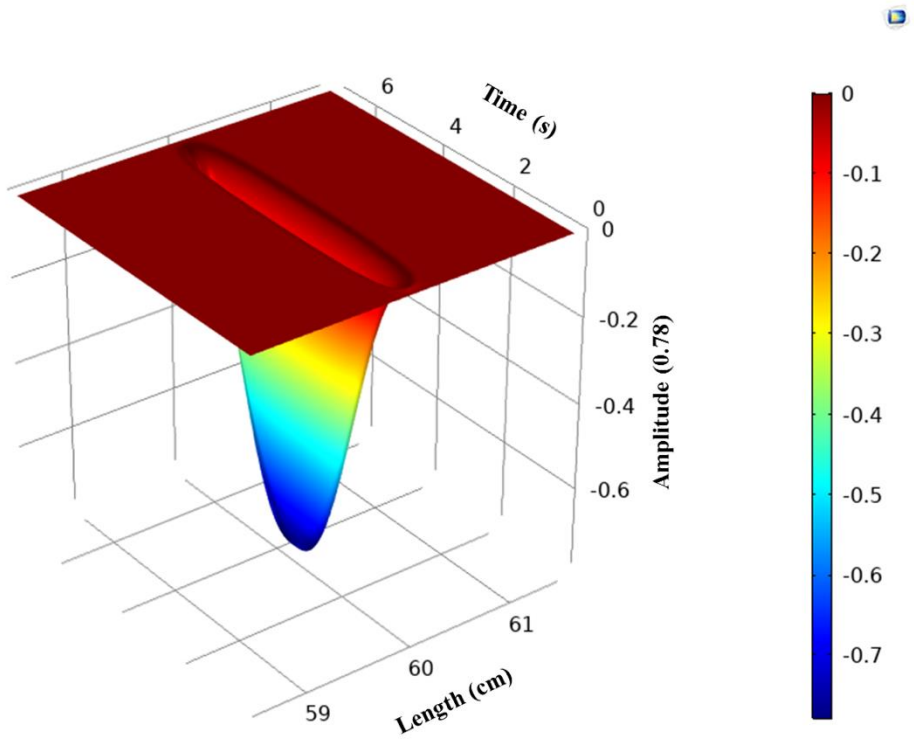

Figure 3.10: Graphical representation of Eq. 3.6 used for generating peristaltic waves in the jejunum fluid flow model

3.7.3. Computational mesh

The computational mesh was created using built-in mesh generating code in COMSOL Multiphysics®. In the 2D-axisymmteric geometry, the mesh was generated using triangular elements connecting 3 nodes at a time, as shown in **Figure 3.9B**. The edges of geometry were built with finer mesh than the remaining geometry for better simulation of peristaltic wave and for accurate calculation of inlet and outlet velocity. The distance between each node varied from 0.305 μm to 0.428 mm depending on the complexity of geometry. For the 2-D axisymmetric jejunum fluid flow model, the domain was discretized into 426,542 elements with 15,000 boundary elements. For the 2-D axisymmetric ileum

fluid flow model, the domain was discretized into 478,260 elements with 18,294 boundary elements. The governing equations were solved for these finite elements at appropriate nodes with the time step of 0.1 s. The computational time needed to solve one peristaltic wave (7 s) in a jejunum or ileum fluid flow model was about 3.5 min on a Dell® workstation with Intel® Xeon® CPU E5-2643 0 processor @ 3.30 GHz and 64.0 GB RAM.

3.8. Diffusion model

To the fluid flow model, *Transport of diluted species* physics was added to model the flow of carbohydrate species.

3.8.1. Geometry

To simulate the glucose absorption process, it was assumed that the intestine is enclosed in a cylindrical cavity with an intermediate diffusive wall as shown in **Figure 3.11A** (jejunum geometry). In this geometry SI represents small intestine and AT represents the absorption tube of assumed radius 1.135 cm. Carbohydrates enter through boundary 2 and exits through boundary 3. Boundary 4 is the intermediate diffusion wall through which digested glucose diffuses and gets collected in the absorption tube (AT). Due to software limitations, the mass balance of carbohydrate species was not achieved in a moving boundary problem. Therefore, the velocity profile obtained at the boundary 2 (**Figure 3.9A**) of the previously developed dynamic fluid flow model was used as the inlet condition in this similar but static geometry (**Figure 3.11A**), to simulate the flow of carbohydrate species. A fully developed (after 1 min) oscillating velocity profile obtained at boundary 2 of **Figure 3.9A** (Jejunum) is shown in **Figure 3.12**.

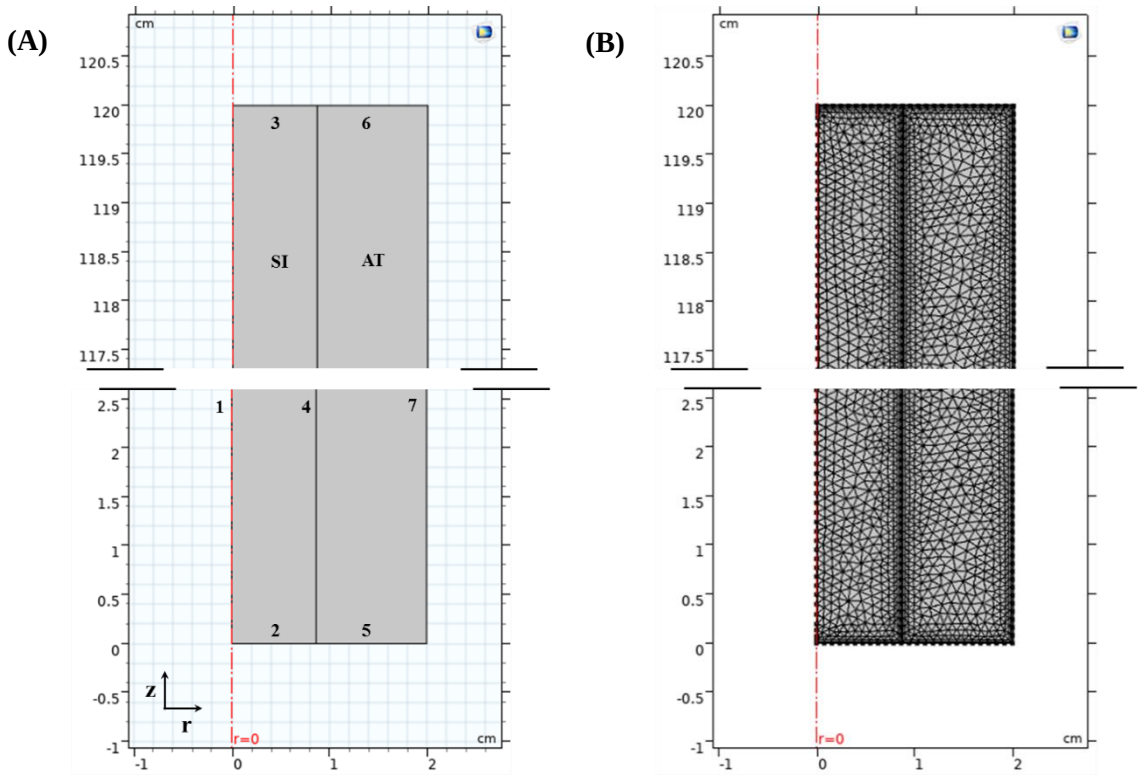

Figure 3.11: (A) 2-D axisymmetry geometry of jejunum used for developing diffusion model and corresponding (B) schematic diagram of mesh used for solving governing equations

This oscillating velocity profile was imposed as the inlet boundary condition at the boundary 2 of **Figure 3.11A**. Similarly, a velocity profile dataset at the boundary 2 of ileum geometry was obtained and used to simulate the ileum diffusion model. The diffusion model was solved using *Laminar flow* physics and *Transport of dilute species* physics.

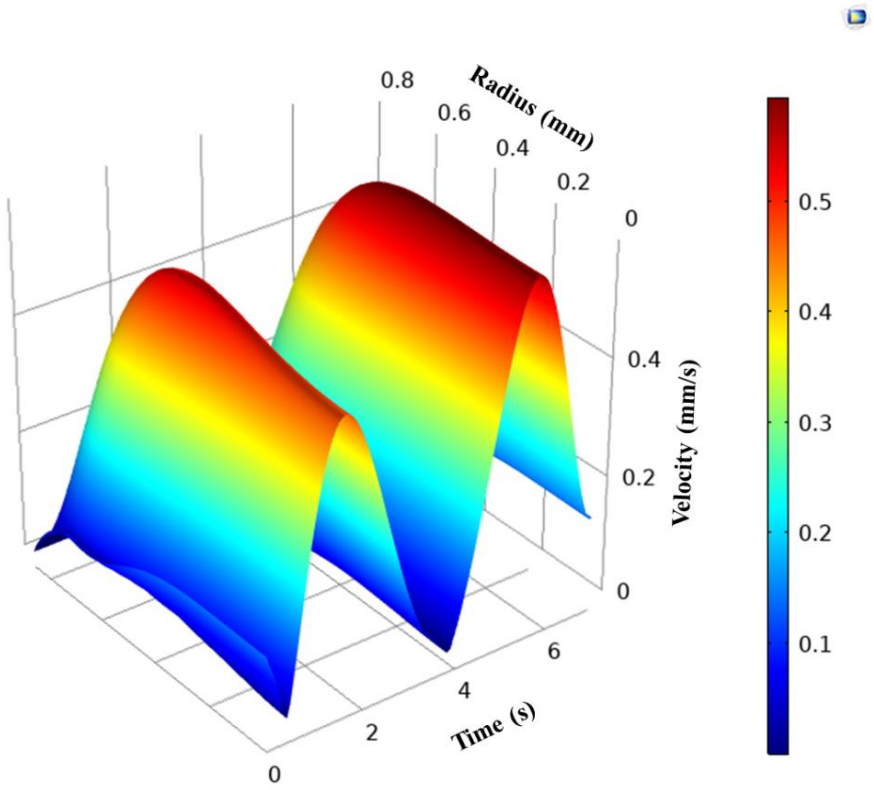

Figure 3.12: Inlet velocity profile at the boundary 2 of the 2D axisymmetric jejunum diffusion model (Figure 3.11A)

3.8.2. Governing equations

3.8.2.1. Laminar flow physics

Fluid properties were defined and solved based on the continuity equation (**Eq. 3.2**) and the Navier-Stokes equation (**Eq. 3.3**), as explained in the previous section, the fluid flow model.

Inlet and Outlet

Boundaries 2 and 5 of **Figure 3.11A** were defined as the inlet boundary condition, which is used to define a net flow into a domain. **Eq. 3.8** was used to solve this boundary condition. In **Eq. 3.8**, U_0 represents the normal inflow speed which was defined by the velocity profile dataset shown in **Figure 3.12** (for jejunum). As shown in **Figure 3.12**, the velocity profile was a function of radius (r-axis coordinates) and time. This velocity profile was repeated every 7 s at the inlet boundary, using the *mod* function. At the boundary 5 of **Figure 3.11A**, the inlet velocity was fixed at an assumed value of 2 mm/s.

$$\boldsymbol{u} = -\boldsymbol{U_0 n} \tag{3.8}$$

Boundaries 3 and 6 of **Figure 3.11A** were defined as the outlet boundary condition, which is used to define net outflow from the domain. **Eq. (3.9)** was used to solve outlet boundary condition. This equation was similar to **Eq. 3.4** explained in the *open boundary* section, in which the summation of pressure force and viscous force was assumed to be zero. The additional function of the outlet boundary condition is that it prevents fluid from entering back into the domain through that boundary, unlike open boundary condition which allows the fluid to flow freely in and out of the domain.

$$[-pI + \boldsymbol{\mu}(\boldsymbol{\nabla u} + (\boldsymbol{\nabla u})^{\boldsymbol{T}})]n = 0 \tag{3.9}$$

Wall

Boundary 7 of **Figure 3.11A** was assumed to be a solid stationary wall and 'no slip' wall condition was used to model the flow. A 'no slip' wall is a wall where the fluid velocity relative to the wall velocity is assumed to be zero. **Eq. 3.10** was used to solve this boundary condition. Interior wall boundary condition was applied to boundary 4 of **Figure 3.11A**, by assuming that this boundary was also a solid stationary wall. **Eq. 3.10** was solved on both the sides of the interior wall.

$$\boldsymbol{u = 0} \tag{3.10}$$

3.8.2.2. Transport of diluted species physics

Transport properties

The chemical species transport was solved using the convective-diffusion equation **(Eq. 3.11)**. In **Eq. 3.11**, c_i is the concentration of the species in mol/m^3, t is the time in s, D_i is the diffusion coefficient of the species in m^2/s, u is the mass average velocity vector in m/s, R_i is the reaction rate expression for the species in mol/(m^3·s).

$$\frac{\partial \boldsymbol{c_i}}{\partial \boldsymbol{t}} - \boldsymbol{\nabla \cdot (D_i \nabla c_i) + u \cdot \nabla c_i = R_i} \tag{3.11}$$

In this study, the term c_m was used to represent the concentration of maltodextrin species and c_g was used to represent the concentration of glucose species. The diffusion coefficient of glucose in the water at 37 °C is ~1×10^{-9} m^2/s **(Converti et al., 1999)**. However, for the current static model, this diffusivity value was too low to facilitate all the

species molecules to move towards the intermediate diffusive wall to diffuse across the intermediate boundary 4 of **Figure 3.11A**. Also, the numerical model assumed that the entire cylindrical geometry was filled with intestinal content. However, under *in vivo* conditions, approximately 50% of small intestinal space would be occupied by gases. This would allow the concentrated chyme to be in contact with the intestinal wall and support the *in vivo* nutrition absorption process. In the numerical diffusion model, since the entire the geometry was filled with intestinal content the nutrient concentrations were comparatively diluted. Therefore, the diffusivity value of intermediate diffusion wall was increased ($1\times10^{-8}\ m^2/s$) based on preliminary simulation results, to assist nutrient transport from the small intestine geometry to the absorption tube. Velocity field values for the term *u* were obtained by coupling this physics interface (*transport of diluted species*) with the solved values of the *laminar flow* physics. This was achieved by using the available multiphysics coupling option called *Flow coupling*. The reaction term R_i represents a source or sink term typically due to a chemical reaction. The reaction term accounts for consumption or production of species per unit volume of medium per unit time. In this study, Michaelis-Menten kinetics model was used to express the rate of maltodextrin consumption (R_m) and glucose generation (R_g), as shown in **Eq. 3.12** and **Eq. 3.13**. Maltodextrin used in the experimental study comprised of approximately 7 glucose units linked with glycosidic bonds, hence the term $\left(\frac{1}{7}\right)$ was incorporated in **Eq. 3.12**. These two equations were applied only to the small intestinal geometry (SI) of **Figure 3.11A.**

$$R_m = -\left(\frac{1}{7}\right) \times \left(\frac{V_{max} \times c_m}{K_m + c_m}\right) \quad \textbf{(3.12)}$$

$$R_g = \left(\frac{V_{max} \times c_m}{K_m + c_m}\right) \quad \textbf{(3.13)}$$

It was assumed that the hydrolysis of maltodextrin to glucose reaction starts and happens only in the jejunal section, which is not true in the real scenario where the hydrolysis reaction starts from the mouth. These two equations were not solved in the ileum diffusion model, because in the human digestive process, most of the nutrients are digested and absorbed in the jejunum section. The remaining digested nutrients get absorbed in the ileum section **(Borgstrom et al., 1957)**. The two Michaelis-Menten parameters, the maximum rate of product formation at saturated substrate concertation (V_{max}) and the Michaelis-Menten constant (K_m), which is the substrate concentration at which the reaction rate is half of V_{max}, were obtained from the literature. The K_m value was assumed to be a constant of 4.8 mol/m^3 **(Schwimmer, 1950)**. The V_{max} value was assumed to vary in the range 0.00365 mol/(m^3·s) to 0.11667 mol/(m^3·s), depending on the extent of short-chained carbohydrate digestion **(Saito et al., 1979; Satomura et al., 1984)**. In the present study, the extent of maltodextrin digestion was varied by changing the initial viscosity of bolus and by the external addition of brush border enzyme (maltose assay kit). While solving the maltodextrin diffusion model, the V_{max} value was varied in the jejunum simulation, to achieve the final amount of base-glucose or total-glucose absorption value obtained from different TIM-1-maltodextrin-based experiments.

Inflow

Species concentration inflow at the inlet boundary 2 of **Figure 3.11A** was defined by using the concentration flux (Danckwerts) inflow boundary condition as shown in **Eq. 3.14**. In the available multiphysics software, Danckwerts flux inflow boundary condition can be used to achieve more stable solutions when oscillating inlet velocity or reaction rates are involved at the inlet.

$$\boldsymbol{n \cdot (D_i \nabla c_i + u c_i) = n \cdot \left(u c_{0,i}\right)} \quad \textbf{(3.14)}$$

$$\boldsymbol{c_{0,i} = 1 - 2^{\left(\frac{t}{t^{1/2}}\right)^{\beta}}} \quad \textbf{(3.15)}$$

The initial inlet concentration of glucose $\left(\boldsymbol{c_{0,g}}\right)$ and maltodextrin $\left(\boldsymbol{c_{0,m}}\right)$ were calculated based on the gastric emptying rate equation shown in **Eq. 3.15**, which was the same equation as **Eq. 3.1**, used in the *in vitro* gastrointestinal model, the TIM-1 system, to control the transit rate of gastric content from the stomach section to the duodenal section. It was assumed that the gastric emptying rate is equivalent to the inflow rate of jejunum. The presence of duodenum was not accounted for in this study. Because of shorter length (25 cm) of *in vivo* duodenum, it was assumed that the rate of intestinal content entering the duodenum is the same as the rate of intestinal content exiting. In **Eq. 3.15**, $c_{0,i}$ represents the fraction of meal exiting stomach or entering jejunum, t is the time of delivery (min), $t^{1/2}$ is the half time delivery, and β is the coefficient describing the shape of the curve. Gastric emptying in the *in vitro* experimental procedure was controlled by this equation, with the parameters $t^{1/2}$ = 80 min and β = 2. Gastric emptying is influenced by physical

properties of food such as form (solid or liquid), viscosity, and factors such as volume, concentration, and composition of gastric content **(Gropper et al., 2009; Ferrua and Singh, 2010)**. The above-mentioned parameters ($t^{1/2}$ and β) may vary for different food systems but was assumed as constants in this study. Based on the molecular weights of glucose (180 g/mol) and maltodextrin (1152 g/mol), respective gastric emptying rates were evaluated, as shown in **Figure 3.13**. These rates were calculated to achieve 5 g inflow of carbohydrates into boundary 2 of jejunum geometry **(Figure 3.11A)**, by the end of 300 min. Inflow at boundary 5 of **Figure 3.11A** i.e., the absorption tube was set at zero for both the species (glucose and maltodextrin).

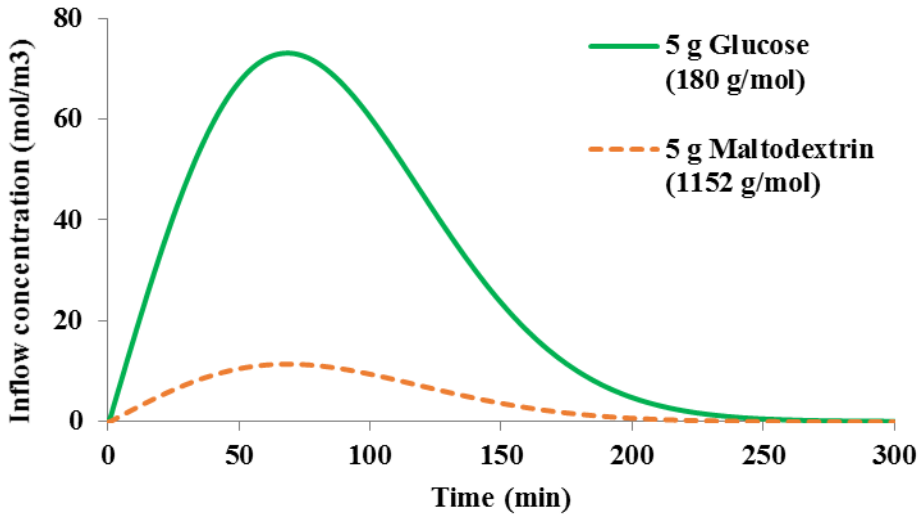

Figure 3.13: Glucose and maltodextrin – jejunal inflow concentration calculated based on gastric emptying rate equation (Eq. 3.15)

Outflow

Outflow boundary condition was set at boundaries 3 and 6 of **Figure 3.11A**, for allowing species to flow through the domains. **Eq. 3.16** was used to solve for the outflow boundary condition.

$$\boldsymbol{n \cdot D_i \nabla c_i = 0} \qquad \textbf{(3.16)}$$

Outflow concentration at boundary 6 of **Figure 3.11A** denotes the absorbed digested glucose concentration in the jejunal section. Outflow concentration at boundary 3 of **Figure 3.11A** was used as the inflow condition of SI tube in the ileum simulation. Also in the ileum simulation, outflow concertation of the absorption tube represents the absorbed digested glucose concentration in the ileal section.

No flux

No flux boundary condition was solved at boundary 7 of **Figure 3.11A**, based on **Eq. 3.17**, indicating no mass flux across that boundary.

$$\boldsymbol{n \cdot D_i \nabla c_i = 0} \qquad \textbf{(3.17)}$$

Thin Diffusion Barrier

Thin diffusion barrier boundary condition was used to model the internal layer, boundary 4 of **Figure 3.11A**, through which species mass was diffused across. This boundary condition helps in avoiding meshing thin structures. By defining the required thickness of the barrier (d_s) and the diffusion coefficient of a species (glucose) across the barrier ($D_{s,g}$), **Eq. 3.18** and **Eq. 3.19** were solved to simulate the thin diffusion barrier boundary condition. The diffusion coefficient of maltodextrin across the barrier was set at zero. In these equations, the subscript *i* and *o* refer to the inside and outside of the thin diffusion barrier. These equations denote that the flux in one direction is driven by concentration gradient across that respective direction and similarly solves for the opposite direction.

$$-\boldsymbol{n} \cdot \boldsymbol{J}_{g,i} = \frac{D_{s,g}}{d_s}\left(\boldsymbol{c}_{g,o-}\, \boldsymbol{c}_{g,i}\right) \tag{3.18}$$

$$-\boldsymbol{n} \cdot \boldsymbol{J}_{g,o} = \frac{D_{s,g}}{d_s}\left(\boldsymbol{c}_{g,i-}\, \boldsymbol{c}_{g,o}\right) \tag{3.19}$$

The thickness of the barrier was set at 2 mm. While solving the glucose diffusion model, the diffusivity value of glucose across the barrier ($D_{s,g}$) was varied separately in the jejunum simulation and the ileum simulation, to achieve the final amount of glucose absorption value obtained from the TIM-1-glucose-based experiments. The finalized diffusivity values were used in the maltodextrin diffusion model simulation.

3.8.3. Computational mesh

The computational mesh consisting of triangular elements was created for the jejunum diffusion model as shown in **Figure 3.11B**. The external and internal boundaries were built with smaller meshes with additional layers than the remaining geometry, for better simulation of concentration inflow, outflow, and diffusion across the thin diffusion barrier. The distance between each node varied from 23.2 μm to 1.56 mm depending on the complexity of geometry. For the 2-D axisymmetric jejunum diffusion model, the domain was discretized into 64,371 elements with 3,805 boundary elements. For the 2-D axisymmetric ileum diffusion model, the domain was discretized into 69,604 elements with 4,640 boundary elements. The governing equations were solved for these finite elements at appropriate nodes. The computational time needed to solve a jejunum or ileum diffusion flow model simulating 5 h of digestion was about 2 days on the Dell® workstation with Intel® Xeon® CPU E5-2643 0 processor @ 3.30 GHz and 64.0 GB RAM.

4. RESULTS AND DISCUSSION

A: *In vitro* experimental procedure

4.1. Viscosity of bolus

Using 5 g glucose or 5 g maltodextrin as the food base, the viscosity of the model bolus solution was varied by changing the proportions of glycerol and water. Five different glycerol to water ratios in w/w (0:100, 50:50, 70:30, 80:20, and 90:10), were used. Typical shear rate vs. shear stress curves for these solutions, obtained using a rheometer, are shown in **Figure 4.1**. The experiment was repeated thrice and the viscosity of each solution was evaluated by calculating the slope of the respective curve because all the curves were linear. The viscosity of model bolus solutions with 5g glucose or 5 g maltodextrin and different glycerol-water ratios are shown in **Figure 4.2** and the values are tabulated in **Table 4.1**.

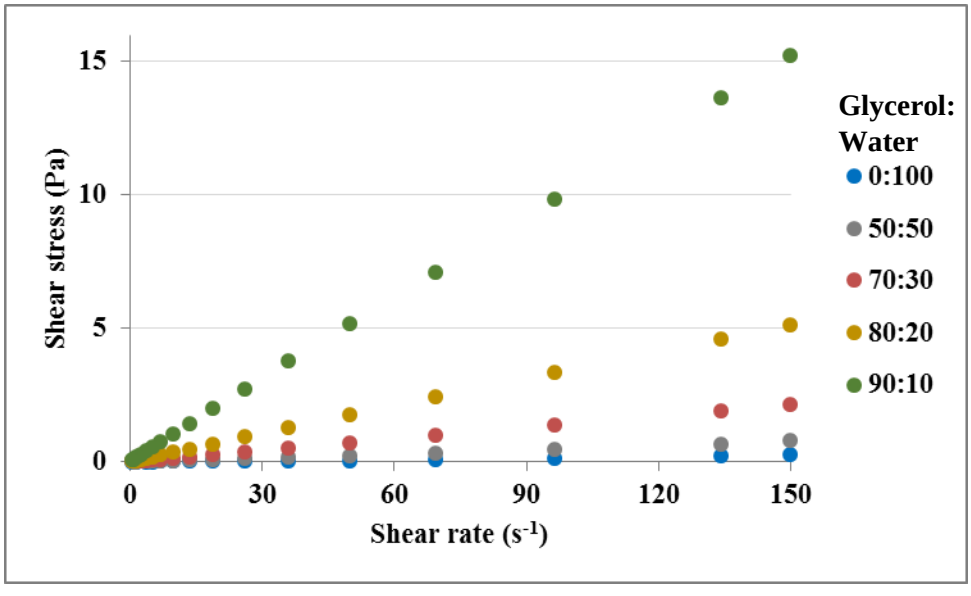

Figure 4.1: Typical shear rate vs. shear stress curves of glucose-based model bolus solutions varying in glycerol to water ratios

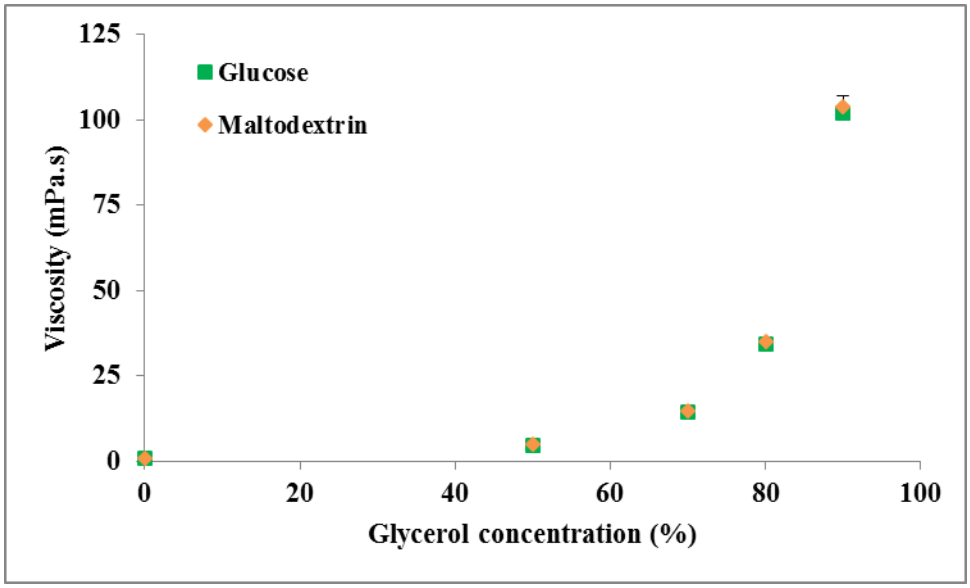

Figure 4.2: Viscosity of glucose-based and maltodextrin-based model bolus solutions as a function of glycerol concentration

Table 4.1: Viscosity of glucose-based and maltodextrin-based model bolus solutions

Glycerol : Water	Viscosity (mPa·s)	
	Glucose solution	Maltodextrin solution
0 : 100	1.00 ± 0.04	1.03 ± 0.10
50 : 50	4.83 ± 0.22	4.97 ± 0.19
70 : 30	14.57 ± 0.34	14.84 ± 0.60
80 : 20	34.51 ± 0.23	34.99 ± 1.23
90 : 10	102.11 ± 2.04	103.89 ± 3.85

From **Figure 4.2**, we could see that the viscosity of the solutions exponentially increased with an increase in glycerol concentration, which is in agreement with previous study **Segur and Oberstar (1951)**. In both glucose-based and maltodextrin-based solutions, when the glycerol to water ratio changed from 0:100 to 70:30 to 90:10, viscosity increased by an order of magnitude, i.e., from one to tens to hundreds, respectively. Therefore, these ratios were chosen to study the effect of bolus viscosity on the *in vitro* digestive process.

4.2. Glucose-based bolus

The initial viscosity values of the three glucose-based bolus solutions were 1.00 mPa·s ± 0.04 mPa·s, 14.57 mPa·s ± 0.34 mPa·s, and 102·11 mPa·s ± 2.04 mPa·s **(Table 4.1)**. For each run, the entire stomach section (300 g) in the TIM-1 system was filled with a specific solution. The digestion of this solution was conducted for 5 h. Since the carbohydrate used was glucose, no carbohydrate digestive reaction was involved. The objective of this experiment was to understand the effect of bolus viscosity on the nutrient (glucose) absorption process in the TIM-1 system. Samples that were absorbed in the jejunum and ileum sections of the TIM-1 system and the unabsorbed efflux were collected periodically. Glucose concentrations in the collected samples were evaluated using the glucose assay kit. A correlation between the absorbance (at 540 nm) value obtained using the kit and the glucose concertation of the known samples was developed (**Figure 4.3)** and used as a standard curve. The glucose absorption curves of glucose-based bolus solutions with three different initial viscosity values obtained from the jejunal and ileal sections of the TIM-1 system are shown in **Figure 4.4 and Figure 4.5**.

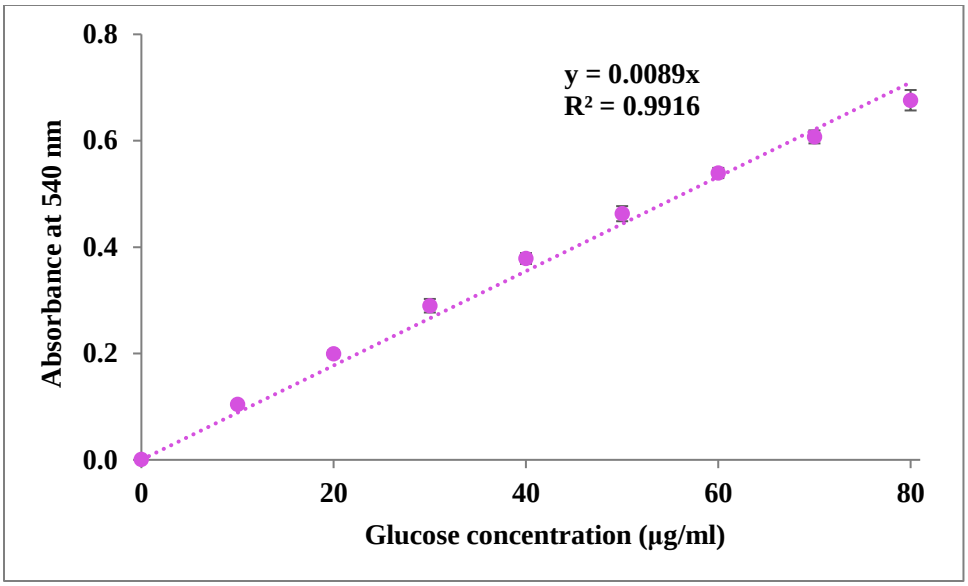

Figure 4.3: Standard curve used to convert the absorbance value at 540 nm to glucose concertation, developed using the glucose assay kit

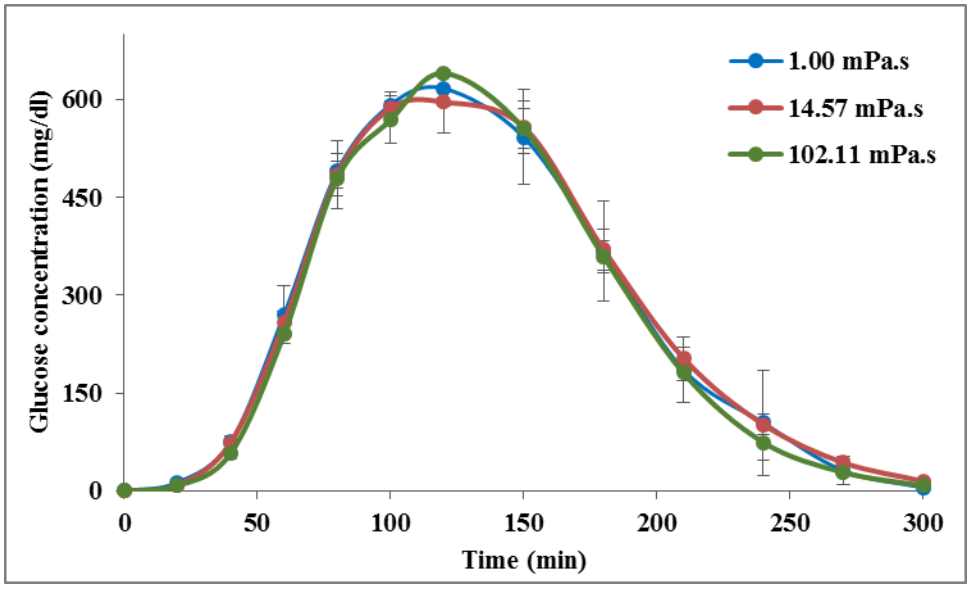

Figure 4.4: Glucose absorption curves of glucose-based bolus (three initial viscosity values) obtained in the jejunal section of the TIM-1 system

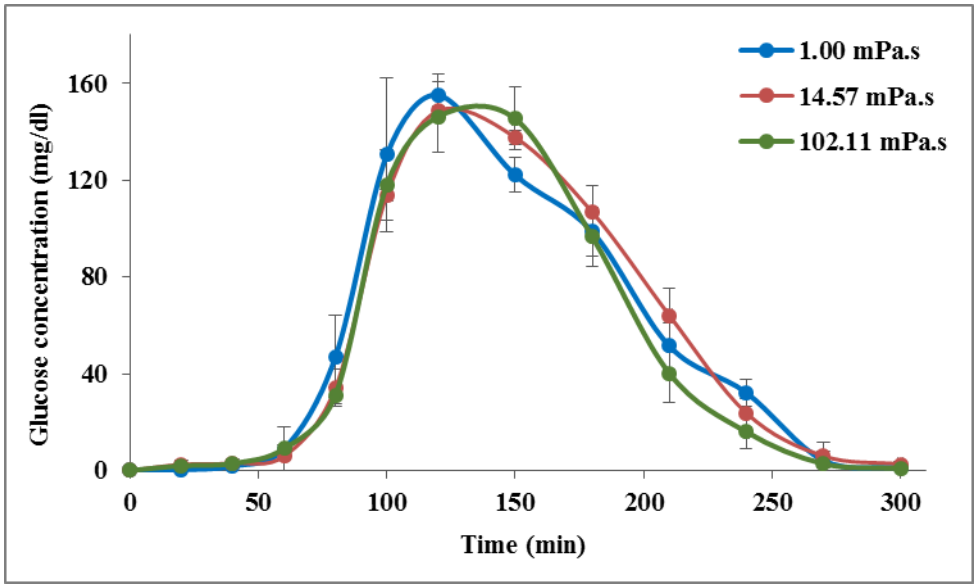

Figure 4.5: Glucose absorption curves of glucose-based bolus (three initial viscosity values) obtained in the ileal section of the TIM-1 system

In both the sections, there was no significant difference between the three glucose absorption curves indicating that glycerol-induced viscosity did not significantly affect the glucose absorption process in the TIM-1 system. Previous *in vitro* studies **(Ferrua and Singh, 2010, Tharakan et al., 2010; AlHasawi et al., 2017)** have reported that increase in bolus viscosity delayed the gastric emptying rate, and an increase in intestinal content viscosity reduced the nutrient absorption rate. However, one of the limitations of the TIM-1 system is that the transit time between the sections are fixed, independent on the bolus viscosity **(Eq. 3.1)**. Also, all three bolus solutions might have resulted in low-viscous intestinal content to significantly affect the glucose absorption process, which is discussed in section 4.4.1. Hence, the presence of glycerol in the gastrointestinal content did not significantly affected the glucose absorption process. In both sections, the highest glucose absorption was observed at 120 min for all three bolus solutions. In the jejunal section, the

highest glucose concentration of the absorbed samples at initial bolus viscosity values of 1.00 mPa·s, 14.57 mPa·s, and 102·11 mPa.s were 616.95 mg/dl ± 33.63 mg/dl, 596.34 mg/dl ± 58.24 mg/dl, and 640.52 mg/dl ± 6.73 mg/dl, respectively. In the ileal section, the highest glucose concentration of the absorbed samples at the same initial viscosity values were 161.76 mg/dl ± 13.49 mg/dl, 148.57 mg/dl ± 2.15 mg/dl, and 146.23 mg/dl ± 17.83 mg/dl, respectively. The absorbed-glucose concentrations were much higher in the jejunal section than in the ileal section. As the jejunal section precedes the ileal section, more glucose was absorbed in the jejunal section. A Similar pattern was observed in many studies with the TIM-1 system and other *in vitro* digestive models **(Speranza et al., 2013**; **Nimalaratne et al., 2015)**. Even while observing *in vivo* human digestive system, most of the macronutrients are absorbed in the proximal portion of the jejunum **(Borgstrom et al., 1957)**.

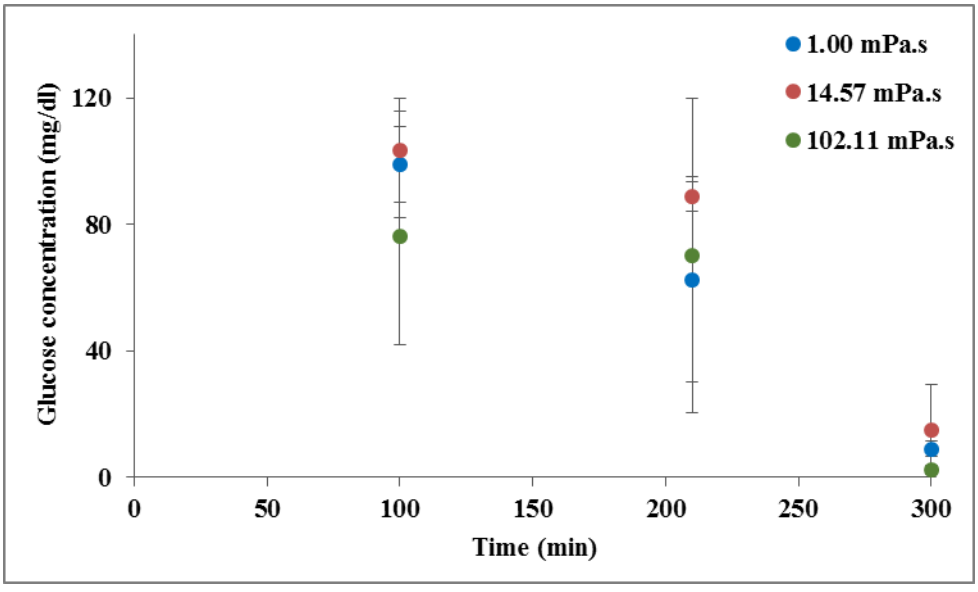

Figure 4.6: Glucose concentrations of unabsorbed efflux obtained during the digestion of glucose-base bolus (three initial viscosity values) in the TIM-1 system

For all three bolus solutions, the glucose concentrations of the unabsorbed efflux decreased with the digestion time, as shown in **Figure 4.6**. By monitoring the volume of collected samples, the mass of glucose absorbed and unabsorbed were calculated **(Table 4.2)**. It was observed that initial bolus viscosity of glucose-based solutions did not significantly affect the amounts of glucose absorbed in the jejunal section, ileal section, and the unabsorbed efflux. For this bolus system, approximately 78% of glucose was absorbed in the jejunal section, 16.5% of glucose was absorbed in the ileal section, and 5.5% glucose was unabsorbed and excreted out of the system.

Table 4.2. Mass of glucose absorbed in the jejunal and ileal sections and in unabsorbed efflux during digestion of 5 g glucose-based bolus (three initial viscosity values) in the TIM-1 system

Glucose-based bolus initial viscosity	Absorbed glucose (g)		Unabsorbed Efflux (g)
	Jejunum	Ileum	
1.00 mPa·s	3.67 ± 0.43^{a}	0.78 ± 0.11^{b}	0.26 ± 0.02^{c}
14.57 mPa·s	3.54 ± 0.38^{a}	0.76 ± 0.70^{b}	0.31 ± 0.01^{c}
102.11 mPa·s	3.54 ± 0.20^{a}	0.71 ± 0.10^{b}	0.24 ± 0.05^{c}

Numbers across a column that do not share the same superscript letter are significantly different based on the Tukey HSD test ($p<0.05$)

4.3. Maltodextrin-based bolus

The initial viscosity values of the maltodextrin-based bolus solutions were 1.03 mPa·s ± 0.10 mPa·s, 14.84 mPa·s ± 0.60 mPa·s, and 103.89 mPa·s ± 3.85 mPa·s **(Table 4.1)**. Since the carbohydrate used was maltodextrin, the amylase digestive reactions would break down maltodextrin to glucose and maltose. The objective of this experiment was to understand the effect of viscosity of bolus on the digestive process in the TIM-1 system. Samples that were absorbed in the jejunum and ileum sections of the TIM-1 system and the unabsorbed efflux were collected periodically. The total-glucose (glucose already present plus glucose converted from maltose) concentrations in the collected samples were evaluated using the maltose assay kit. A correlation between the absorbance (at 570 nm) value obtained using the kit and the maltose (total-glucose) concertation of the known samples was developed (**Figure 4.7)** and used as a standard curve.

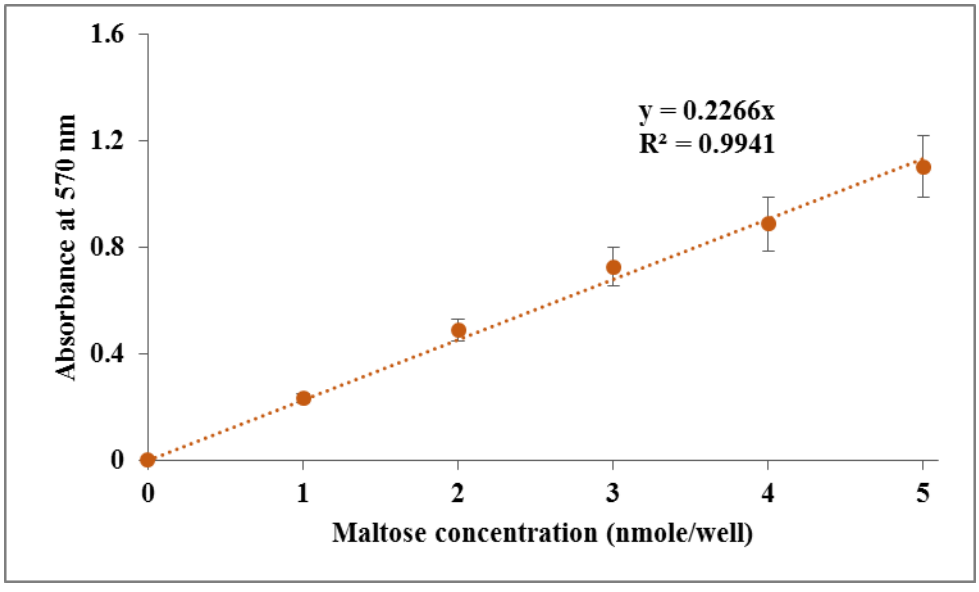

Figure 4.7: Standard curve used to convert the absorbance value at 570 nm to maltose (total-glucose) concentration, developed using the maltose assay kit

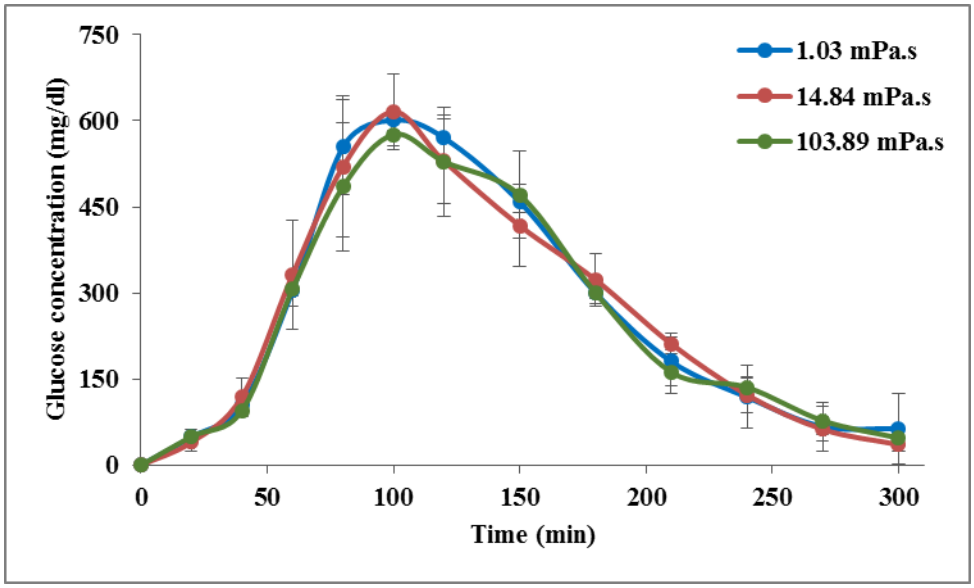

Figure 4.8: Total-glucose absorption curves of maltodextrin-based bolus (three initial viscosity values) obtained in the jejunal section of the TIM-1 system

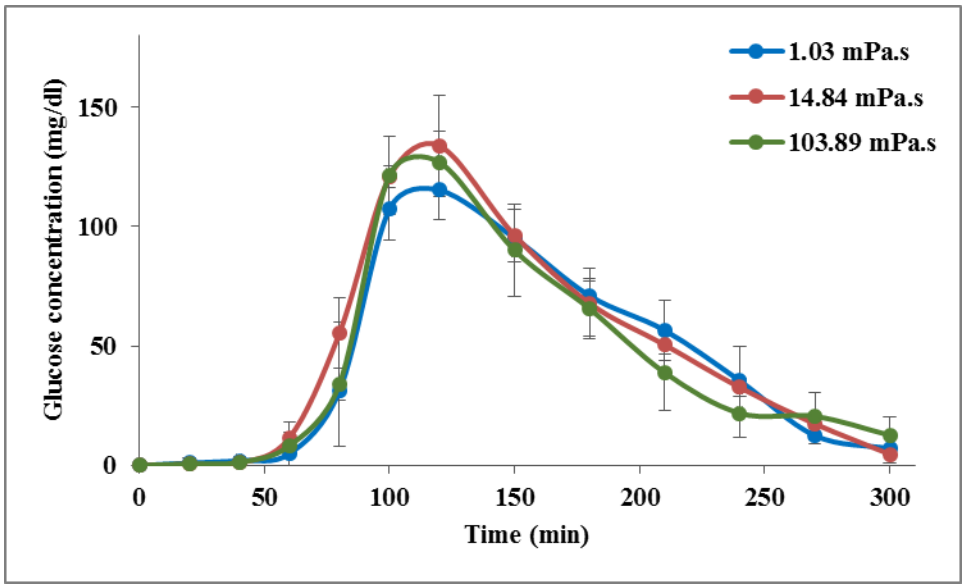

Figure 4.9: Total-glucose absorption curves of maltodextrin-based bolus (three initial viscosity values) obtained in the ileal section of the TIM-1 system

The total-glucose absorption curves of maltodextrin-based bolus solutions obtained from the jejunal and ileal sections of the TIM-1 system are shown in **Figure 4.8 and Figure 4.9**, respectively. These curves follow a similar trend as the curves of glucose-based bolus solutions **(Figure 4.4 and Figure 4.5)**. No significant difference between the three total-glucose curves was observed. This trend indicated that the glycerol-induced viscosity did not significantly affect the nutrient absorption process in the TIM-1 system. For all three bolus solutions, the highest total-glucose absorption was observed at 100 min in the jejunal section and at 120 min in the ileal section. In the jejunal section, the highest total-glucose concertation of the absorbed samples at initial bolus viscosity values of 1.03 mPa·s, 14.84 mPa·s, and 103.89 mPa·s were 601.17 mg/dl ± 5.96 mg/dl, 615.88 mg/dl ± 65.14 mg/dl, and 576.09 mg/dl ± 1.83 mg/dl, respectively. In the ileal section, the highest total-glucose concentration of the absorbed samples at the same initial bolus viscosity values were 115.29 mg/dl ± 15.00 mg/dl, 133.92 mg/dl ± 25.80 mg/dl, and 125.24 mg/dl ± 17.93 mg/dl, respectively. As seen in the results of glucose-based bolus solutions, more glucose was absorbed in the jejunal section than in the ileal section. For all three bolus solutions, the total-glucose concentrations of the unabsorbed efflux decreased with the digestion time, as shown in **Figure 4.10**. By monitoring the volume of samples collected, the masses of total-glucose absorbed and unabsorbed were calculated **(Table 4.3)**. It was observed that the initial bolus viscosity of maltodextrin-based solutions did not significantly affect the amounts of total-glucose absorbed. For this bolus system, approximately 82% of total-glucose was absorbed in the jejunal section, 14.5% of total-glucose was absorbed in the ileal section, and 3.5% total-glucose was unabsorbed and ejected out of the system.

Table 4.3. Mass of glucose absorbed in the jejunal and ileal sections and in unabsorbed efflux during digestion of 5 g maltodextrin-based bolus (three initial viscosity values) in the TIM-1 system

Maltodextrin-based bolus initial viscosity	Absorbed glucose (g)				Unabsorbed Efflux (g)	
	Jejunum		Ileum			
	Total-glucose	Base-glucose	Total-glucose	Base-glucose	Total-glucose	Base-glucose
1.03 mPa·s	3.74 ± 0.39^{a}	1.07 ± 0.16^{b}	0.66 ± 0.06^{d}	0.21 ± 0.03^{e}	0.17 ± 0.01^{g}	0.08 ± 0.004^{i}
14.84 mPa·s	3.82 ± 0.27^{a}	0.69 ± 0.07^{c}	0.68 ± 0.06^{d}	0.14 ± 0.01^{f}	$0.16 \pm 0.02^{g,h}$	0.04 ± 0.003^{j}
103.89 mPa·s	3.61 ± 0.08^{a}	0.69 ± 0.09^{c}	0.62 ± 0.08^{d}	0.13 ± 0.03^{f}	0.13 ± 0.01^{h}	0.03 ± 0.005^{j}

Numbers across a column that do not share the same superscript letter are significantly different based on the Tukey HSD test ($p<0.05$)

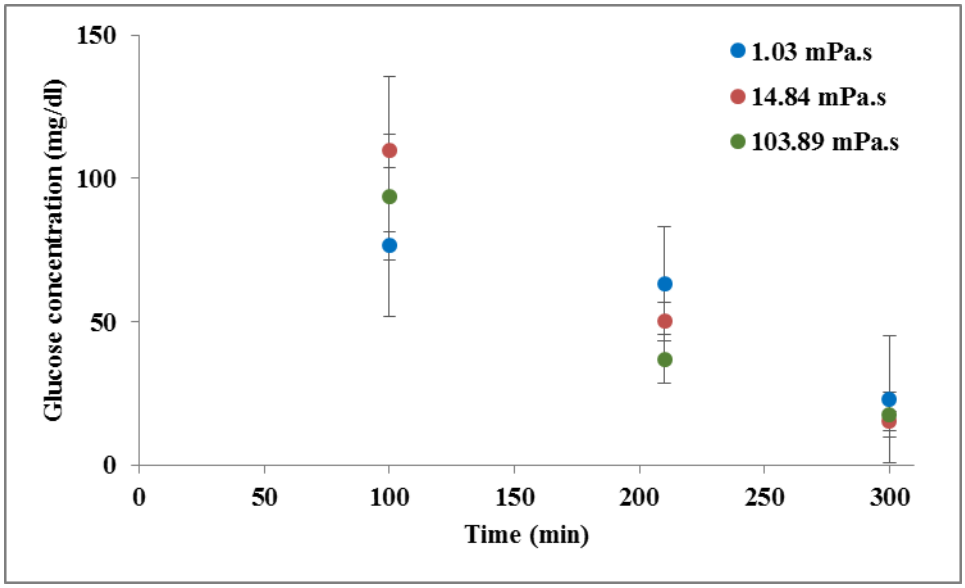

Figure 4.10: Total-glucose concentrations of unabsorbed efflux obtained during the digestion of maltodextrin-base bolus (three initial viscosity values) in the TIM-1 system

The base-glucose (glucose already present in the sample) absorption curves for maltodextrin-based bolus solutions with three different initial viscosity values obtained from the jejunal and ileal sections are shown in **Figure 4.11** and **Figure 4.12**. In both these figures, it can be observed that more glucose units were broken down from maltodextrin when the bolus had no glycerol. This pattern suggested that glycerol-induced viscosity affected carbohydrate digestive reactions. A possible reason for this could be that high viscous environment might have limited the motility of digestive enzymes and their access to the starch substrate **(Rainbird and Low, 1986; Tharakan, 2010)**. For all three bolus solutions, the highest base-glucose absorption rate was observed at 80 min in the jejunal section and at 120 min in the ileal section.

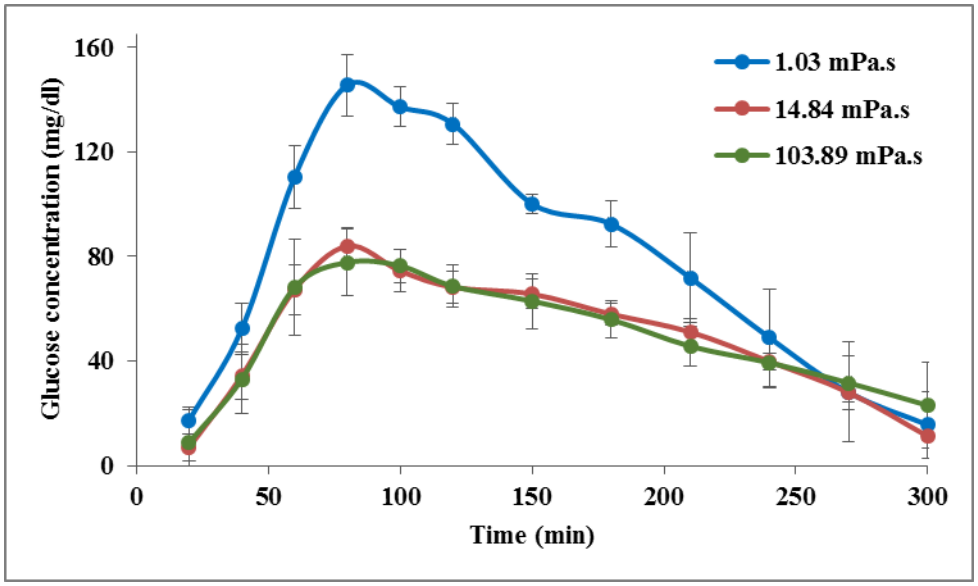

Figure 4.11: Base-glucose absorption curves of maltodextrin-based bolus (three initial viscosity values) obtained in the jejunal section of the TIM-1 system

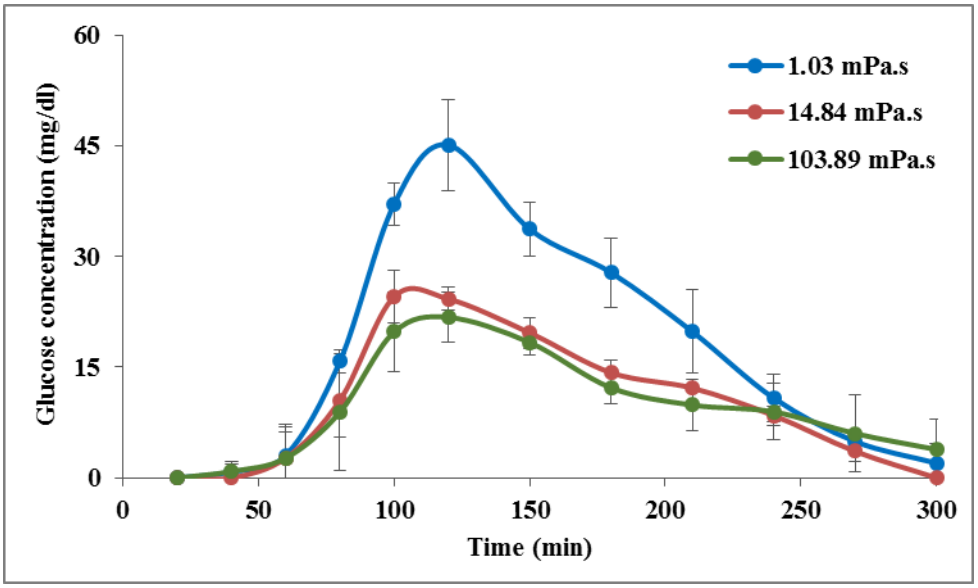

Figure 4.12: Base-glucose absorption curves of maltodextrin-based bolus (three initial viscosity values) obtained in the ileal section of the TIM-1 system

In the jejunal section, the highest base-glucose concentration of the absorbed samples at initial viscosity values of 1.03 mPa·s, 14.84 mPa·s, and 103.89 mPa·s were 145.73 mg/dl ± 13.60 mg/dl, 85.96 mg/dl ± 10.01 mg/dl, and 77.70 mg/dl ± 9.85 mg/dl respectively. In the ileal section, the highest base-glucose concentration of the absorbed samples at the same initial bolus viscosity values were 41.67 mg/dl ± 10.94 mg/dl, 24.90 mg/dl ± 1.91 mg/dl, and 24.07 mg/dl ± 4.25 mg/dl respectively. For all three bolus solutions, the base-glucose concentrations of the unabsorbed efflux decreased with the digestion time as shown in **Figure 4.13**.

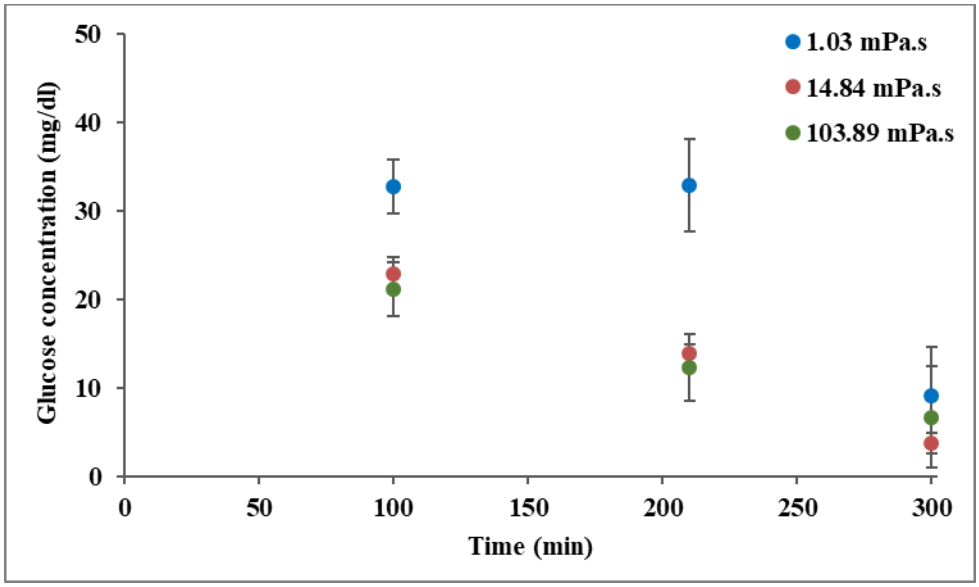

Figure 4.13: Base-glucose concentrations of unabsorbed efflux obtained during the digestion of maltodextrin-base bolus (three initial viscosity values) in the TIM-1 system

By monitoring the volume of samples collected, the masses of base-glucose absorbed and unabsorbed were calculated **(Table 4.3)**. A significant difference in base-glucose absorption was observed between the bolus solutions with and without glycerol. It can be observed that the initial bolus viscosity non-linearly influenced the maltodextrin digestive process. A fourteen-fold increase in initial bolus viscosity (from 1.03 mPa·s to 14.84 mPa·s) decreased the maltodextrin to base-glucose conversion by 35%. However, beyond 14.84 mPa.s, a seven-fold increase in the initial bolus viscosity did not significantly affect the digestive reactions. Based on these results, it can be concluded that there could be a critical viscosity limit (~15 mPa·s) for this bolus system, until which the viscosity significantly influenced the maltodextrin digestion and beyond that, no significant effect was observed. A similar non-linear pattern was observed by **Hardacre et al. (2016)** while analyzing the effect of shear rate on *in vitro* carbohydrate digestion in intestinal content. They reported that an increase in shear rate from 0.1 s^{-1} to 1 s^{-1}, significantly increased the rate of carbohydrate digestion. However, increasing the shear rate further from 1 s^{-1} to 10 s^{-1} did not significantly increase the rate of carbohydrate digestion. The rate and extent of carbohydrate digestion have a major effect on the postprandial glucose levels **(Englyst et al., 1996; Goni et al., 1997)**. Hence, understanding the effect of bolus viscosity on carbohydrate digestion could be useful in reducing available glucose for intestinal absorption.

4.4. Fluorescence viscosity correlation

A specific concentration (10 μM) of Fast Green was added to the model bolus solutions filled in transparent glass tubes. After negating the effect of background signals obtained from control tubes, the normalized fluorescence signals obtained from one set of the model glucose-based and one set of the model maltodextrin-based bolus solutions are shown in **Figure 4.14** and **Figure 4.16**, respectively. The fluorescence data of these two sets of solutions were similar. It can be seen that the fluorescence intensity increased with an increase in the viscosity of the solution. The normalized peak intensity of model glucose-based bolus solutions at viscosity values of 1.00 mPa·s ± 0.04 mPa·s , 4.83 mPa·s ± 0.22 mPa·s, 14.57 mPa·s ± 0.34 mPa·s, 34.51 mPa·s ± 0.23 mPa·s, and 102.11 mPa·s ± 2.04 mPa·s were 0.03 ± 0.00, 0.10 ± 0.01, 0.26 ± 0.02, 0.47 ± 0.01, and 1.00 ± 0.03, respectively. The normalized peak intensity of model maltodextrin-based bolus solutions at viscosity values of 1.03 mPa·s ± 0.10 mPa·s, 4.97 mPa·s ± 0.19 mPa·s, 14.84 mPa·s ±0.60 mPa·s, 34.99 mPa·s ± 1.23 mPa·s, and 103.89 mPa·s ± 3.85 mPa·s were 0.03 ± 0.01, 0.11 ± 0.01, 0.24 ± 0.02, 0.48 ± 0.03, and 1.00 ± 0.03, respectively. **Figure 4.15** and **Figure 4.17** correlate the viscosity of the model glucose-based and model maltodextrin-based bolus solutions with their respective normalized peak intensity values (the average of maximum normalized intensity achieved by a solution). From these figures, it could be observed that the normalized peak intensity exponentially increased with an increase in the viscosity of the solution. The correlations between the viscosity of solutions and the normalized peak intensity values were used to predict the viscosity of gastrointestinal content.

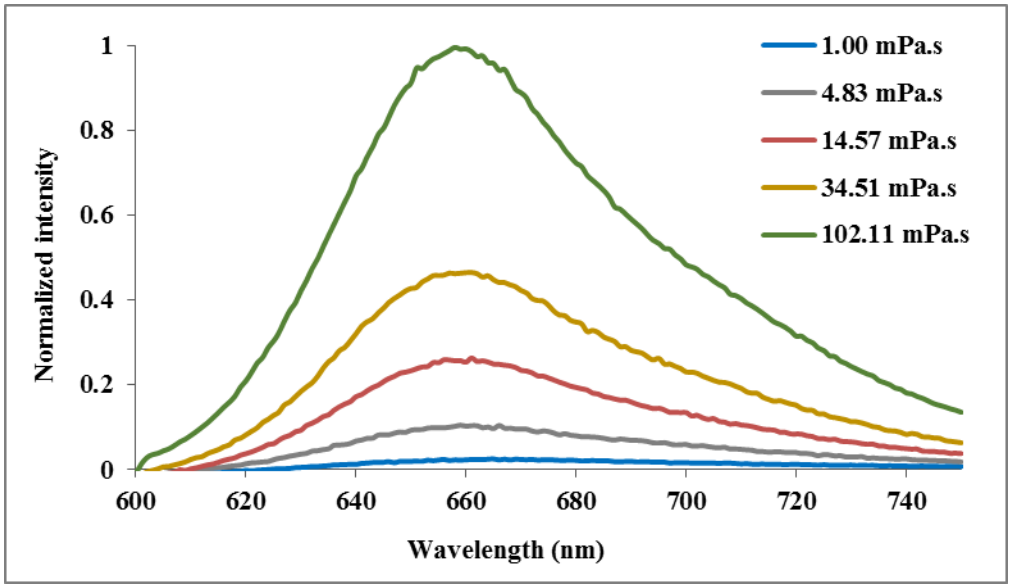

Figure 4.14: Normalized emission spectra of Fast Green in model glucose-based bolus solutions with different viscosity values, after subtracting background fluorescence signal

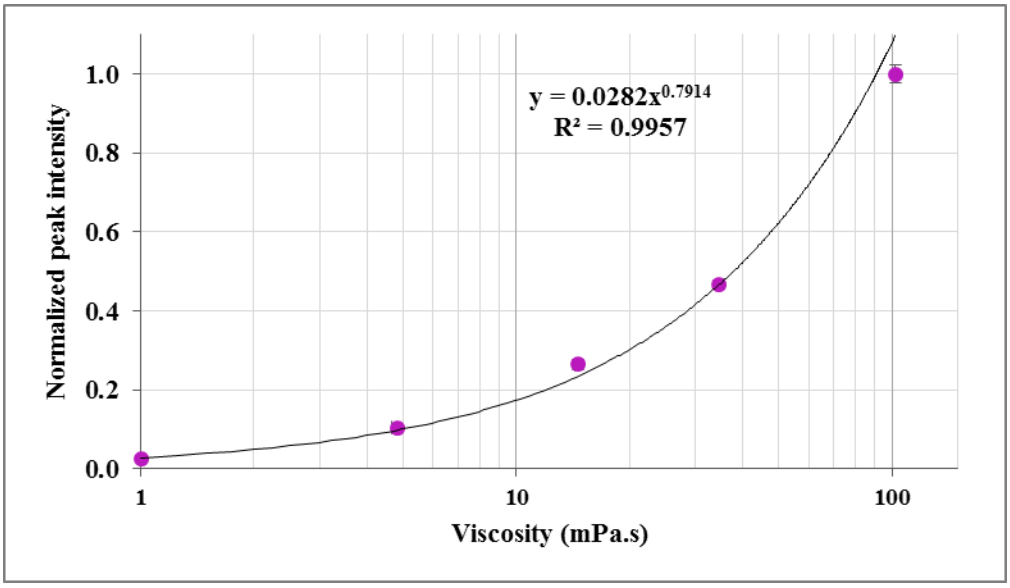

Figure 4.15: Correlation between the viscosity of model glucose-based bolus solutions and their corresponding normalized peak intensity values

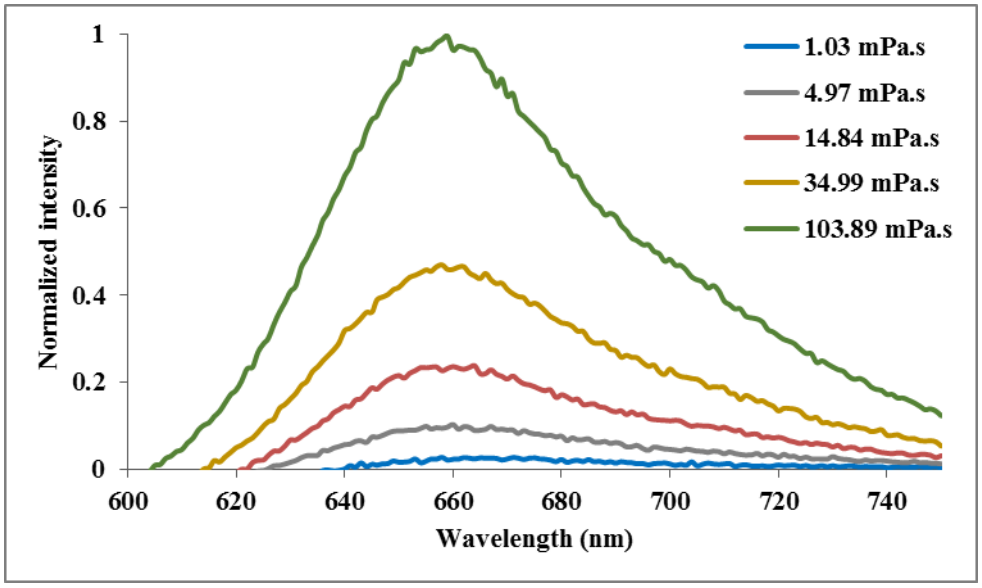

Figure 4.16: Normalized emission spectra of Fast Green in model maltodextrin-based bolus solutions with different viscosity values, after subtracting background fluorescence signal

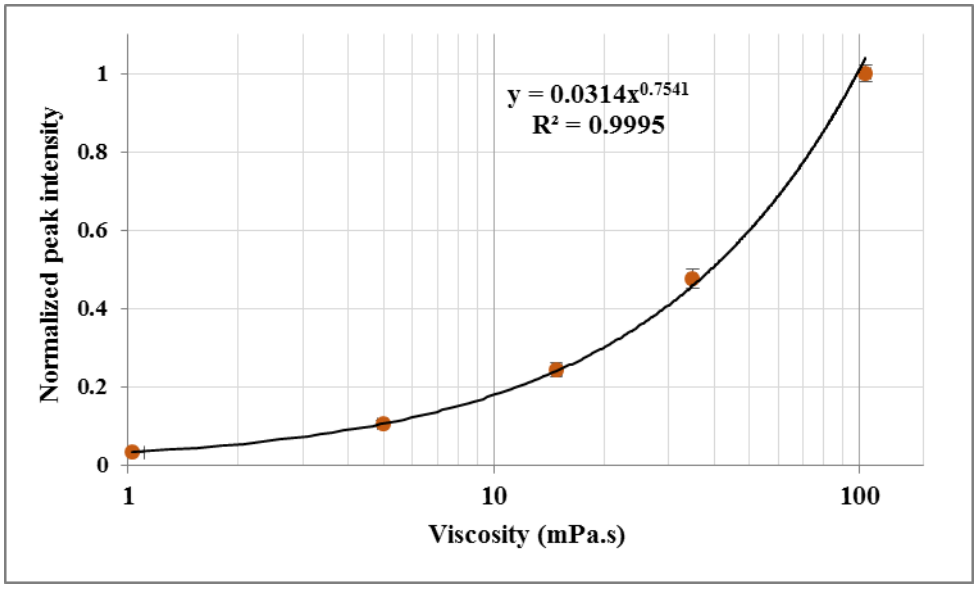

Figure 4.17: Correlation between the viscosity of model maltodextrin-based bolus solutions and their corresponding normalized peak intensity values

4.4.1. In-line fluorescence intensity monitoring

Fluorescence emission spectra were recorded in the TIM-1system during digestion of glucose-based and maltodextrin-based bolus solutions with different initial viscosity values. For each bolus system, the signals were monitored at the four sections of the TIM-1 system, namely stomach, duodenum, jejunum, and ileum. Control runs were performed for the respective bolus composition with no dye in the entire system. After negating the signals obtained from the control experiment, the normalized peak intensity as a function of time at each section of the TIM-1 system was plotted, as shown in **Figures 4.18** to **4.25**.

Figure 4.18 shows the changes in normalized peak intensity of gastric content during digestion of three maltodextrin-based bolus solutions in the TIM-1 system. These curves can be interpreted as the viscosity changing pattern of the gastric content during digestion of the three bolus solutions. It can be observed that when the initial bolus viscosity was 1.03 mPa·s, the viscosity of the gastric content remained almost the same throughout the entire digestion period. When the initial viscosity was 14.84 mPa·s, the viscosity of the gastric content gradually decreased to approximately 1 mPa·s. In the case of the highly viscous bolus (103.89 mPa·s), the viscosity of the gastric content drastically dropped by 70% within an hour and then gradually decreased. Similar viscosity changing patterns were reported by **Villemejane et al. (2015) and AlHasawi et al. (2017)**, while analyzing the gastric content in a TIM-1 system using a dynamic rheometer and the Fast Green dye, respectively.

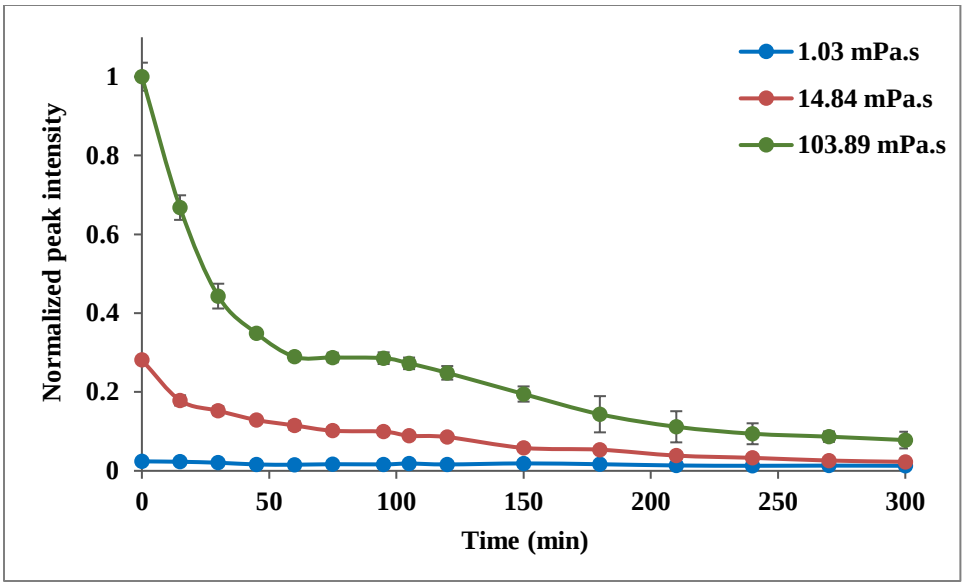

Figure 4.18: Normalized peak intensity of Fast Green periodically measured at the stomach section of the TIM-1 system during the digestion of maltodextrin-based bolus with three initial viscosity values

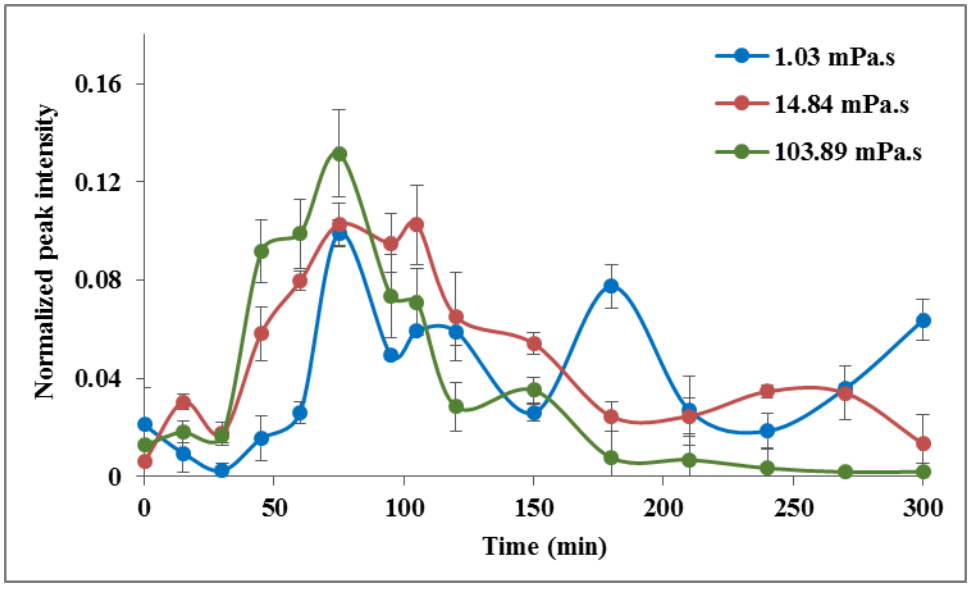

Figure 4.19: Normalized peak intensity of Fast Green periodically measured at the duodenal section of the TIM-1 system during the digestion of maltodextrin-based bolus with three initial viscosity values

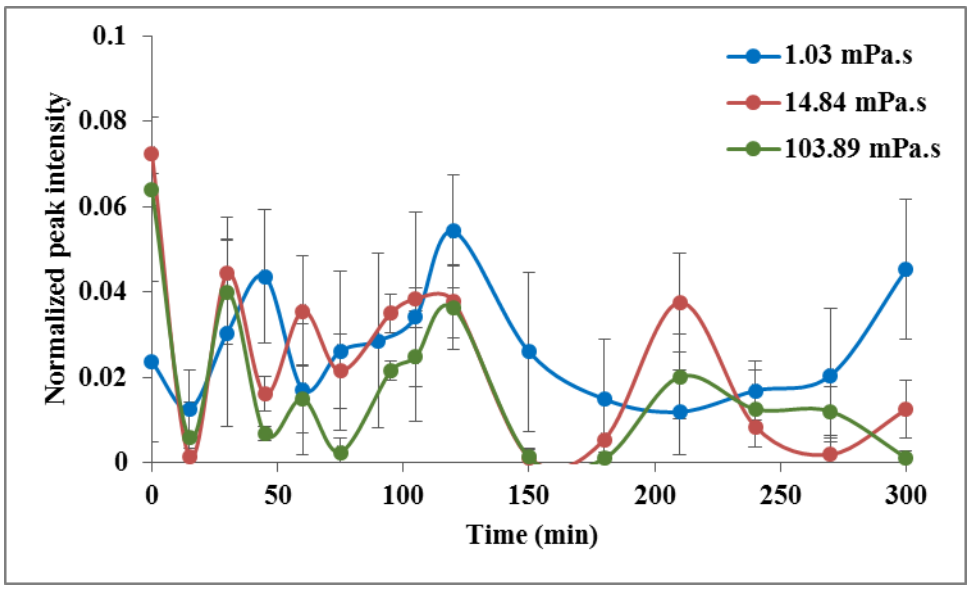

Figure 4.20: Normalized peak intensity of Fast Green periodically measured at the jejunal section of the TIM-1 system during the digestion of maltodextrin-based bolus with three initial viscosity values

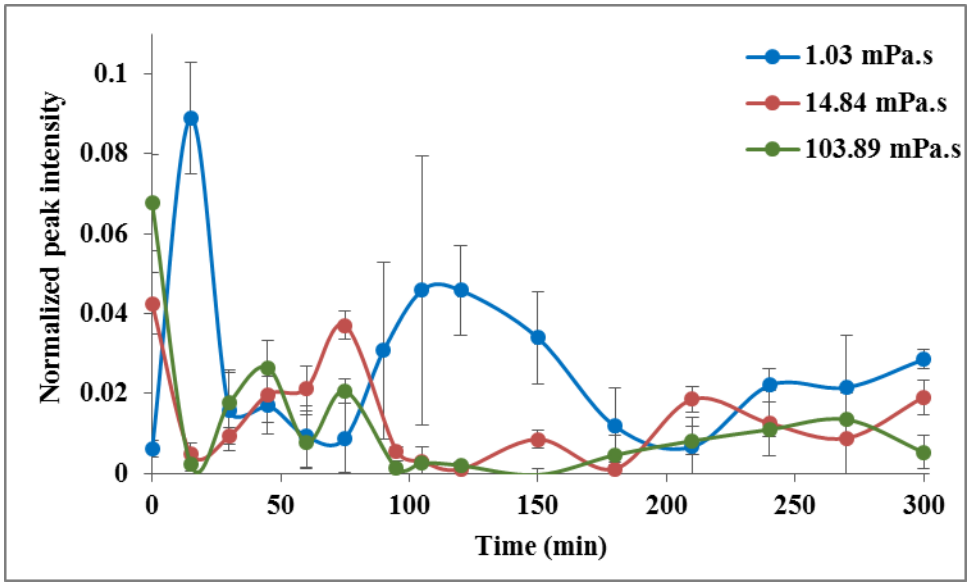

Figure 4.21: Normalized peak intensity of Fast Green periodically measured at the ileal section of the TIM-1 system during the digestion of maltodextrin-based bolus with three initial viscosity values

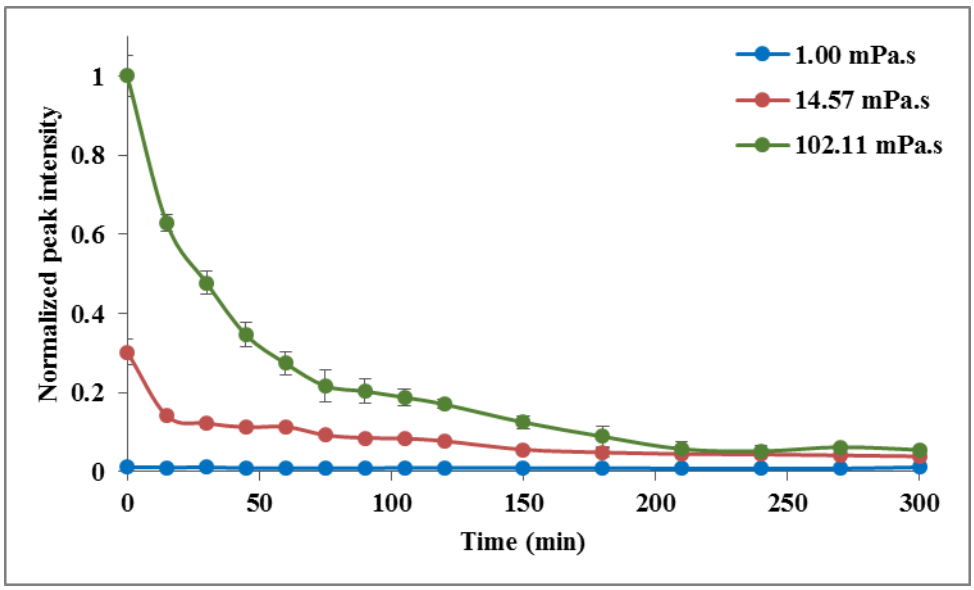

Figure 4.22: Normalized peak intensity of Fast Green periodically measured at the stomach section of the TIM-1 system during the digestion of glucose-based bolus with three initial viscosity values

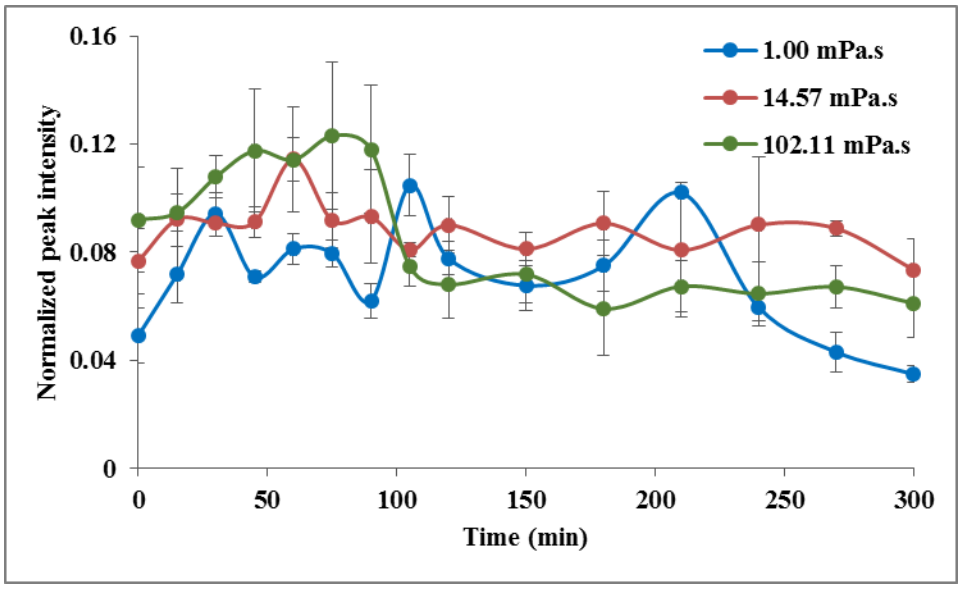

Figure 4.23: Normalized peak intensity of Fast Green periodically measured at the duodenal section of the TIM-1 system during the digestion of glucose-based bolus with three initial viscosity values

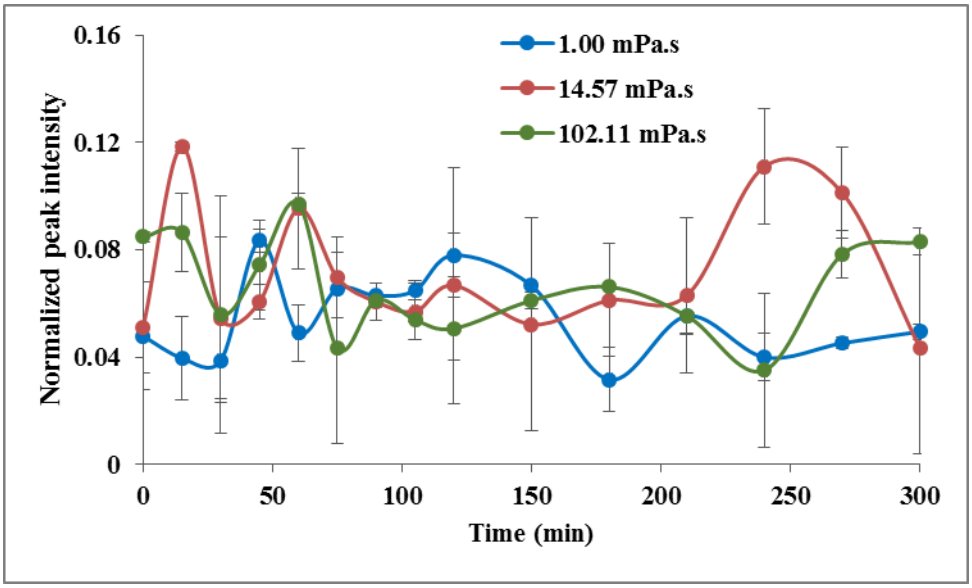

Figure 4.24: Normalized peak intensity of Fast Green periodically measured at the jejunal section of the TIM-1 system during the digestion of glucose-based bolus with three initial viscosity values

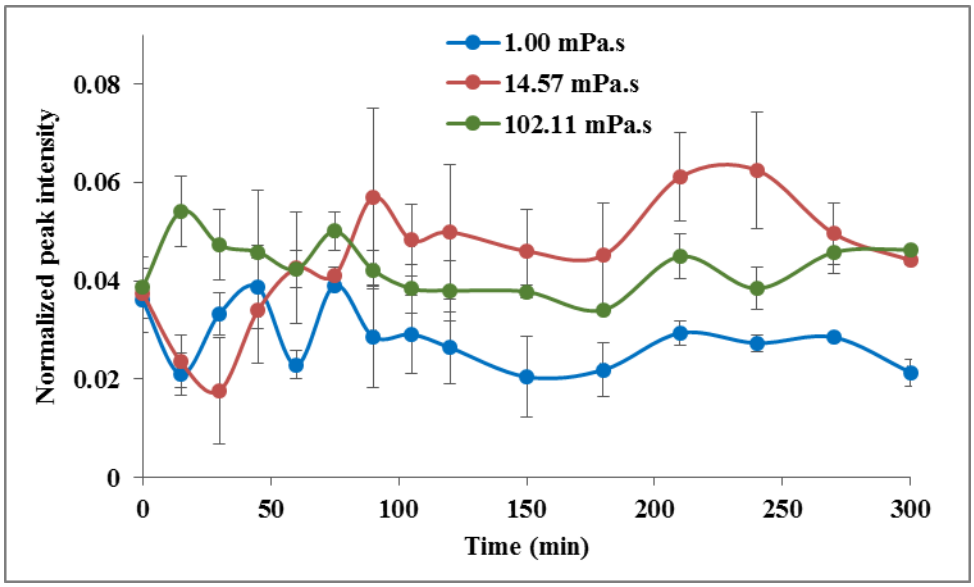

Figure 4.25: Normalized peak intensity of Fast Green periodically measured at the ileal section of the TIM-1 system during the digestion of glucose-based bolus with three initial viscosity values

Figure 4.19 shows the changes in normalized peak intensity of duodenal content during digestion of three maltodextrin-based bolus solutions. These curves can be interpreted as the viscosity changing pattern of the duodenal content during digestion. The viscosity of duodenal content was comparatively lower than the gastric content which can be inferred from the low normalized peak intensity range. Based on the viscosity-normalized peak intensity correlation, the normalized peak intensity of 0.12 approximately corresponds to 6 mPa·s. For all three bolus solutions, the viscosity changing pattern followed a similar trend. Initially, the viscosity was very low, and at 90 min, there was a sudden increase in viscosity, and then it dropped. The possible reason for this could be the initiation of gastric content transfer from the stomach section and the secretion of high-viscous bile at 90 min which might have increased the viscosity of duodenal content. Later the viscosity might have been reduced due to the secretion of less-viscous electrolyte solutions. Similar viscosity changing patterns were reported by **Villemejane et al. (2015) and AlHasawi et al. (2017)** while analyzing the viscosity of duodenal content in a TIM-1 system.

In the jejunal **(Figure 4.20)** and ileal **(Figure 4.21)** sections, the viscosity of intestinal content was very low to influence the molecular rotor property of this particular dye, Fast Green. It can be inferred that the viscosity of the intestinal content might be closer to 1 mPa·s for all the three bolus solutions during the entire digestion period. Similar low viscosity values were reported by **Villemejane et al. (2015) and AlHasawi et al. (2017)**. Such low viscosity values might be the reason for obtaining overlapping total-glucose absorption curves independent of the initial bolus viscosity. Fluorescence-based viscosity

measurements confirmed that the presence of glycerol in the bolus did not significantly affect the viscosity of jejunal and ileal content in the TIM-1 system. These fluorescence data provided a basic understanding of the influence of the bolus viscosity on the viscosity of gastrointestinal content during and the subsequent nutrient absorption process.

The fluorescence peak intensity patterns monitored during the digestion of glucose-based bolus solutions **(Figures 4.22** to **4.25)** were similar to the patterns monitored discussed for maltodextrin-based bolus solutions (**Figures 4.18** to **4.21**). **Figure 4.24** and **Figure 4.25** indicate that the viscosity on jejunal and ileal content was too low. This might be the reason for obtaining overlapping glucose absorption curves. This confirmed that the glycerol-induced viscosity did not significantly affect the rate of glucose absorption in the TIM-1 system. These fluorescence data provided a basic understanding of the influence of the bolus viscosity on the viscosity of gastrointestinal content during and the subsequent nutrient absorption process.

B: Numerical simulation

4.5. Fluid flow model predictions

A 2-D axisymmetric jejunum fluid flow model (radius: 8.65 mm and length: 1.2 m) and an ileum fluid flow model (radius: 8.65 mm and length: 1.8 m) were developed to simulate the fluid flow (based on the continuity equation and the Navier-Stokes equation) due to peristalsis. Intestinal motility parameters were obtained from the literature and the peristaltic wave condition was imposed on the walls of the geometry as described earlier. Fully developed velocity profile in a section of the jejunum fluid flow model, at different time intervals between 63 s and 70 s, induced by a peristaltic wave, is shown in **Figure 4.26**. In the figure, the colors represent velocity levels, blue being the lowest and red being the highest. Small black arrows indicate the direction of fluid flow. The maximum fluid velocity observed was approximately 3 mm/s and the average fluid velocity was approximately 0.24 mm/s. Similarly, the ileum fluid flow model was developed and analyzed. To validate the intestinal geometry and motility parameters obtained from the literature **(Ohkubo et al., 2013)**, the intestinal diameter at the center of the geometry (z = 60 cm) was compared with the reported graph and the results are shown in **Figure 4.27**. On considering the limitations in matching the real-time intestinal diameter variations, the fluid flow model simulated the peristaltic wave with an average error of 1.8 mm. The assumed parameters used in this numerical model: contraction cycle (7 s) and amplitude (78%) could be used in the future to simulate intestinal motility. The numerical fluid flow model was successfully developed to predict the velocity profile induced by peristalsis.

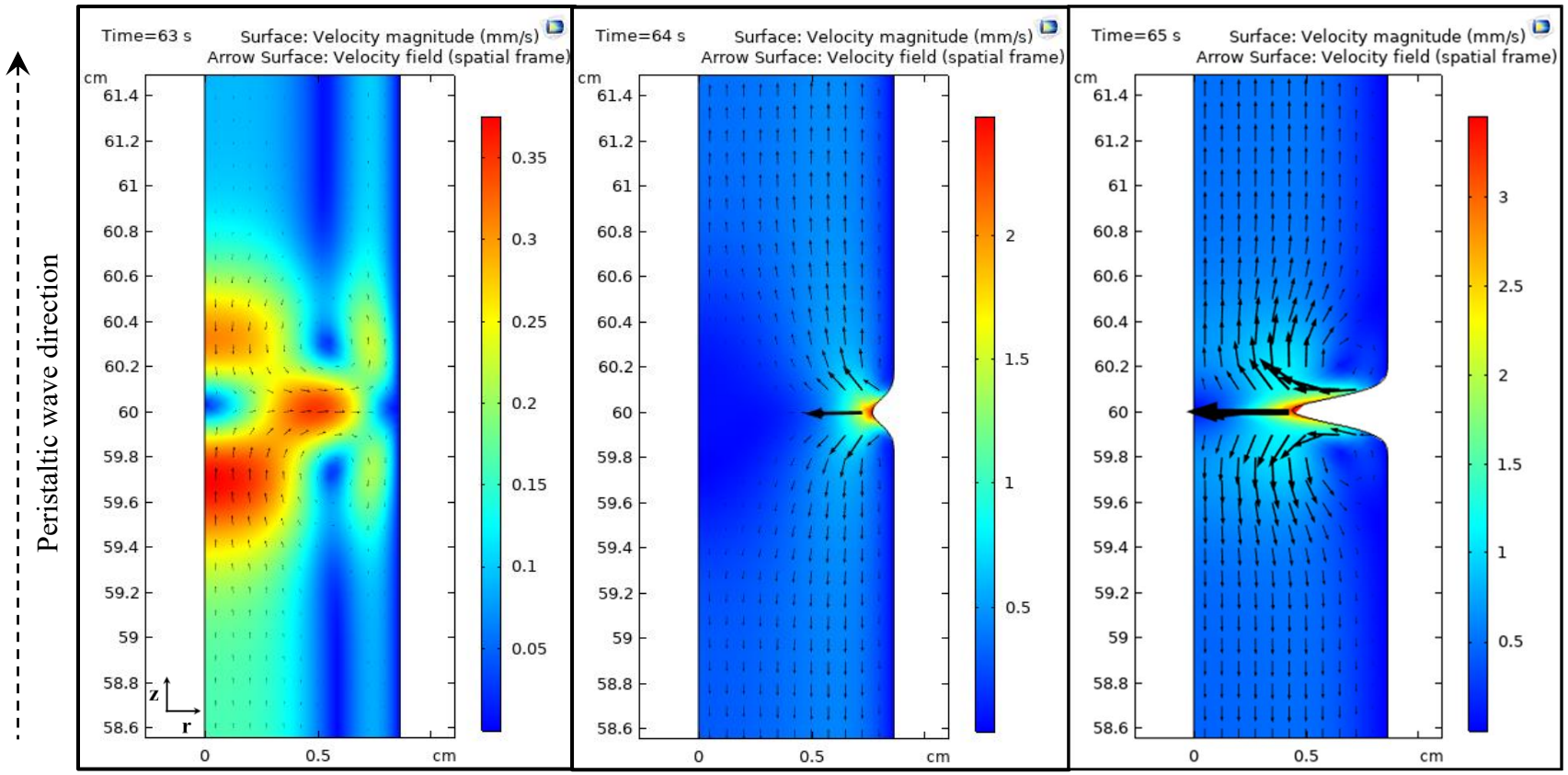

t = 63 s **t = 64 s** **t = 65 s**

Figure 4.26: Velocity profile in a section of the jejunum fluid flow model at different time intervals, induced by a peristaltic wave, predicted by COMSOL Multiphysics®

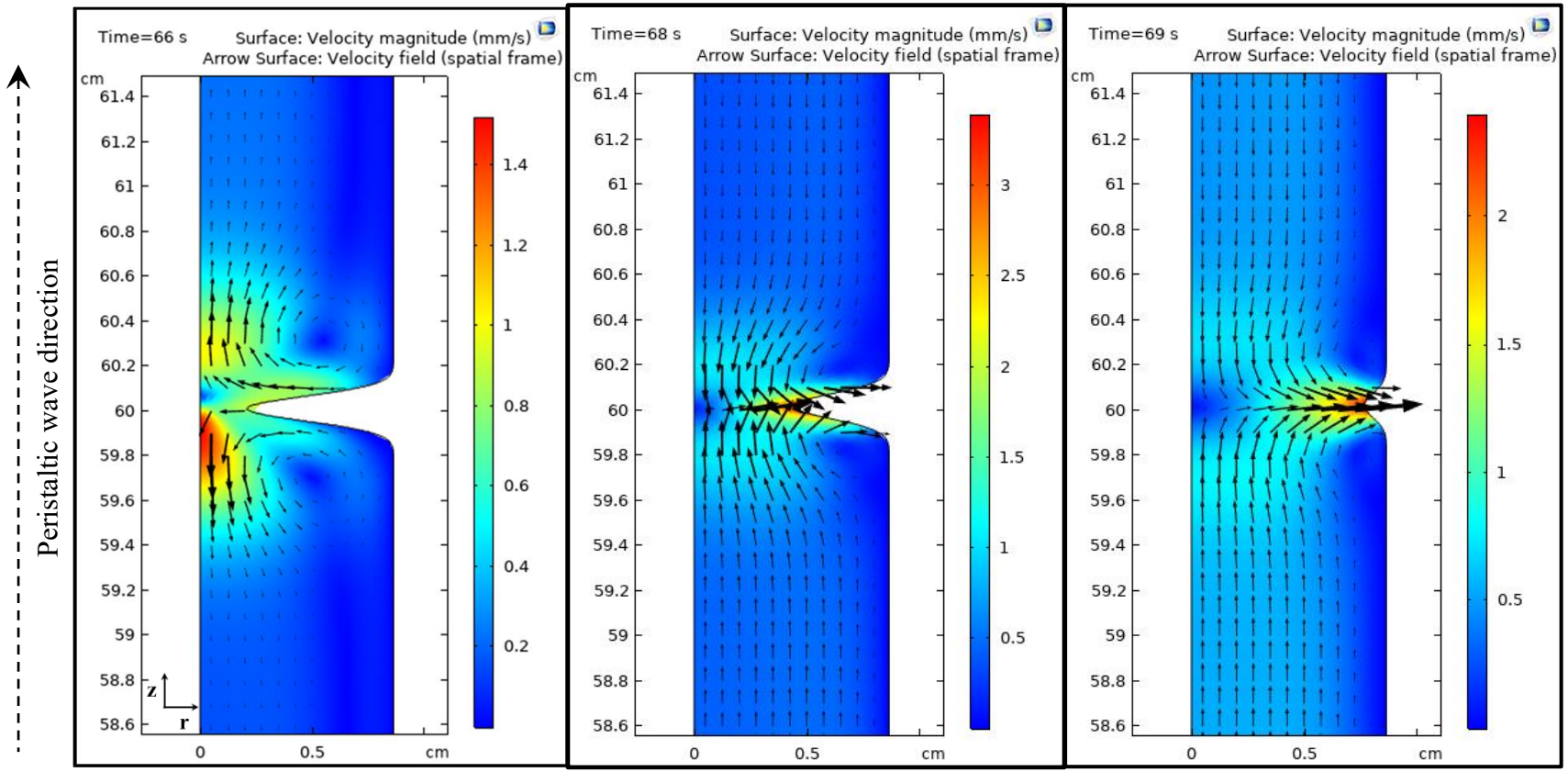

t = 66 s **t = 68 s** **t = 69 s**

Figure 4.26: Velocity profile in a section of the jejunum fluid flow model at different time intervals, induced by a peristaltic wave, predicted by COMSOL Multiphysics®

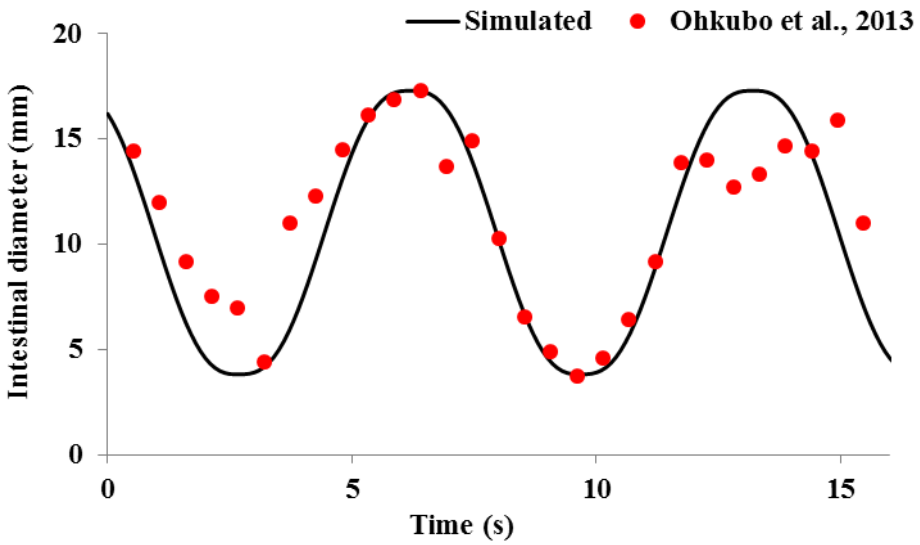

Figure 4.27: Comparison of intestinal diameter variations between simulated results and data obtained from the literature (Ohkubo et al., 2013)

4.6. Diffusion model predictions

As mentioned in the materials and methods section, the velocity profile obtained from the dynamic fluid flow model was used as the inlet condition in the static diffusion model. The 5 g glucose diffusion model was simulated first to finalize the thin diffusion barrier properties before incorporating reaction kinetics to the model. From **Table 4.2**, it can be seen that 5 g glucose-based bolus (1.00 mPa·s) experiment resulted in 3.67 g of glucose absorbed in the jejunum section and 0.78 g of glucose absorbed in the ileal section. In the jejunum diffusion model and the ileum diffusion model, the diffusivity value of glucose across the thin diffusion barrier ($D_{s,g}$) was varied independently, to achieve the above-mentioned final glucose absorption values. For the jejunum diffusion model, the thin

diffusion barrier of thickness 2 mm and glucose diffusivity of 5.25×10^{-9} m^2/s was able to achieve the cumulative experimental glucose absorption value of 3.67 g. The experimental-numerical comparison of cumulative glucose absorption curves is shown in **Figure 4.28**. The comparison has an average error of 0.07 g and an RMSE value of 0.1.

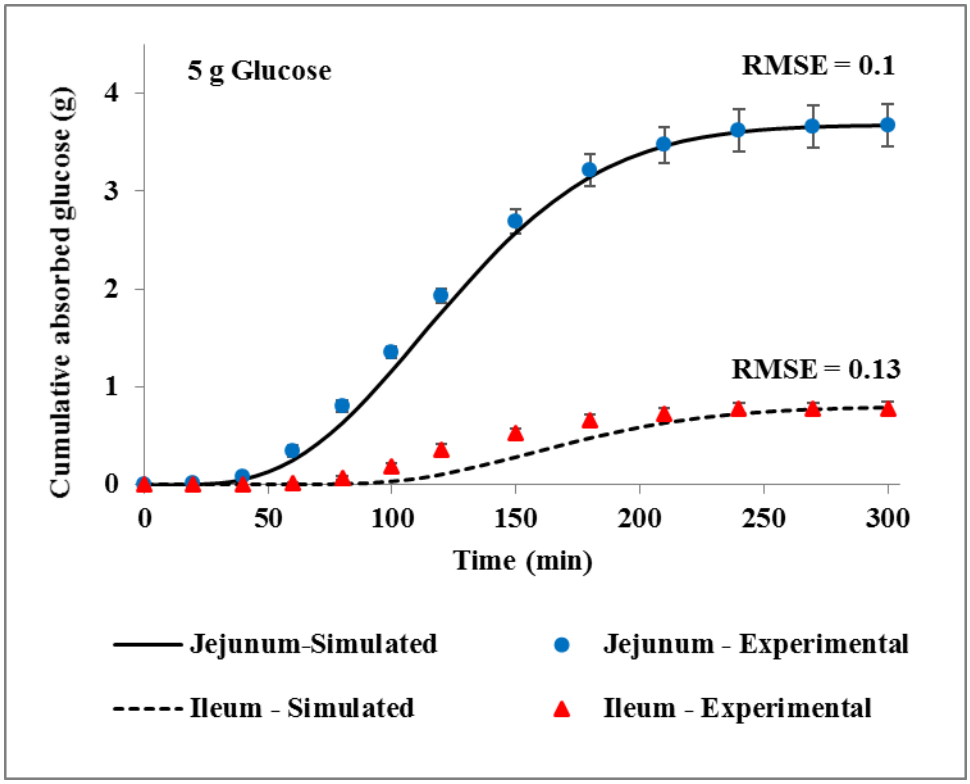

Figure 4.28: Comparison of simulated and experimental cumulative glucose absorption curves of 5 g glucose feed (diffusivity in jejunum model = 5.25×10^{-9} m^2/s and diffusivity in ileum model = 2.5×10^{-8} m^2/s)

In the case of ileum diffusion model, only $1/4^{th}$ of the actual ileum geometry length (0.45 m) was simulated, instead of the entire length (1.8 m). The reduction in the length of the ileum geometry was implemented because of the experimental glucose absorption value. Due to experimental limitations, only ~90% of the fed carbohydrate was able to recover in the absorption sections, ~75% in the jejunal section and ~15% in the ileal section. To maintain this proportion, only 45 cm of the ileum section was simulated, instead of the entire length. With the diffusion barrier thickness of 2 mm and glucose diffusivity value of 2.5×10^{-8} m^2/s, the ileum diffusion model could achieve the cumulative experimental glucose absorption value of 0.78 g. The experimental-numerical comparison of cumulative glucose absorption curves is shown in **Figure 4.28**. The comparison has an average error of 0.08 g and an RMSE value of 0.13.

The other two 5 g glucose-based bolus solutions of viscosity values 14.57 mPa·s and 102.11 mPa·s resulted in 3.54 g of glucose absorbed in the jejunum section, and 0.76 g and 0.71 g of glucose absorbed in the ileum section, respectively, as shown in **Table 4.2**. These values were not significantly different from previously used amount glucose absorbed during the digestion of 1.00 mPa·s glucose-based bolus (3.67 g in jejunum and 0.78 g in ileum). In the experimental procedure, the gastric emptying rate was kept constant for all three bolus system and there was no digestive reaction involved. Therefore, the same jejunum and ileum diffusion models were used to predict their glucose absorption curves, without changing any variables. In the case of 14.57 mPa·s glucose-based bolus, the jejunum diffusion model predicted the experimental glucose absorption curve with an average error of 0.08 and an RMSE value of 0.10 and the ileum diffusion model predicted

the experimental glucose absorption curve with an average error of 0.07 and an RMSE value of 0.10. In the case of 102.11 mPa·s glucose-based bolus, the jejunum diffusion model predicted the experimental glucose absorption curve with an average error of 0.06 and an RMSE value of 0.08 and the ileum diffusion model predicted the experimental glucose absorption curve with an average error of 0.07 and an RMSE value of 0.10.

4.6.1. Diffusion model incorporated with reaction kinetics

Based on the finalized thin diffusion barrier properties (jejunum model: 2 mm thickness and 5.25×10^{-9} m^2/s glucose diffusivity and ileum model: 2 mm thickness and 2.5×10^{-8} m^2/s glucose diffusivity), maltodextrin diffusion simulations were carried out by incorporating reaction kinetics to the model. While performing *in vitro* digestive experiments, the extent of maltodextrin digestion was varied by either externally adding brush border enzyme (maltose assay kit) or by changing the initial viscosity of bolus. Depending on the extent of digestion, 5 g maltodextrin-based bolus experimental variables were divided into three categories.

(1) Complete hydrolysis - external addition of brush border enzyme, from the maltose assay kit, which gives the total-glucose absorption values **(Table 4.3)**. No significant difference in glucose absorption values was found based on the initial bolus viscosity values, 1.03 mPa·s, 14.84 mPa·s, and 103.89 mPa·s. Therefore the 1.03 mPa·s system (maltodextrin in water, no glycerol) was used as the reference to developing this simulation model.

(2) Partial hydrolysis - absence of brush border enzyme and absence of glycerol. In the actual TIM-1 experiments, due to the absence of brush border enzyme, maltodextrin was partially hydrolyzed to glucose and maltose molecules and was collected. The concentration of glucose molecules in the collected samples were quantified using the glucose assay kit and termed as base-glucose **(Table 4.3)**. Amount of absorbed base-glucose changes with respect to the glycerol-induced viscosity. Case 2 diffusion model was developed based on cumulative base-glucose absorption values of 1.03 mPa·s bolus (maltodextrin in water, no glycerol)

(3) Partial hydrolysis - absence of brush border enzyme and presence of glycerol. Case 3 diffusion model was developed based on cumulative base-glucose absorption values of 14.84 m Pa.s bolus (maltodextrin in 70:30 glycerol to water). No significant difference between glucose absorption values of 14.84 mPa·s and 103.89 mPa·s bolus system was observed **(Table 4.3)**.

While solving all three cases of maltodextrin diffusion models, the K_m value was assumed to be a constant of 4.8 mol/m^3. The V_{max} value was varied in the jejunum diffusion, in the range 0.00365 mol/(m^3·s) to 0.11667 mol/(m^3·s), depending on the extent of maltodextrin digestion (three cases), to achieve the respective final amount of base-glucose or total-glucose absorption values mentioned in **Table 4.3**. As mentioned in the materials and methods section, it was assumed that the maltodextrin digestion reaction happened only in the jejunum model, not in the ileum model.

Case 1: Complete hydrolysis with the external addition of brush border enzyme

From **Table 4.3**, it can be seen that 5 g maltodextrin in water bolus system (1.03 mPa·s) resulted in 3.74 g total-glucose absorbed in the jejunum section and 0.66 g of total-glucose absorbed in the ileal section. The jejunum diffusion model with the K_m value of 4.8 mol/m^3 and V_{max} value of 0.065 mol/(m^3·s), predicted the cumulative jejunal total-glucose absorption value of 3.74 g. The experimental-numerical comparison has an average error of 0.20 g with an RMSE value of 0.30, as shown in **Figure 4.29**. Case 1 ileum diffusion model, with no reaction kinetics equation, predicted 0.66 g of ileal cumulative total-glucose absorption value with an average error of 0.13 g and an RMSE value of 0.19 **(Figure 4.29)**.

The other two 5 g maltodextrin-based bolus solutions of viscosity values 14.84 mPa·s and 103.89 mPa·s resulted in 3.82 g and 3.61 g of total-glucose absorbed in the jejunum section, respectively, and 0.68 g and 0.62 g of total-glucose absorbed in the ileum section, respectively, as shown in **Table 4.3**. These values were not significantly different from previously used values of total-glucose absorbed during the digestion of 1.03 mPa·s maltodextrin-based bolus (3.74 g in jejunum and 0.66 g in ileum). In the experimental procedure, the gastric emptying rate was kept constant for all three bolus system. Therefore, the same jejunum and ileum diffusion models were used to predict their glucose absorption curves, without changing any variables. In the case of 14.84 mPa·s maltodextrin-based bolus, the jejunum diffusion model predicted the experimental total-glucose absorption curve with an average error of 0.22 and an RMSE value of 0.33 and the ileum diffusion model predicted the experimental total-glucose absorption curve with an

average error of 0.08 and an RMSE value of 0.05. In the case of 103.89 mPa·s maltodextrin-based bolus, the jejunum diffusion model predicted the experimental total-glucose absorption curve with an average error of 0.21 and an RMSE value of 0.27 and the ileum diffusion model predicted the experimental total-glucose absorption curve with an average error of 0.15 and an RMSE value of 0.11.

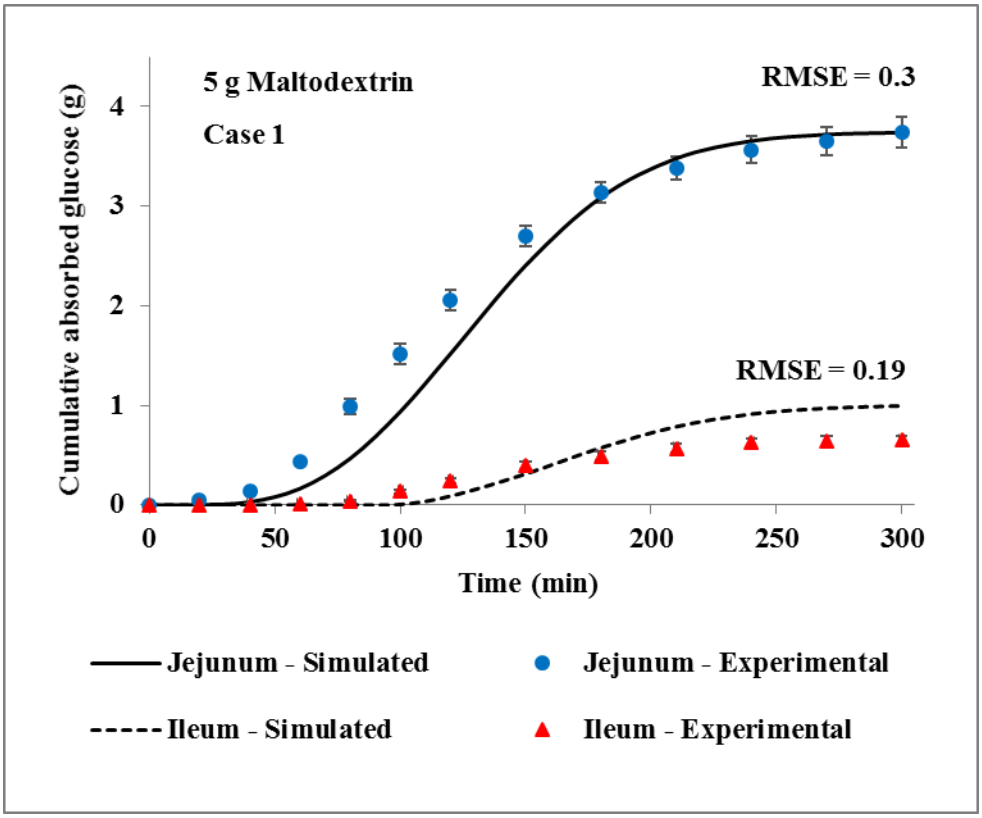

Figure 4.29: Comparison of simulated and experimental cumulative glucose absorption curves of 5 g maltodextrin feed - Case 1: Complete hydrolysis with the external addition of brush border enzyme

(K_m = 4.8 mol/m^3 and V_{max} = 0.065 mol/(m^3·s))

Case 2: Partial hydrolysis with the absence of brush border enzyme and absence of glycerol

From **Table 4.3**, it can be seen that 5 g maltodextrin in water bolus system (1.03 mPa·s) resulted in 1.07 g of base-glucose absorbed in the jejunum section and 0.21 g of base-glucose absorbed in the ileal section.

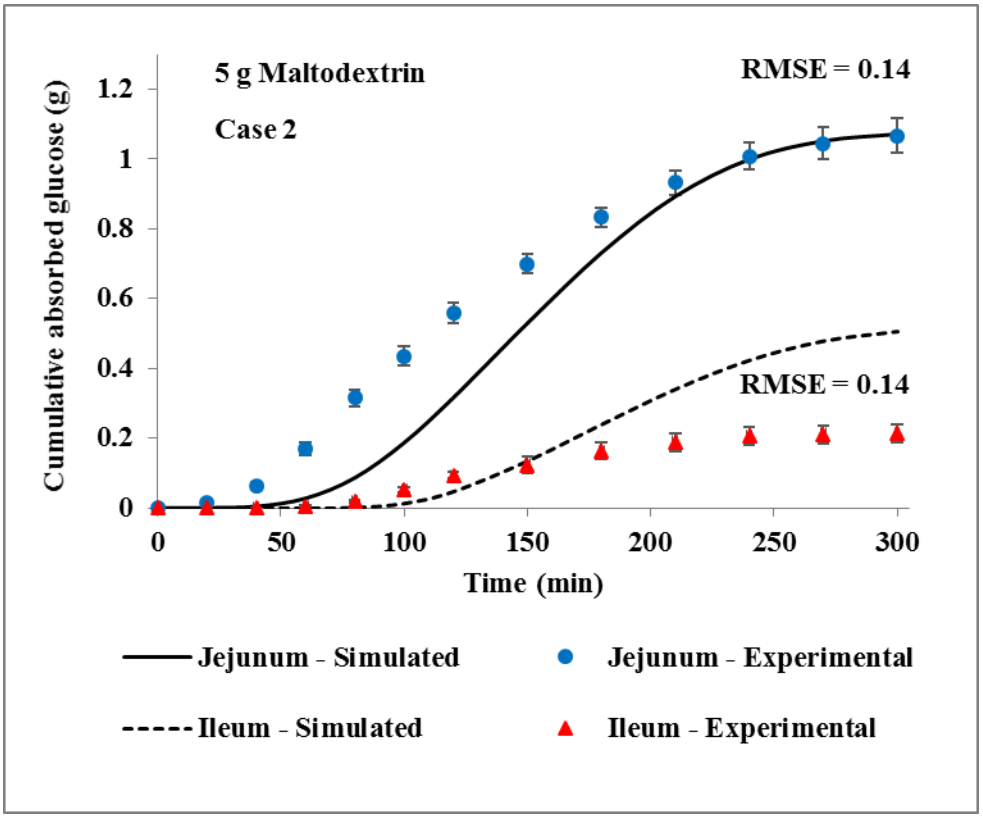

Figure 4.30: Comparison of simulated and experimental cumulative glucose absorption curves of 5 g maltodextrin feed - Case 2: Partial hydrolysis with absence of brush border enzyme and absence of glycerol

(K_m = 4.8 mol/m^3 and V_{max} = 0.0063 mol/(m^3·s))

The jejunum diffusion model with the K_m value of 4.8 mol/m^3 and V_{max} value of 0.0063 mol/(m^3·s), predicted the cumulative jejunal base-glucose absorption value of 1.07 g. The experimental-numerical comparison has an average error of 0.1 g with an RMSE value of 0.14, as shown in **Figure 4.30**. Case 2 ileum diffusion model, predicted 0.21 g of ileal cumulative base-glucose absorption value with an average error of 0.09 g and an RMSE value of 0.14 **(Figure 4.30)**.

Case 3: Partial hydrolysis with the absence of brush border enzyme and presence of glycerol

From **Table 4.3**, it can be seen that 5 g maltodextrin–based bolus with an initial viscosity of 14.84 mPa·s resulted in 0.69 g of base-glucose absorbed in the jejunum section and 0.14 g of base-glucose absorbed in the ileal section. The jejunum diffusion model with the K_m value of 4.8 mol/m^3 and V_{max} value of 0.0039 mol/(m^3·s), predicted the cumulative jejunal base-glucose absorption value of 0.69 g. The experimental-numerical comparison has an average error of 0.05 g with an RMSE value of 0.08, as shown in **Figure 4.31**. Case 3 ileum diffusion model predicted 0.14 g of ileal cumulative base-glucose absorption value with an average error of 0.06 g and an RMSE value of 0.09 **(Figure 4.31)**.

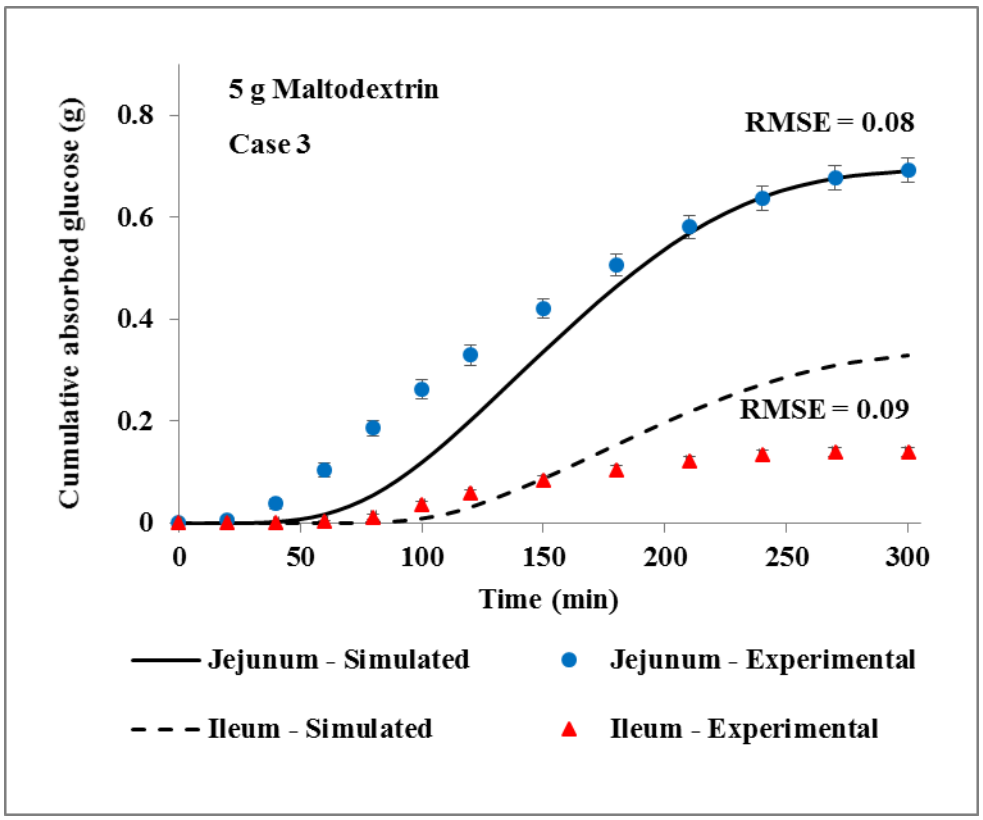

Figure 4.31: Comparison of simulated and experimental cumulative glucose absorption curves of 5 g maltodextrin feed - Case 3: Partial hydrolysis with absence of brush border enzyme and presence of glycerol (K_m = 4.8 mol/m^3 and V_{max} = 0.0039 mol/(m^3·s))

The other 5 g maltodextrin-based bolus solution of initial viscosity 103.89 mPa·s resulted in 0.69 g of base-glucose absorbed in the jejunum section and 0.13 g base-glucose absorbed in the ileum section, as shown in **Table 4.3**. These values were not significantly different from previously used values of base-glucose absorbed during the digestion of 1.03

mPa·s maltodextrin-based bolus (0.69 g in jejunum and 0.14 g in ileum). In the experimental procedure, the gastric emptying rate was kept constant for all the bolus system. Therefore, the same jejunum and ileum diffusion models were used to predict the glucose absorption curves, without changing any variables. In the case of 103.89 mPa·s maltodextrin-based bolus, the jejunum diffusion model predicted the experimental base-glucose absorption curve with an average error of 0.05 and an RMSE value of 0.07. The ileum diffusion model predicted the experimental base-glucose absorption curve with an average error of 0.06 and an RMSE value of 0.01.

The overshoot in ileum predictions in all 3 cases is due to the fact explained in the previous section. While performing numerical simulation, 100% mass balance was achieved as opposed to the experimental procedure which was able to achieve only ~90% mass balance. In a real-life scenario and *in vitro* experimental procedures, the rate and amount of glucose absorbed in the jejunum section hold more importance than the amount of glucose absorbed in the ileum section. Values such as glycemic index are being calculated within 2-hours of food consumption, which predominantly represents the amount of glucose absorbed in the jejunum section. In the future, more importance should be given to the jejunum diffusion model simulation, for predicting the cumulative glucose absorption rate and value.

To simulate the jejunum and ileum diffusion model and to successfully predict the cumulative glucose absorption rates and values, three parameters of a given food product have to be obtained either experimentally or through literature.

1) Carbohydrate composition of the food (amylose or amylopectin, chain length)

2) Initial bolus viscosity, which could be experimentally obtained by the addition of gastric juices to the food product and analyzing its viscosity. Based on the initial bolus viscosity, the gastric emptying rate has to be predicted. Many research articles have been published relating 'expected' gastric emptying rate depending on a wide variety of food products

3) Amylase reaction kinetics for the given food product, which can be obtained by conducting lab-scale experiments.

The first two parameters are used to define the *inflow* boundary condition of the diffusion model. The third parameter is used to define the reaction kinetics (K_m and V_{max}). With these three parameters, the diffusion model would be able to predict the cumulative glucose absorption values.

5. CONCLUSIONS

An *in vitro* gastrointestinal model, the TIM-1 system, was successfully used to study the effect of bolus viscosity on the digestion and nutrient absorption processes. From nutrient absorption curves, it was observed that the glycerol-induced viscosity did not significantly affect the nutrient absorption process in the TIM-1 system. However, the initial bolus viscosity non-linearly influenced the *in vitro* maltodextrin digestion process. For the maltodextrin-based bolus, there was a critical viscosity limit (~15 mPa·s), until which an increase in viscosity significantly reduced the maltodextrin digestion process. Increasing the viscosity above ~15 mPa·s did not significantly affect the maltodextrin digestion. Further research has to be done to explore the effect of viscosity on the digestive process of other carbohydrate-based food systems. With real-time challenges in tracking viscosity changes of gastrointestinal content, the usage of the Fast Green dye proved to be a successful 'non-invasive' methodology while performing *in vitro* studies. The data obtained from this procedure provided a basic understanding of the viscosity changing pattern of the *in vitro* gastrointestinal content during digestion.

This numerical simulation study explored the possibility of mathematically analyzing and predicting the human digestive process. COMSOL Multiphysics® was successfully used to simulate fluid flow due to peristalsis based on real-time motility parameters. The velocity field obtained from a moving boundary dynamic model was successfully imposed on a static model to simulate the transport of carbohydrates, digestion, and nutrient absorption processes. The thin diffusion barrier properties of 2 mm

thickness with glucose diffusivity value of 5.25×10^{-9} m^2/s for the jejunum geometry and 2.5×10^{-8} m^2/s for the ileum geometry, were able to predict cumulative experimental glucose absorption value with an average error of 0.1 g. For a given food product, three parameters have to be known to run this model: 1) carbohydrate composition, 2) gastric emptying rate, 3) amylase reaction kinetics. With these three parameters, this model would be able to predict the cumulative glucose absorption value. This model could further be developed to predict the glycemic index of a given food product.

Research in this direction can aid food industry and related researchers in understanding the possibility of reducing the nutrient/caloric intake by altering the viscosity of food matrix/bolus and can help in predicting the glucose absorption pattern in the human small intestine. Formulating innovative food products with predictive viscosity behavior and glucose absorption process would be helpful in controlling excessive caloric intake and in turn may reduce the chances of obesity-related health risks.

6. FUTURE WORK

In vitro experimental procedure

This study analyzed *in vitro* digestion of simple carbohydrate-based food systems, namely glucose and maltodextrin. *In vitro* digestion of more carbohydrate-based food systems, with different chain length and complexity (branched chains) have to be analyzed to confirm the reliability of this *in vitro* experimental procedure. Glycerol was used in this study to change the initial viscosity of bolus. Different thickening agents could be tried to confirm the effect of viscosity on the overall digestive process.

Absorbed glucose and maltose concentration quantification

To quantify the absorbed nutrients (glucose and maltose) chemical assay kits purchased from Sigma Aldrich was used in this study. These assay kits analyzed a small sample volume of sample (less than 50 μL) and some of the additional enzymes added during the assay experiments was as low as 2 μL. Working with such a low quantity might increase the chances of experimental error. Implementing a more robust method such as analyzing the samples using HPLC to quantify these carbohydrates would help in reducing human and instrumental error.

Fluorescence emitting dye

Fast Green dye was used in this study, to monitor the changes in viscosity of *in vitro* gastrointestinal content during digestion. This dye was helpful in tracking the viscosity changing pattern without interrupting the *in vitro* digestive experiment. However,

in the jejunum and ileum sections of the TIM-1 system, the intestinal content viscosity was too low to influence the molecular rotor property of this dye. Different fluoresce emitting in a wide variety of food systems can be analyzed to identify a better sensitive dye at lower viscosity changes.

Numerical simulation

This study was one of the few initial attempts at incorporating the digestive reaction and diffusion process to a fluid flow numerical model. Because of the complexity involved in the multistage digestion process, many assumptions were made to develop this model, such as, the geometry of small intestine is a long cylinder, entire geometry is filled with intestinal content, only one peristaltic wave in each section of the small intestine, the digestive reaction happens only in the jejunum section, glucose-sodium transport was assumed as a diffusion model, etc. This numerical model could be improved by addressing these assumptions. Also, by comparing the experimental glucose absorption curves of more carbohydrate-based food systems, this model could be improved to increase the accuracy of glucose absorption predictions.

7. REFERENCES

AlHasawi, F. M., Dondaco, D., Ben-Elazar, K., Ben-Elazar, S., Fan, Y. Y., Corradini, M. G., Ludescher, R. D., Bolster, D., Carder, G., Chu, Y., Chung, Y., Kasturi, P., Johnson, J., and Rogers, M. A. (2017). *In vitro* measurements of luminal viscosity and glucose/maltose bioaccessibility for oat bran, instant oats, and steel cut oats. *Food Hydrocolloids*, 70, 293-303.

AlHasawi, F. M., Corradini, M. G., Rogers, M. A., and Ludescher, R. D. (2018). Potential applications of luminescent molecular rotors in food science and engineering. *Critical Reviews in Food Science and Nutrition*, 58(11), 1902-1916.

Anson, N. M., Selinheimo, E., Havenaar, R., Aura, A. M., Mattila, I., Lehtinen, P., Bast, A., Poutanen, K., and Haenen, G. R. (2009). Bioprocessing of wheat bran improves *in vitro* bioaccessibility and colonic metabolism of phenolic compounds. *Journal of Agricultural and Food Chemistry*. 57, 6148-6155.

Betts, J. G., Desaix, P., Johnson, E., Johson, J. E., Korol, O., Kruse,D., Poe, B., Wise, J.A., Womble, M., Young, K.A. (2013). Anatomy and Physiology: The Digestive System. OpenStax College textbook. Rice University, Texas. (Chapter 23). Retrieved from: https://opentextbc.ca/anatomyandphysiology/chapter/23-5-the-small-and-large-intestines/
Last accessed on: April 09, 2019

Billa, N., Yuen, K., Khader, M. A. A., and Omar A. (2000). Gamma-scintigraphic study of the gastrointestinal transit in vivo dissolution of a controlled release diclofenac sodium formulation in xanthan gum matrices. International Journal of Pharmaceutics. 201(2000), 109-120.

Blundell, J. E. (1999). The control of appetite: basic concepts and practical implications. *Schweiz Med Wochenschr*. 129, 182-188.

Brasseur, J. G., Banco, G. G., Ailani, A. C., Wang, Y., Neuberger, T., Smith, N. B., and Webb, A. G. (2009). Motility and absorption in the small intestines: Integrating MRI with Lattice Boltzmann models. *IEEE International Symposium on Biomedical Imaging: From Nano to Macro*. 374-377.

Boisen, S. and Eggum, B. O. (1991). Critical evaluation of *in vitro* methods for estimating digestibility in simple stomached animals. *Nutrition Research Reviews*. 4, 141-162.

Borgstrom, B., Dahlqvist, A., Lundh, G., and Sjovall, J. (1957). Studies of intestinal digestion and absorption in the human. *The Journal of Clinical Investigation*, 36, 1521-1536.

Caspary, W. F. (1992). Physiology and pathophysiology of intestinal absorption. *The American Journal of Clinical Nutrition*. 55(1), 299S-308S.

Clark, M. J., and Slavin, J. L. (2013). The effect of fiber on satiety and food intake: A systematic review. *Journal of the American college of Nutrition.* 32(3), 200-211.

Coles, L. T., Moughan, P. J., and Darragh, A. J. (2005). *In vitro* digestion and fermentation methods, including gas production techniques, as applied to nutritive evaluation of foods in the hindgut of humans and other simple-stomached animals. *Animal Food Science and Technology*. 123-124. 421-444.

Converti, A., Zilli, M., Arni, S., Felice, R. D., and Borghi, M. D. (1999). The effects of temperature and viscsoity on glucose diffusivity through *Saccharomyces cerevisiae* biofilms. *The Canadian Journal of Chemical Engineering*. 77, 618-626.

Corradini, M. G., and Ludescher, R. D. (2015). Making sense of luminescence from GRAS optical probes. *Current Opinion in Food Science*. 4, 25-31.

Coupe, A. J., Davis, S. S., and Wilding, I. R. (1991). Variation in gastrointestinal transit of pharmaceutical dosage forms in healthy subjects. *Pharmaceutical Research*. 8(3), 360-364.

Davis, S. S., Hardy, J. G., and Fara, J. W. (1986). Transit of pharmaceutical dosage through the small intestine. *Gut: Alimentary tract and pancreas*. 27, 886-892.

Dickinson, P. A., Rmaileh, R. A., Ashworth, L., Barker, R. A., Burke, W. M., Patterson, C. M., Stainsforth, N., and Yasin, M. (2012). An investigation in to the utility of a multi-compartmental, dynamic, system of the upper gastrointestinal tract to support formulation development and establish bioequivalence of poorly soluble drugs. *American Association of Pharmaceutical Scientists*. 14(2), 196-205.

Du, H., Kim, C., Corradini, M. G., Ludescher, R. D., and Rogers, M. A. (2014). Micro-viscosity of liquid oil confined in colloidal fat crystal networks. *Soft Matter*. 10, 8652-8658.

Elashoff, J. D., Reedy, T. J., and Meyer, J. H. (1982). Analysis of gastric emptying data. *Gastroenterology*, 83, 1306-1312.

Englyst, H. N., Veenstra, J., and Hudson, G. J. (1996). Measurement of rapidly available glucose (RAG) in plant foods: a potential in vitro predictor of the glycaemic response. *British Journal of Nutrition*. 75(3), 327-337.

Etcheverry, P., Grusak, M. A., and Fleige, L. E. (2012). Applications of *in vitro* bioaccessibility and bio availability methods for calcium, carotenoids, folate, iron, magnesium, polyphenols, zinc, and vitamins B_6, B_{12}, D, and E. *Frontiers in Physiology*. 3(317).

Etienne-Mesmin, L., Livrelli, V., Privat, M., and Blanquest-Diot, S. (2011). Effect of a new probiotic Saccharomyces cerevisiae strain on survival of Escherichia coli o157, H7 in a dynamic gastrointestinal model. *Applied and Environmental Microbiology*. 77, 1127-1131.

Ferrua, M. J. and Singh, R. P. (2010). Modeling the fluid dynamics in a human stomach to gain insight of food digestion. *Journal of Food Science*. 75(7), R151-R162.

Ferrua, M. J. and Singh, R. P. (2011). Computational modeling of gastric digestion using computational modeling. *Procedia Food Science*. 1, 1465-1472.

Ferrua, M. J. and Singh, R. P. (2013). Computational modeling of gastrointestinal fluid dynamics. In: Cheng, L. K., Pullan, A. J., and Farrugia, G. (Eds.) New Advances in Gastrointestinal Motility Research. Springer Science+Business Media, Dordrecht.

Finkelstein, E. A., Trogdon, J. G., Cohen, J. W., and Dietz, W. (2009). Annual medical spending attributes to obesity: Payer-and service-specific estimates. *Health Affairs*. 28(5), 822-831.

Flegal, K. M., Kruszon-Moran, D., Carroll, M. D., Fryar, C. D., and Ogden, C. L. (2016). Trend in obesity among adults in the United State, 2005 to 2014. *The Journal of the American Medical Association*. 315(21), 2284-2291.

Foster-Powell, K., Holt, S. H., and Brand-Miller, J. C. (2002). International table of glycemic index and glycemic load values: 2002. *The American Journal of Clinical Nutrition*. 76, 5-56.

Goni, I., Garcia-Alonso, A., and Saura-Calixto, F. (1997). A starch hydrolysis procedure to estimate glycemic index. *Nutrition Research*, 17(3), 427-437.

Gropper, S. S., Smith, J. L., and Groff, J. L. (2009). Advanced nutrition and human metabolism. (5th ed.). California, Wadsworth Cengage Learning. (Chapter 2).

Guerra, A., Etienne-Mesmin., Livrelli, V., Denis, S., Blanquet-Diot, S., Alric, M. (2012). Relevance and challenges in modeling human gastric and small intestinal digestion. *Trends in Biotechnology*. 30, 591-600.

Haidekker, M. A., and Theodorakis, E. A. (2010). Environment-sensitive behavior of fluorescent molecular rotors. *Journal of Biological Engineering*. 4, 11.

Halton, T. L., and Hu, F. B. (2004). The effects of high protein diets on thermogenesis, satiety and weight loss: a critical review. *The Journal of American College of Nutrition*. 23(5), 373-385.

Hardacre, A.K., Lentle. R. G., Yap, S., and Monro, J. A. (2016). Does viscosity or structure govern the rate at which starch granules are digested? *Carbohydrate polymers*, 136, 667-675.

Hari, B., Bakalis, S., and Fryer, P. (2012). Computational modelling and simulation of the human duodenum. *Excerpt from the Proceedings of the 2012 COMSOL Conference in Milan*.

Howarth, N. C., Saltzman, E., and Roberts, S. B. (2001). Dietary fiber and weight regulation. *Nutrition Reviews*. 59, 129-139.

Hur, S. J., Lim, B. O., Decker, E. A., and McClements, D. J. (2011). *In vitro* human digestion models for food applications. *Food Chemistry*. 125, 1-12.

Jamieson, G., and Wong, J. (2006). Chapter 11: Small bowel resection; ileostomy; ileal pouches and the use of ileal conduits to replace the oesophagus: the anatomy of the small bowel. In Jamieson, G. G. (Eds.), *The Anatomy of General Surgical Operations.* (pp. 56). UK Longman Group UK limited and Elsevier Limited.

Kashi, A., Waxman, S. M., Komaiko, J. S., Draganski, A., Corradini, M. G., and Ludescher, R. D. (2015). Potential use of food synthetic colors as intrinsic luminescent probes of the physical state of foods. In: Guthrie, B., Beauchamp, J., Buettner, A., and Lavine, B. K. (Eds.) The Chemical Sensory Informatics of Food: Measurement, Analysis, Integration. ACS Symposium Series, American Chemical Society, Washington, DC, 2015.

Kennedy, J. F., Knill, C. J., and Taylor, D. W. (1995). Maltodextrins. In: Kearsley, M. W. and Dziedzic, S. Z. (Eds.) Handbook of starch hydrolysis products and their derivatives. Springer Science+Business Media, Dordrecht. (Chapter 3).

Kong, F., Oztop, M. H., Singh, R. P., McCarthy, M. J. (2011). Physical changes in white and brown rice during simulated gastric digestion. *Journal of Food Science*. 76(6), E450-E457.

Kopelman, P. G. (2000). Obesity as a medical problem. *Nature*, 404, 635-643.

Kostewics, E. S., Abrahamsson, B., Brewster, M., Brouwers, J., Butler, J., Carlert, S., Dickinson, P. A., Dressman, J., Holm, R., Klein, S., Mann, J., McAllister, M., Minekus, M., Muenster, U., Mullertz, A., Verwei, M., Vertzoni, M., Weitschies, W., Augustijns, P. (2014). *In vitro* models for the prediction of *in vivo* performance of oral dosage forms. *European Journal of Pharmaceutical Sciences*. 57, 342-366.

Kotttas, G. S., Clarke, L. I., Horinek, D., and Michl, J. (2005). Artificial molecular rotors. *Chemical Reviews*. 105(4), 1281-1376.

Kristensen, M., Jensen, M. G., Riboldi, G., Petronio, M., Bugel, S, toubro, Soren, Tetens, I., and Astrup, A. (2010). Wholegrain vs. refined wheat bread and pasta. Effect on postprandial glycemia, appetite, and subsequent *ad libitum* energy intake in young healthy adults. *Appetite*. 54, 163-169.

Lentle, R. G., and Janssen, P. W. M. (2010). Manipulating digestion with foods designed to change the physical characteristics of digesta. *Critical Reviews in Food Science and Nutrition*. 50, 130-145.

Lentle, R. G., and Janssen, P. W. M. (2011). The physical processes of digestion. Springer Science+Business Media, New York. (Chapter 3).

Lin, A. S. H., Buist, M. L., Smith, N. P., Pullan, A. J. (2006). Modelling slow wave activity in the small intestine. *Journal of theoretical Biology*. 242, 356-362.

Linton, P. H., Conley, M., Kuechenmeister, C., and McClusky, H. (1972). Satiety and Obesity. *The American Journal of Clinical Nutrition*, 25, 368-370.

Liu, S., Willet, W.C., Stampfer, M.J., hu, F.B., Franz, M., Sampson, L., and Hennekens, C.H. (2000). A prospective study of dietary glycemic load, carbohydrate intake and risk of coronary heart disease in US women. *The American Journal of Clinical Nutrition*. 71, 1455-1461.

Maljaars, J. Peters, H. P. F., and Masclee, A. M. (2007). Review article: the gastrointestinal tract: neuroendocrine regulation of satiety and food intake. *Alimentary Pharmacology & Therapeutics*. 26(2), 241-250.

McDonald, D. E., Pethick, D. W., Mullan, B. P., and Hampson, D. J. (2001). Increasing viscosity of the intestinal contents alters small intestinal structure and intestinal growth, and stimulates proliferation of enterotoxigenic *Escherichia coli* in newly-weaned pigs. *British Journal of Nutrition*. 86. 487-498.

Minekus, M., Marteau, P., Havenaar, R., Huis in't Veld, J. H. J. (1995). A multi-compartmental dynamic computer-controlled model simulating the stomach and small intestine. *Alternatives to Laboratory Animals*. 23, 197-209.

Minekus, M. (2015). The TNO Gastro-Intestinal Model (TIM) (Chapter 5). In: Verhieckx, K., Cotter, P., Lopez-Exposito, I., Kleiveland, C., Lea, T., Mackie, A., Requena, T., Swiatecka, D., Wichers, H. (Eds.), The impact of food bioactives on health: *in vitro* and *ex vivo* models. Springer, Cham, Switzerland.

Moxon, T. E., Gouseti, O., and Bakalis, S. (2016). *In silico* modelling of mass transfer & ansorption in the human gut. *Journal of Food engineering*. 176, 110-120.

Nimalaratne, C., Savrad, P., Gauthier, S. F., Schieber, A., and Wu, J. 2015. Bioaccessibility and digestive stability of carotenoids in cooked eggs studied using a dynamic *in vitro* gastrointestinal model. *Journal of Agricultural and Food Chemistry*. 63(11), 2956-2962.

NIH. (2012). National Heart, Lung, and Blood Institute (U.S. Department of Health & Human Services). Overweight and Obesity.
Retrieved from: http://www.nhlbi.nih.gov/health/health-topics/topics/obe/
Last assessed on: April 06, 2019.

Ohkubo, H., Kessoku, T., Fuyuki, A., Lida, H., Inamori, M., Fujii, T., Kawamura, H., Hata, Y., Manabe, N., Chiba, T., Kwee, T. C., Haruma, K., Matsuhashi, N., Nakajima, A., and Takahara, T. (2013). Assessment of small bowel motility in patients with chronic intestinal pseudo-obstruction using cine-MRI. *The American Journal of Gastroenterology*. 108(7), 1130-1139.

Paddon-Jones, D., Westman, E., Mattes, R. D., Wolfe, R. R., Astrup, A., Westerterp-Plantenga, M. (2008). Protein, weight management, and satiety. *The American Journal of Clinical Nutrition*. 87(5), 1558S-1561S.

Pal, A., Indireshkumar, K., Schwizer, W., Abrahamson, B., Fried, M., and Brasseur, J. G. (2004). Gastric flow and mixing studied using computer simulation. *Proceedings of the Royal Society of London B*. 271, 2587-2594.

Pallotta, N., Baccini, F., and Corazziari, E. (1999). Contrast ultrasonography of the normal small bowel. *Ultrasound in Medicine & Biology*, 25(9), 1335-1340.

Pan, A. and Hu, F. B. (2001). Effects of carbohydrates in satiety: differences between liquid and solid food. *Current Opinion in clinical Nutrition and Metabolic Care*. 14, 385 - 390.

Patton, K. T., and Thibodeau, G. A. (2016). Anatomy & Physiology. (9th ed.) Missouri, Elsevier. (Chapter 9).

Potier, M., Darcel, N., Tome, D. (2009). Protein, amino acids and the control of food intake. *Current Opinion in Clinical Nutrition and Metabolic Care*. 12, 54-58.

Pozrikidis, C. (1987). A study of peristaltic flow. *Journal of Fluid Mechanics*, 180, 515-527.

Rainbird, A., and Low, A. (1986). Effect of guar gum on gastric emptying in growing pigs. *British Journal of Nutrition*, 55, 87-98.

Sacks, F. M., Bray, G. A., Carey, V. J., Smith, S. R., Ryan, D. H., Anton, S. D., McManus, K., Champagne, C. M., Bishop, L. M., Laranjo, N., Leboff, M. S., Rood, J. C., Jonge, L. D., Greenway, F. L., Loria, C. M., Obarzanek, E., and Williamson, D. A. (2009). Comparison of weight-loss diets with different compositions of fat, protein, and carbohydrates. *The New England Journal of Medicine*. 260(9), 859-873.

Saito, N., Horiuchi, T., Yoshida, M., and Imai, T. (1979). Action of human pancreatic and salivary α-amylases on maltooligosaccharides: Evaluation of kinetic parameters. *Clinica Chimica Acta*. 97, 253-260.

Salovaara, S., Alminger, M. L., Eklund-Jonsson, C., Andlid, T., and Sandberg, A. (2003). Prolonged transit time through the stomach and small intestine improves iron dialyzability and uptake *in vitro*. *Journal of Agricultural and Food Chemistry*. 51, 5131-5136.

Satomura, S., Okajima, S., Hamanaka, T., Shintani, A., Miyashita, Y., and Sakata, Y. (1984). Kinetics of human pancreatic and salivary α-amylases with carboxymethylamyloses as substrates. *Clinica Chimica Acta*. 138, 21-29.

Segur, J. B. and Oberstar, H. E. (1951). Viscosity of glycerol and its aqueous solutions. *Industrial and Engineering Chemistry*. 43(9), 2117-2120.

Schwimmer, S. 1950. Kinetics of malt α-amylase action - Enzyme research division contribution No.126. *The Journal of Biological Chemistry*. 186, 181-193.

Schulze, K. (2006) Imaging and modeling of digestion ion the stomach and the duodenum. *Neurogastroenterolgy & Motility*. 18(3), 172-183.

Singh, S. K. (2007). Fluid flow and disintegration of Food in human stomach. Doctoral Thesis. University of California, Davis.

Slavin, J. and Green, H. (2007). Dietary fibre and satiety. *Nutrition Bulletin*. 32, 32-42.

Smeets-Peeters, M., Minekus, M., Havenaar, R., Schaafsma, G., Verstegen, M. (1999). Description of a dynamic in vitro model of the dog gastrointestinal tract and an evaluation of various transit times for protein and calcium. *Alternatives to Laboratory Animals*. 27, 935-949.

Snyder, W. S., Cook, M. J., Nasset, E. S., Karhausen, L. R., Howells, G. P., and Tipton, I. H. (1992). Report of the task group on reference man. International Commission on Radiological Protection. Publication 23. Pergamon press Oxford, UK. (Chapter VII. Digestive system, 144).

Speranza, A., Corradini, M. G., Hartman, T. G., Ribnicky, D., Oren, A., and Rogers, M. A. (2013). Influence of emulsifier structure on lipid bioaccessibility in oil-water nanoemulsions. *Journal of Agriculture and Food Chemistry*. 61, 6505-6515.

Taghipoor, M., Barles, G., Georgelin, C., Licois, J. R., and Lescoat, P. (2014). Digestion modeling in the small intestine: Impact of dietary fiber. *Mathematical Biosciences*. 101-112.

Tharakan, A. (2008). Modelling of physical and chemical processes in the small intestine. *Doctoral thesis*, University of Birmingham, England.

Tharakan, A., Norton, I. T., Fryer, P. J., and Bakalis, S. (2010). Mass transfer and nutrient absorption in a simulated model of small intestine. *Journal of Food Science*. 75(6), 339-346.

Tighe, P., Duthie, G., Vaughan, N., Brittenden, J., Simpson, W. G., Duthie, S., Mutch, W., Wahle, K., Horgan, G., and Thies, F. (2010). Effect of increased consumption of whole-grain foods on blood pressure and other cardiovascular risk markers in healthy middle-aged persons: a randomized controlled trial[1-3]. *The American Journal of Clinical Nutrition*. 92, 733-740.

Turro, N. J., Ramamurthy, V., and Scaiano, J. C. (2010). Modern molecular photochemistry of organic molecules. University Science Books. Sausalito, CA.

Uzhinov, B. M., Ivanov, V. L., and Melnikov, M. Y. (2011). Molecular rotors as luminescence sensors of local viscosity and viscous flow in solutions and organized systems. *Russian Chemical Reviews*. 80(12), 1179-1190.

Villemejane, C., Wahl, R., Aymard, P., Denis, S., Michon, C. (2015). *In vitro* digestion of short-dough biscuits enriched in proteins and/or fibres, using a multi-compartmental and dynamic system (1): Viscosity measurement and prediction. *Food Chemistry*. 182, 55-63.

Wachters-Hagedoorn, R. E., Priebe, M. G., Heimweg, J. A. J., Marius Heiner, A., Englyst, K. N., Holst, J. J., Stellaard, F., and Vonk, R. J. (2006). The rate of intestinal glucose absorption is correlated with plasma glucose-dependent insulinotropic polypeptide concentrations in healthy men. The Journal of Nutrition. 136(6), 1511-1516.

WHO. (2015). World Health Organization. Obesity and Overweight.
Retrieved from: http://www.who.int/mediacentre/factsheets/fs311/en/
Last assessed on: April 06, 2019.

Williams, P. G., Grafenauer, S. J., and O'Shea, J. E. (2008). Cereal grains, legumes, and weight management: a comprehensive review of the scientific evidence. *Nutrition Reviews*. 66(4), 171-182.

Yuen, K.H., Deshmukh, A. A., Newton, j. M., Short, M., Melchor, R. (1993). Gastrointestinal transit and absorption of theophylline from a multiparticulate controlled release formulation. *International Journal of Pharmaceutics*, 97, 61-77.

Yuen, K. H. (2010). The transit of dosage forms through the small intestine. *International Journal of Pharmaceutics*, 395(1-2), 9-16.